LIGHT ACTIVATION OF MECHANOSENSITIVE ION CHANNELS

vorgelegt von:
Fucsia Crea

Erstgutachter:
Prof. Joachim Heberle

Zweitgutachter:
Prof. Rumiana Dimova

Date of the thesis defense: 29th January 2025

Declaration of authorship

Name: Fucsia Crea

I declare to the Freie Universität Berlin that I have completed the submitted dissertation independently and without the use of sources and aids other than those indicated. The present thesis is free of plagiarism. I have marked as such all statements that are taken literally or in content from other writings. This dissertation has not been submitted in the same or similar form in any previous doctoral procedure.

I agree to have my thesis examined by a plagiarism examination software.

15th October 2024
Fucsia Crea

Acknowledgments

This thesis would not have been possible without the support, guidance, and friendship of many people, to whom I owe my deepest gratitude.

First, I would like to thank the entire AG Heberle group, both current and former members, for creating such a happy and collaborative atmosphere. Most of all, I am deeply grateful for your friendship, as I have shared an important part of both my scientific and personal life with you. I am especially grateful to my supervisor, Prof. Joachim Heberle, for the main idea behind this work, and for the continuous encouragement that pushed me forward, even in challenging times. I am also grateful for the many opportunities he provided for me to present my work at conferences, which have been invaluable for my development as a scientist. A special thanks to Dr. Kenichi Ataka for his guidance in the lab and for sharing his experience, which was crucial to this research. I also want to thank Aoife Redlich for her valuable input in discussing data and experimental design, for making the lab a fun place to work, and for proofreading this thesis. I owe special thanks to Rubèn Cruz for running the DFT calculations and helping me interpret the results, as well as to Federico Baserga for his interest and collaboration on nanodiscs.

I am especially indebted to Dr. Ramona Schlesinger and her lab for their expertise on membrane proteins and for providing the MscL sample. In particular, my thanks go to Kirsten Hoffman and Dorothea Heinrich, who taught me all about protein expression in E. coli and purification, and to Antreas Vorkas for producing the samples and taking over the electrophysiology measurements.

I am grateful to Prof. Dirk Trauner's group for providing the photolipids, especially Dirk Trauner for contributing to the main idea of this thesis and to James Frank and Johannes Morstein for synthesizing the lipids. Additionally, I would like to thank Prof. Rumiana Dimova for our collaboration, with a special mention to Mina Aleksanyan and Vasil Georgiev for running the experiments on AzoPC-containing GUVs. I would also like to thank Dr. Christian Schwieger for his generosity in inviting me to use his setup for IRRAS measurements and for sharing his invaluable expertise in this area. Finally, I would like to acknowledge Prof. Adam Lange, with whom I did not directly collaborate but

iv

whose contribution in providing the MscL plasmid was essential for this project.

To my friends, thank you for your endless curiosity, for always asking questions, and for being enthusiastic spectators in this journey. Your interest and support were a constant source of motivation. Lastly, to my partner Fab, thank you for always being there for me, especially during the difficult times when discouragement got the better of me.

Abstract

Mechanosensors play a crucial role in translating physical stimuli into chemical signals, governing numerous biological processes and serving as targets for various diseases. There is a need for precise and remote control over mechanosensitive ion channels. In this thesis, we focused on constructing a basic benchmark system by reconstituting the mechanosensitive ion channel of large conductance, MscL, an ion channel gated solely by membrane tension, in a bilayer containing a photoswitchable lipid, AzoPC. AzoPC is a phospholipid with a substituted azobenzene. When illuminated with blue or UV light it can take two different conformations that create pressure or tension in the membrane. The photolipid's light-to-tension conversion was examined in the monolayer on a Langmuir-Blodgett trough, while structural reorientations during light switching were analyzed using polarized FTIR spectroscopy. A DFT simulation of AzoPC helped with the assignment of the characteristic absorption bands and with the interpretation of the reorientations occurring in the lipids. The tension created with AzoPC in the mebrane can be applied to MscL in order to gate the channel with light. MscL was reconstituted in a free standing bilayer, a multilayer, liposomes and nanodiscs containing AzoPC. The response of the ion channel to light-induced tension was observed with FTIR spectroscopy, revealing a clear reversible movement in the protein backbone. In the black lipid membrane, MscL could be gated to an intermediate subconducting state. Through the combination of rheology, spectroscopic experimental techniques, and functional tests, this thesis provides the foundations of the light-induced modulation of mechanosensitive ion channels. These findings not only advance our understanding of fundamental biological processes but also offer promising avenues for the development of innovative therapeutic biological tools.

Zusammenfassung

Mechanosensoren spielen eine entscheidende Rolle bei der Umwandlung physikalischer Reize in chemische Signale, steuern zahlreiche biologische Prozesse und dienen als Angriffspunkte für verschiedene Krankheiten. Es besteht ein Bedarf an präziser und ferngesteuerter Kontrolle über mechanosensitive Ionenkanäle. In dieser Arbeit haben wir ein einfaches Referenzsystem für solche Ionenkanäle konstruiert. Dafür haben wir den mechanosensitiven Ionenkanal mit großer Leitfähigkeit, MscL, in einer Doppelschicht rekonstruiert. MscL ist ein Kanal, der ausschließlich durch die Membranspannung gesteuert wird. Die Membranspannung wird in diesem Fall über ein photoschaltbares Lipid, welches ebenfalls in der Membran eingebaut ist, gesteuert. Bei dem Lipid handelt es sich um AzoPC, einem Phospholipid mit einem substituierten Azobenzol. Wenn AzoPC mit blauem oder UV-Licht beleuchtet wird kann es zwei verschiedene Konformationen annehmen, die Druck oder Spannung in der Membran erzeugen. Die Umwandlung des Photolipids von Licht in Spannung wurde in der Monoschicht auf einem Langmuir-Blodgett-Trog untersucht, während die strukturellen Umorientierungen während des Lichtwechsels mit Hilfe der polarisierten FTIR-Spektroskopie analysiert wurden. Eine DFT-Simulation von AzoPC half bei der Zuordnung der charakteristischen Absorptionsbanden und bei der Interpretation der in den Lipiden auftretenden Umorientierungen. MscL wurde in einer freistehenden Doppelschicht, in einer Multilayer, in Liposomen und in Nanodiscs mit AzoPC rekonstituiert. Die Reaktion des Ionenkanals auf lichtinduzierte Spannung wurde mit FTIR-Spektroskopie beobachtet, wobei eine deutliche reversible Bewegung im Proteingerüst festgestellt wurde. In der schwarzen Lipidmembran konnte MscL in einen subkonduktiven Zwischenzustand gebracht werden. Durch die Kombination von Rheologie und spektroskopischen experimentellen Techniken sowie funktionellen Tests liefert diese Arbeit die Grundlagen für die lichtinduzierte Modulation von mechanosensitiven Ionenkanälen. Diese Erkenntnisse bringen nicht nur unser Verständnis grundlegender biologischer Prozesse voran, sondern bieten auch vielversprechende Möglichkeiten für die Entwicklung innovativer therapeutischer biologischer Werkzeuge.

Publications related to this thesis:

- F. Baserga, A. Vorkas, F. Crea, L. Schubert, J. L. Chen, A. Redlich, M. La Greca, J. Storm, S. Oldemeyer, K. Hoffmann, R. Schlesinger, J. Heberle (2022). "Membrane Protein Activity Induces Specific Molecular Changes in Nanodiscs Monitored by FTIR Difference Spectroscopy." *Frontiers in Molecular Biosciences*, 602.

- F. Crea, A. Vorkas, A. Redlich, R. Cruz, C. Shi, D. Trauner, A. Lange, R. Schlesinger, J. Heberle (2022). "Photoactivation of a Mechanosensitive Channel." *Frontiers in Molecular Biosciences*, 676.

- M. Aleksanyan, A. Grafmüller, F. Crea, V. N. Georgiev, J. Heberle, R. Dimova. "Modulating membrane shape and mechanics of minimal cells by light: area increase, softening and interleaflet coupling of membrane models doped with azobenzene-lipid photoswitches." (*in preparation*)

Contents

Forces mediate all physical interactions. Mechanical forces are the most commonly experienced at all life scales. From the paramecium to the blue whale, the ability to sense mechanical forces was developed as a way to survive, develop and exchange information.

1.1 Mechanobiology and mechanosensors

Understanding mechanosensation and mechanotransduction, the mechanisms by which a cell senses a mechanical stimulus and then translates it to a different signal, is of utter importance in all branches of biology. Gene expression, homeostasis and secretion, morphogenesys and embryogenesis, movement, proprioception, the senses of touch and hearing are all strongly dependent on sensing mechanical forces.[1–6] The field of science which investigates the action of mechanical forces on cells is commonly referred to as mechanobiology.[7,8]

In the membrane of eukaryotes and prokaryotes, mechanical stress is sensed by mechanosensitive ion channels.[9] These are integral membrane proteins that can open or close a channel across a membrane and whose state and conductance is regulated by tensions and pressures. Some criteria have been proposed to help classify mechanosensitive ion channels: 1) the protein should be required for a response to a mechanical stimulus, 2) it should be expressed in a mechanosensory organ, allowing for mechanosensation, 3) in knockout mutants, cells or organisms where the genes for protein expression are either silenced or removed, loss of sensory function should be observed, 4) the mechanical response should be altered by mutations that change the channel properties, 5) the response to mechanical stimuli should be proven in heterogously expressed

proteins.[10,11]

These criteria are only meant to be an indication and not as strong constraints for classification, as many channels do not fulfill all five criteria but are nonetheless considered mechanosensors. Furthermore, several other families of ion channels show mechanosensitivity to some degree, although not as the main trigger; for example the large family of transient receptor potential (TRP) channels, which respond to a large variety of stimuli such as light, temperature, pH and ligand binding, or the two-pore domain thermosensitive TREK/TRAAK potassium channels.[12,13]

1.2 Force-from-lipids principle

The way the tension acts upon the protein structure can vary widely depending on the protein architecture, but a main distinction can be drawn between two categories: gating mechanisms that require an involvement of the extracellular matrix or the cytoskeleton, usually referred to as tethered models, and gating mechanisms, typical of bacterial mechanosensors, that can be triggered solely by membrane tension.[13] In this second class of mechanisms, the force acts *via* the lipids onto the protein without the intermediation of any other cellular component[9,12,14] and the model is often referred to as the "force-from-lipids" model.[15]

MscL as a benchmark protein

Due to the simplicity of its activation mechanism, the class of ion channels that do not require any additional molecular machinery to be gated is of high interest in the perspective of protein re-engineering and medical applications. Among those ion channels, the Mechanosensitive Ion Channel of Large conductance, MscL, first isolated by Boris Martinac and colleagues from the *E. coli* plasma membrane,[16] but with several homologous channels in other bacteria,[17,18] has been adopted as a benchmark protein for the study of tension-gated mechanosensors.[14,19] MscL requires a single gene, *mscl*, to be expressed[20] and it is gated purely by a change in lateral pressure in the bilayer.[21]

The force-from-lipids theory was indeed born out of research on MscL: Martinac had observed that this mechanosensitive ion channel could be activated by addition of amphiphilic molecules to the bilayer, therefore indicating some relevance of the protein-lipid interaction to the gating mechanism.[22] The fact that the response of MscL to mechanical stress could also be observed in reconstituted systems confirmed that no other molecular machinery or cellular component is needed for the activation of the channel.[20,23] The reconstitution of functional MscL in a bilayer of specific lipid composition, either in standard

liposomes[23–26] or in more recently developed droplet interface bilayers[27,28] and droplet hydrogel bilayers,[29] is now a common sample preparation for the study of this protein.

Mechanics of membrane pulling

But how are the lipids exactly acting on the ion channel in order to gate it? Non-mutually exclusive hypotheses have been proposed.

First, a strong interaction between some lipids and part of the protein could be maintained while the bilayer tension increases, therefore the movement of the lipids would directly induce a conformational change in the protein. This seems to be the case for the N-term helix in MscL, which has been suggested to strongly interact with some acyl chains from the membrane. The lipid tails protruding into a protein cavity are effectively moving the helix when tension is applied.[30–32] This principle extends to other mechanosensors as well, such as the smaller conductance mechanosensitive ion channel MscS, but also the Piezo channels.[31,33]

A second idea is that the conformational change induced in the protein is a consequence of the deformation of the membrane annular lipids, those in close proximity to the protein. A change in membrane tension results in a thinning or thickening of the bilayer. Upon stretching, the membrane thickness decreases and hydrophobic transmembrane regions of the protein get exposed to the acqueous environment. This results in a hydrophobical mismatch between the bilayer section and the protein surface that are in contact. The consequent change in the force vectors of the lipid-protein interaction induces then the structural rearrangement in the protein.[34] The hydrophobic mismatch contribution to gating is substantiated also by the fact that the thickness of the bilayer influences the open probability of MscL, whose curve is shifted towards lower pressures when reconstituted in shorter acyl chain lipid membranes.[35]

The MscL activation from the membrane therefore lies with the interplay of hydrophobic mismatch and pulling forces acting on the protein, arising from strong and long lasting lipid-protein interactions.[32]

1.3 MscL structure and gating mechanism

In 1998 a pentameric structure of the closed state was resolved for *Mycobacterium tuberculosis* MscL[18], revised in 2007[36] (Figure 1.1), then in 2009 a tetrameric structure was published for *Staphylococcus aureus*[37] MscL. There is still no observed structure for the *Escherichia coli* MscL, but all known homologues share highly conserved sequences that are compatible with the
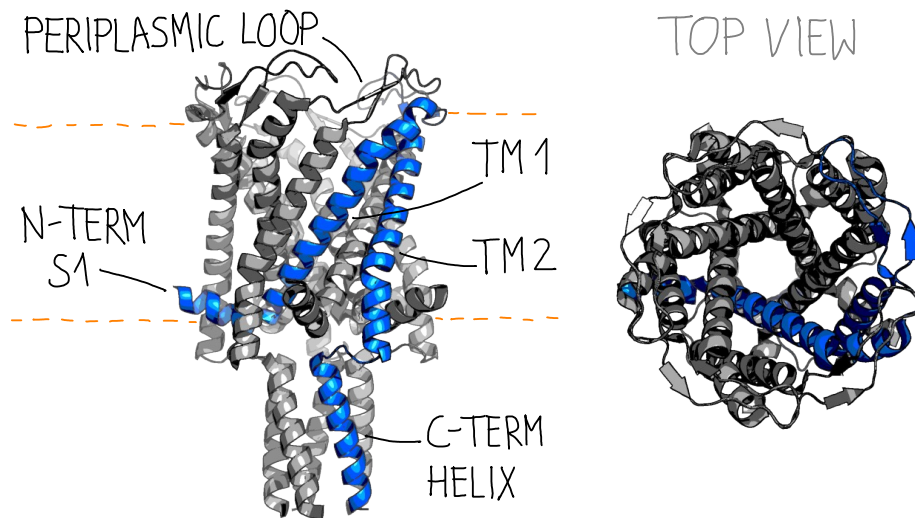
FIGURE 1.1: Structure of *Mycobacterium tubercolosis* MscL (PDB ID: 2OAR). A single monomer is colored in blue. TM: transmembrane helix domain, N-TERM: N-terminus, C-TERM: C-terminus.

topology of the known structures: two transmembrane (TM) helices connected by a periplasmic loop, a cytoplasmic helix at the C-terminus and a shorter helix at the N-terminus.[17,18,38,39]

Mutagenesis has had an impact in understanding the role of specific amino acids in the gating and in the relationship between the ion channel and the lipids of the bilayer. Together with the action of the lipid membrane on the protein outer surface just described, the intra-protein interactions between some internal residues were found to be also crucial for the gating of MscL. Here I will present the latest model of MscL gating, based on the available structures, the homology models of *Escherichia coli* MscL, the experimental evidence collected mostly from mutagenesis and the *in silico* simulations.

Topology

Prior to the first X-ray crystal structure of MscL much information could already be inferred from other techniques. H/D exchange showed that two thirds of the ion channel are water accessible.[40] From PhoA fusion, it was discovered that this protein has two transmembrane (TM) domains,[41] confirmed to be α-helices from CD spectroscopy,[40] and that both the C-terminus and the N-terminus were on the cytoplasmic side.[41,42] A working topologic model of a MscL monomer (Figure 1.2) was then available.[41]
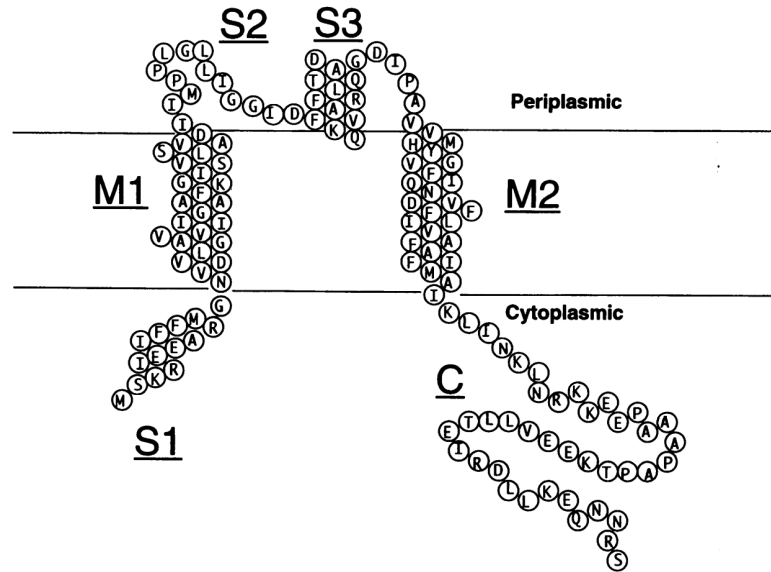
FIGURE 1.2: Topology model of *E. coli* MscL, adapted from the first one published by Blount *et al.*[43]

The extramembrane domains

The relevance to the gating of the S1 subdomain at the N-terminus had been identified early: by adding amino acids to the N-terminus the activity of the ion channel was unchanged, but its gating properties were altered in case of deletions or substitutions.[44] In particular, a deletion of three amino acids ($\Delta 2$ - 4) didn't have any effect, but a deletion of eleven ($\Delta 2$ - 12) meant a complete loss of function.[43,44]

Although already suspected from the amphipathic nature of its sequence, the secondary structure of S1 could only be shown to be α-helical after a revision of the first crystal structure,[36] where initally this segment was not clearly resolved. It was first hypothesized that, in the oligomeric form, these helices would form a bundle and constitute a cytoplasmic gate.[45–47] This was part of the first gating mechanism proposed, known as the Sukharev-Guy model.

After the revision, the currently accepted position for the N-terminal helix is parallel to the bilayer. This position and the helix sliding movement along the cytoplasmic membrane during channel opening were proposed after a thorough investigation focused on the N-terminus which adopted several methods: cysteine scanning, *in vivo* functional characterization, *in vivo* substituted cysteine accessibility method, electrophysiological studies, and disulfide-trapping experiments.[48] Combining evidence from EPR data, FRET data and simulations, the N-term helix was identified as a stabiliser for the TM1 domain in the

closed state and as a pulling element crucial to the gating, strongly interacting with the lipids of the bilayer on its hydrophobic side.[30,49,50]

The C-terminus function is still not completely clear. In the oligomeric state, the C-terminus helices form a bundle.[51] A study which combines EPR data and MD simulations of *E. coli* MscL demonstrates that only the residues from A110 to E118 dissociate when the channel opens.[52] Deletion of 27 terminal amino acids (Δ110-136) does not impair *E. coli* MscL function,[43] but deletion of 33 (Δ104-136) does.[44] Indeed the RKKEEP sequence that makes the difference, a charged cluster at the base of the TM2 domain, must be necessary to the channel opening.[44] An influence of cytoplasmic pH on the C-term helical structure was observed: different proton concentrations determined a shift in protein sensitivity to the triggering lateral pressure, effectively highlighting the RKKEE cluster as a pH sensor.[53]

For the *M. tubercolosis* homologue, in total absence of the C-terminal domain (cutting after G101, corresponding to E107 in *E. coli*) the functionality is preserved, although with some sensitivity differences and the oligomeric state is a pentamer,[54] whereas C-terminal deletions in *E. coli* MscL seem to result in different distributions of oligomers.[55] The incomplete picture of the cytoplasmic helix function suggests a role of oligomer stabilisation element. Since the conductance of the channel can be modulated by changing the length of the linker between TM2 and the cytoplasmic bundle, a function of molecular sieve has also been proposed.[51,56]

The other extramembrane domain is the periplasmic loop that connects TM1 to TM2. Enzimatic cleavage of this loop does not impair protein function,[57] indicating little involvement in channel activity, but selective mutations at the rim of the funnel on the periplasmic side create loss-of-function variants.[58] Expression of the TM domains separately produced a gating channel with increased pressure sensitivity,[59] hinting to a regulatory function of the loop to the mechanosensation. This was later confirmed by a study on chimeras where it was shown that exchanging I49 and F47 from the loops of *E. coli* and *S. aureus* MscL could change dwell times and that the F47L *S. aureus* mutant would lead to hysteresis in the opening/closing of the channel.[60] A shifted sensitivity is observed also for Q56 mutants, a residue of the loop.[43] These findings suggest for the periplasmic loop the role of a spring.

The iris model

MscL has a huge single channel conductance of 3.8 nS.[61] Since there is no structure available for the fully open state, the pore dimensions were investigated with molecular sieving experiments and with FRET spectroscopy. The FRET data on the pore size suggest a pore larger than 25 Å,[62] confirming the

EPR based simulation of the open structure;[34] varying sizes of poli-L-lysines were transferred through the pore, resulting in an estimated diameter of 37 Å.[61] Among the proteins successfully transferred, the highest molecular weight was that of the fluorescently labelled bovine pancreas trypsin inhibitor, which is 65kDa.[63]

The pore is lined mostly by the TM1 helices,[34,62] which indeed seem to play a major role in the gating. Through random mutagenesis, the actual gate of the channel was identified around residue G22, in the lower part of TM1.[64] When the cluster of hydrophobic residues around that position gets exposed to water, the opening is initiated.[65] Variants of MscL where G22 is mutated to more hydrophilic residues have a lower energy barrier to the channel opening, *vice versa* variants with hydrophobic substitutions require an increased tension to gate.[66]

The mutation G22C has therefore been exploited to locally bind methanethio-sulfonates, positively or negatively charged, to gate the channel in absence of tension.[67] Another glycine close to the pore constriction, G26, has also been proven a good site for the same modifications.[68] Altered gating properties as a consequence of mutagenesis in TM1 indicate this transmembrane helix as highly relevant to the gating.[34,49,62] Many other residues were screened by random mutagenesis. The involvment in the gating of mutated residues was evaluated on the 408 MscL variants by their osmotic downshock curves, revealing a library of gain-of-function as well as loss-of-function variants.[69]

The consensus on the gating mechanism of MscL is that, when tension is applied to the membrane, the lipids start pulling on the S1 domain. The S1 helix is anchored to the membrane and, as it moves, it pulls on the base of the TM1 helix.[30,48–50] Intermediate states have been hypothesized, where the channel has changed conformation, but does not yet gate.[45–47] In particular, it is possible that an expanded non conducting state would allow a change of hydrophobicity at the gate, disrupting interactions in the pore and allowing then for complete opening.[65] There are indications that the movement of the TM1 helix is a combination of a tilt and a twist, which collectively results in a lateral expansion and a thinning of the protein and the adjacent lipids, opening a pore similarly to a camera iris.[30,34,48,70,71]

Stoichiometry

Initially, since a fusion protein consisting of two MscL channels expressed in sequence was proven to be conducting, it was hypothesized that the ion channel would be composed by an even number of subunits, in particular a hexamer, as it seemed from the oligomer molecular weight.[41,42] The oligomerization state of MscL has then been observed to be by far mostly pentameric *in vivo*, but it

could range from tetrameric to hexameric *in vitro.*[38,72,73]

1.4 Azobenzene switches and the photo-switching of lipid molecules

Azobenzene is a photoswitchable molecule composed of two phenyl rings bound to an N=N bond. It has two metastable states, the *trans* and *cis* state. The *trans* state is the lowest in energy and it can be switched to *cis* with UV illumination. The reversed transition can either be induced thermally or *via* blue light illumination.[74,75] The azobenzene chemical structure is shown in the upper half of Figure 1.3.
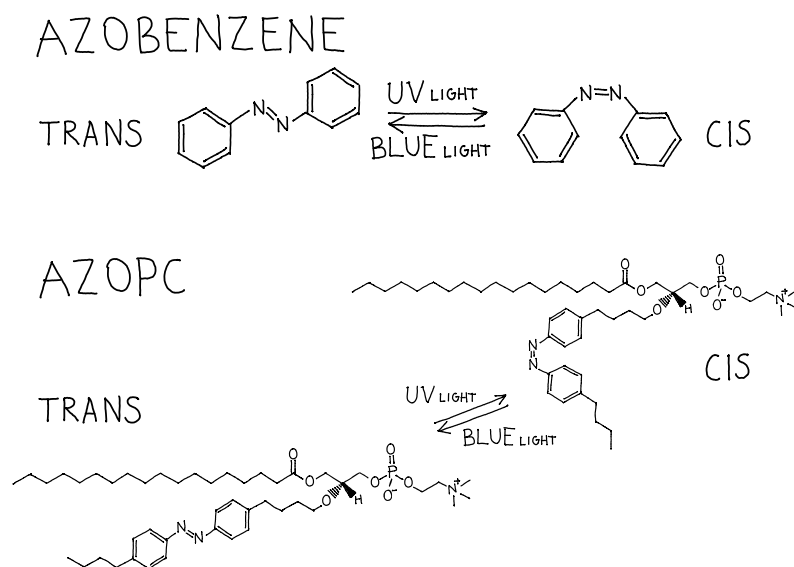
FIGURE 1.3: Chemical structure of azobenzene in its two isomeric states and of an AzoPC lipid molecule.

This reversible molecular switch is used to make all kind of biological molecules light sensitive: from peptides and proteins to nucleic acids and oligonucleotides. Carbohydrates and lipids have also been a target of modifications to make them photo-switchable. A vast collection of azobenzene-modified photosystems has been amassed and reviewed.[74,76,77] Combining photo-switches with lipids can result in a high time/space resolution in controlling membrane properties, lipid binding to specific receptors, and modulation of protein activity.[78]

We focused on a glycerophospholipid developed and synthesized by the Trauner group from New York University, called AzoPC (its structure in the lowest half of Figure 1.3). Based on the natural lipid 1,2-distearoyl-sn-glycero-3-phosphocholine (DSPC), it has an azobenzene substituted in the *sn*-2 alkyl chain, between carbons C5-C14.[79] Its phosphatidylcholine (PC) headgroup is compatible with MscL, as we know from previous reconstitution experience.[23,80] A membrane containing AzoPC modifies its properties upon light illumination: switching between blue and UV light changes the morphology of vescicles, inducing budding, pearling and the genesis of tubes,[79] it affects lipids organization and domains formation when in mixtures,[81] and it influences diffusion and membrane thickness.[82] The light-induced changes occurring in an AzoPC membrane can be used to influence protein activity, shown recently by Doroudgar *et al.* with *E. coli* diacylglycerol kinase, as a proof-of-principle.[83]

In order to keep the pushing/pulling forces developed by the bilayer upon isomerization of the *azo*-lipids, a rigid boundary condition is needed. Some sort of constraint not yet quantified is offered by a nanodisc assembly. These structures are small patches of lipids, between 100 and 200 lipid molecules or the amount needed to surround a membrane protein, encircled by a membrane scaffold protein (MSP). These are helical proteins that, depending on their length, determine the exact size of the nanodisc (in a range of 10 to 20 nm in diameter).[84]

Nanodiscs have seen an exponential increase in use in the last ten years[85] and not without reason: they turned out to be an extremely valuable tool in the study of membrane proteins.[86,87] They offer a way of solubilizing membrane proteins, while reconstituting them in a close-to-native environment.

A previous attempt at testing the constraining properties of nanodisc structures to lateral pressure in the membrane was reported in the past, but with a much different system.[88] The nanodiscs were bound by styrene-maleic acid, a polymer instead of a MSP, and the lateral pressure in the membrane was exerted by a lipid-like compound containing azobenzene, far from an actual lipid molecule. The ability of these molecules to switch in the enclosed environment was confirmed, but no quantitative measurement on the developed lateral pressure was considered.

1.5   Photo-activation of a mechanosensor

The idea at the base of this thesis is to investigate the properties and characteristics of a photoswitchable lipid molecule, AzoPC, with the specific perspective of using the change in lateral pressure, occurring in an AzoPC-containing

membrane upon light illumination, to gate mechanosensitive proteins.

Thanks to its large pore and conductance, MscL has been early identified as a good candidate for a nanovalve and a target for molecular engeneering. Methods that have been explored to control its activity until now comprise ultrasound and light. With ultrasound, it is possible to activate MscL reconstituted in liposomes,[89] expressed in neuron cells *in vitro*[90] and *in vivo* in mice[91]. Light-activation was developed by the Koçer group, *via* an internal ligand that changes its charge upon photolysis, inducing reversible channel opening.[92–94]

A precursory attempt at gating MscL with light by photoswitching the membrane was done using a light-sensitive pseudolipid and *L. lactis* MscL years ago. There they could show activity from the ion channel by measuring single channel currents in patch clamp,[95] but that research has then been discontinued.

With the advent of newly synthesized photoswitches, the remote activation of mechanosensors with light became a possibility again. In the context of photopharmacology, combining a photoswitchable membrane with MscL can provide a powerful tool for precise and localized control of membrane tension and transport processes.

First, the ability of the photolipids to induce a change in the lateral pressure upon illumination was tested. This was measured for an AzoPC monolayer in a Langmuir-Blodgett (LB) trough. The lipids have then been observed switching in the IR, to characterize their changes in the vibrational spectrum. To combine these two methods, InfraRed Reflection Absorption Spectroscopy (IRRAS) was applied to AzoPC.

Later on, the mechanosensor was reconstituted in various lipidic systems containing the photoswitchable PC lipid and the effects of light switching on the protein were observed. To give a constraint to the forces developed by the switching of the photolipids, MscL was moved into nanodiscs. We confirmed the functionality of MscL in a membrane containing AzoPC with electrophysiology on a free standing bilayer. As an additional functional test, a standard calceine efflux assay on liposomes has been adapted for our photo-activatable system.

This thesis is structured traditionally: what follows this Introduction is a Materials and Methods chapter where all details of the conducted experiments are reported, having in mind that other people will continue to work on this project, and a rather dry description of the methods, necessary to the understanding of the Results and Discussion chapters that follow. The Results chapter is divided into two parts: a first one on the photolipids only

and a second one focusing on the protein. The Discussion chapter combines all collected information from the various methods to convey the core findings of this work. A Conclusions chapter briefly sums up the content of this thesis and offers some directions for future development.

The line of thought that guided me during this work, and that I would like to guide the reader as well, is sketched in Figure 1.4.
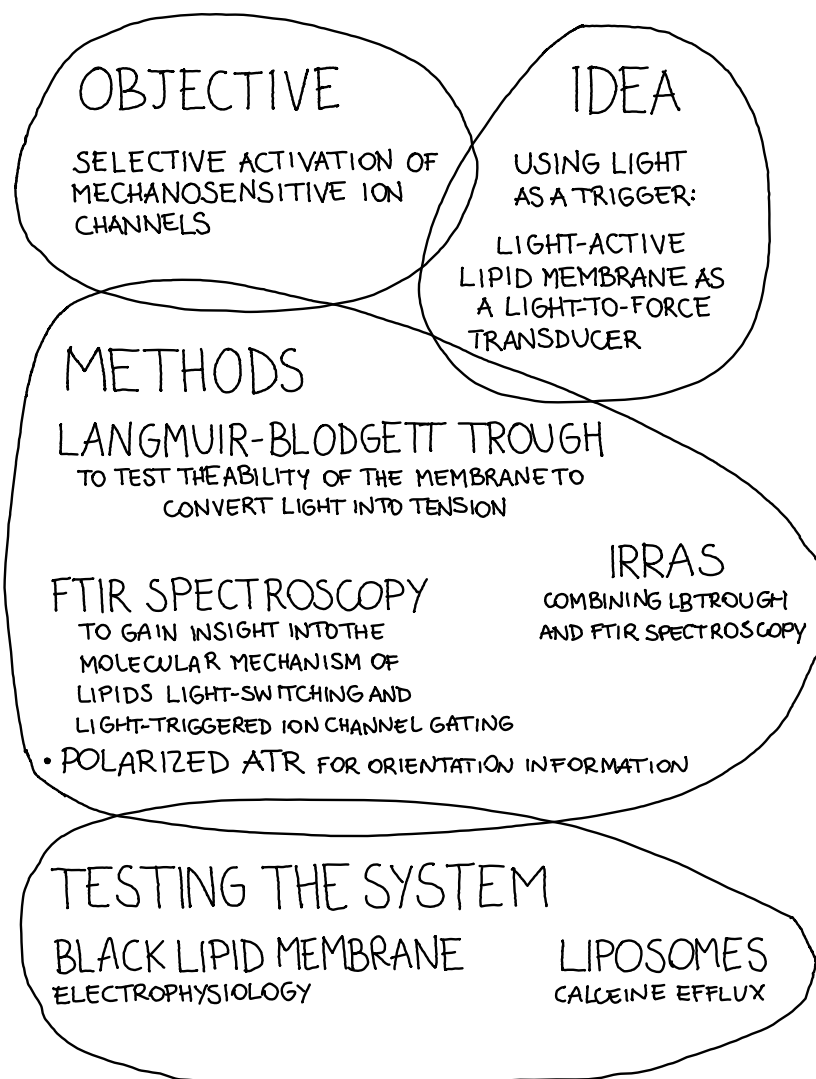

FIGURE 1.4: Schematic representation of the approach adopted to investigate the photo-activation of MscL *via* AzoPC lipids.

2.1 MscL sample production

The protein sample used in this work has been systematically produced in the genetic laboratory of Dr. Ramona Schlesinger, Freie Universität Berlin. With the help of the technical assistants Dorothea Heinrich and Kirsten Hoffmann, we adapted the protocol from Prof. Boris Martinac[25] to the laboratory's well established protocol for membrane proteins expression in *E. coli*. Initially, I have been expressing and purifying the protein myself, whereas, since July 2019, my colleague Antreas Vorkas, from the group of Dr. Schlesinger, has been providing me with the purified sample in detergent or reconstituted in nanodiscs. The methods to express, purify and then reconstitute in lipids MscL are explained in detail in the following sections.

2.1.1 MscL expression and purification

Expression

The *mscl* gene for the wildtype was generously provided by the research group of Prof. Adam Lange, Leibniz-Forschungsinstitut für Molekulare Pharmakologie. Another gene of the G22C F90W mutant was kindly given to us by the research group of Paula Booth, King's College London. In both cases the primary structure of both genes has been confirmed by sequencing before expression.

The dYT culture medium for the *E. coli* cells is prepared with 160 g of tryptone, 100 g of yeast extract and 50 g of NaCl each 10 L of water and then it is autoclaved to exclude any contamination. Usually starting with a total of 12 L of dYT liquid cell culture medium, the procedure that follows would

be done in parallel on 6 equal batches, resulting in about 10 mg of protein in total at the end of the purification.

To start, 1 µL of the plasmid containing *mscl* is inserted into 50 µL of thawed competent cells (strain BL21-CodonPlus(DE3)-RP) *via* electrotransformation, followed by the immediate addition of 1 mL of Brain Heart Infusion (BHI) medium. The solution is left shaking at 37°C for one hour. It is then centrifuged at 7000 g for 2 minutes, 300 µL of the supernatant are discarded, the pellet is resuspended in the remaining solution and then deposited on an agar plate for overnight incubation at 37°C. The agar plates had been previously prepared with BHI agar and 1 µL/mL ampicillin, an antibiotic. The plasmid used to deliver *mscl* contains an ampicillin resistance gene to select for the MscL-expressing *E. coli* cells.

The following day, the cell culture is scratched from the agar plate with the help of about 30 mL of dYT medium and distributed in four flasks. Each flask contains about 0.5 L of dYT medium and 500 µL of additional ampicillin. The flasks are then left on the orbital shaker at 37°C. The optical density at 600 nm (OD_{600}) can be used to qualitatively track the growth of the cellular population. In this case the initial value of OD_{600} is between 0.15 and 1.20. When after 2-3 hours an OD_{600} of 0.9 is reached, the expression is induced by the addiction of 100 µL of 1 M isopropyl -d-1-thiogalactopyranoside (IPTG). IPTG is a non-metabolic mimic of lactose that binds to the lac repressor, which otherwise inhibits, by binding to the lac operator, the transcription from the RNA polimerase of the target gene. After 3 hours the culture is centrifuged at 8000 g for 15 minutes at 4°C and then the supernatant is discarded. The pellet is then resuspended in PBS buffer at pH 7.2, using about 1 mL of buffer per gram of cells, and left overnight at -20°C.

The third day the cells get broken with a cell disruptor at 1.7 kbar for two times. Cell lysis can be qualitatively checked under an optical microscope. Protease inhibitors, 1 mL of phenylmethylsulfonyl fluoride (PMSF) from a 20 mg/mL solution, is added to prevent protein degradation after cell lysis. A tip of a spatula of DNase is also dissolved in the mixture to degrade the DNA content. The cell lysate is centrifuged at 8000 g for 30 minutes at 4°C to remove debris. The collected supernatant is then ultracentrifuged at 186000 g for 4 hours at 4°C. The supernatant is then discarded and the pellet is resuspended in about 100 mL PBS buffer in a glass homogenizing potter. To solubilize the membrane proteins a detergent, n-Dodecyl -D-maltoside (DDM), is added to a final concentration of 2 % w/v and the mixture is left to stir overnight at 4°C.

Purification

The expressed MscL is already tagged at the C terminus with an His-Tag, a sequence of several histidines, which has a strong affinity to nickel. The purification is therefore performed by running the solution containing the DDM-solubilized protein through a column filled with nickel-chelating nitrilo-triacetic acid (Ni-NTA) agarose resin. First the target proteins will bind to the column, while all the rest will run through the column and be discarded. The His-tagged proteins gets then eluted by a continuous gradient of imidazole, a competitor to His-tags, and retrieved. The whole process is run in the ÄKTA pure, an automated chromatography maschine.

Two buffers are prepared: PBS buffer with 1 mM DDM and PBS buffer with 1 mM DDM and 500 mM imidazole, both at pH 6.7. The Ni-NTA column volume amounts to 10 mL. Initially the column is equilibrated with the imidazole-free buffer for several cycles, then the sample is loaded completely onto the column. The column is first washed with 70 mL of imidazole-free buffer, to remove everything not binding to the column. Then for the elution, the ÄKTA mixes the two buffers in order to linearly increase the imidazole content of the eluting solution from 0 to 500 mM for a total of 600 mL.

During elution it is possible to track the absorption of a specific wavelength to look for the fraction containing the protein. The wavelength is usually set at 280 nm, the absorption maximum of tryptophan, unless otherwise determined by the presence of a chromophore. Unfortunately wildtype MscL does not contain any tryptophan residue, the absorption of the other aromatic amino acids (10 phenylalanines and 1 tyrosine per monomer) is too low to be detected, as it is also the case for the G22C F90W mutant, therefore all eluted samples are collected. Test samples from all fractions are let run on a sodium dodecyl sulfate - polyacrylamide gel electrophoresis (SDS-PAGE) to look for the presence of MscL. A band corresponding to the monomeric molecular weight of MscL, about 16 kDa, appears in all eluted samples starting from an imidazole concentration of 180 mM. All eluted fractions showing a strong band for the MscL monomer are then combined. For an example of a typical chromatogram and SDS gel, see Appendix A.1.

To store the protein and before any reconstitution in lipids, the amount of DDM is lowered to its critical micellar concentration (CMC), the minimal amount of detergent in solution that still allows it to condensate in micelles. For DDM this value is 0.17 mM in standard conditions (in water, at room temperature), but can be lower in the presence of salts. To partially remove the detergent the protein sample is put in a 30 kDa amicon filter tube, PBS buffer without DDM is layered on top and the tube is centrifuged. This procedure washes as well the imidazole.

Quantification of protein sample

Since MscL is transparent to UV-visible light, direct spectroscopic methods commonly adopted for the quantification of protein yield cannot be used, but other methods can be applied instead.[96] For the time I have been expressing and purifying MscL, the Bradford assay[97] has been used. It is based on the absorption of a dye (Coomassie Brilliant Blue G-250) that can bind unselectively to the protein backbone. The unbound dye has an absorption maximum at 465 nm, while the bound form at 595 nm. A calibration curve is recorded with bovine serum albumin (BSA) for a range of known concentrations around the expected value for the concentration of MscL: samples of equal volume (100 µL) containing different amounts of BSA, the one with MscL and a control of PBS buffer are stained with the same amount of dye (5 mL) and left to react for 15 to 30 minutes (no significant difference is observed after the first 15 minutes). The OD_{595} is then plotted against protein concentration for the BSA samples and the resulting curve can be used to estimate the concentration of MscL, given its OD_{595}.

Antreas Vorkas has used a Lowry assay instead. Although based on a different reaction, the protein concentration is still determined by photometry, in this case at 750 nm, in comparison to a BSA calibration curve. The Lowry calibration curve and the MscL data for all expressions are reported in Appendix A.2. A usual round of MscL production, starting with 12 L of liquid growth medium, yields about 10 mg of purified protein.

2.1.2 Reconstitution into lipid membranes

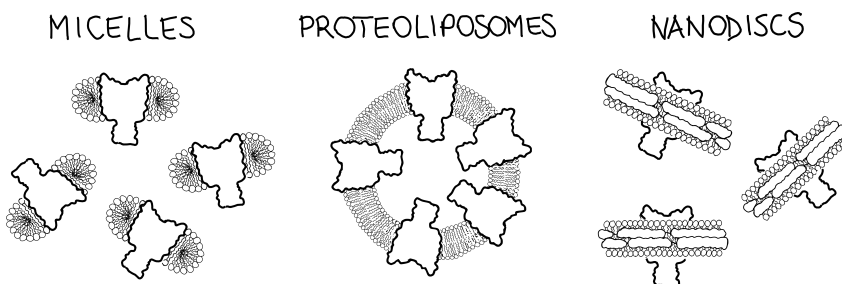FIGURE 2.1: MscL reconstitution in lipids. Illustration of the three forms of lipid reconstitution used in this work. In micelles the hydrophobic portion of the protein is covered by a belt of lipids, making it soluble. Proteoliposomes are vescicles where the ion channel is embedded in the bilayer. Nanodiscs are portions of bilayer surrounding the target protein, held together by scaffold proteins.

The physiological environment of MscL is the lipid bilayer of a bacterial plasma membrane. After solubilization, the protein is surrounded by a belt of detergent and immersed in 1 mM DDM. In order to reconstitute it into a lipid membrane, the detergent has to be removed and substituted with lipids, without inducing protein aggregation and precipitation. Several are the methods developed to achieve that.[98,99] Depending on the experiment, the requirements for the preparation might differ. For example in a spectroscopic experiment it is important to maximise the protein:lipids ratio, and this is best achieved with micelles rather than with liposomes. In turn, liposomes are essential if an efflux assay has to be run. The preparations that follow are the basic protocols of reconstitution commonly used in our lab and necessary to the experiments of this work: recostitution in micelles, liposomes and nanodiscs[84] (in figure 2.1 an illustration). They have been developed by merging literature evidence, colleagues' experience and trial and error.

Micelles

The protein:lipids ratio chosen for the preparation of micelles is 1:200 in moles for a pentameric oligomer of MscL (which then equals 1:40 per monomer).

The desired amount of lipids is dissolved in chloroform, then deposited at the bottom of a glass vial and the solvent is evaporated by putting the vial under 50 mbar of vacuum. The amount of chloroform is not relevant, but indicatively the concentration of the lipids in chloroform solution is in the order of 1 mg/mL. The larger the volume to be evaporated, the longer the vial is left under vacuum: after the liquid chloroform is not visible anymore and the bottom of the vial is at room temperature again - it cooles down due to evaporative cooling during evaporation of the chloroform - the sample is still left under vacuum an additional time of 30 minutes to make sure of complete solvent depletion.

On top of the dry lipid film, the PBS buffer, pH 7.2, is added to the vial, to a final concentration of lipids in buffer of 2 mg/mL. The closed vial is then sonicated in a water bath sonicator until the sample looks turbid but homogeneous. The sonication helps the dry film to get first swollen and then to get into solution in the form of multilamellar vescicles.

MscL in detergent is added to match the desired protein:lipids ratio and is left shaking for 1 hour at room temperature. During this time the detergent and the lipids should be mixing, competing in the interaction with the protein. Afterwards, a tip of a spatula of biobeads, polisterene macroporous beads that adsorb detergent molecules, is added to the solution and the sample is put on a shaker at 4°C. After 2 hours another slightly larger amount of biobeads

is added and the sample is left on the shaker overnight. The next day, the detergent molecules have been removed by adsorption to the biobeads and lipid molecules have substituted them around the proteins. The solution can be removed from the biobeads sucking it up with a pipette with a fine tip and can be used.

Large unilammelar vescicles (LUVs) and proteoliposomes

To prepare liposomes, the desired amount of lipids in chloroform are deposited in a round-bottomed flask. The solvent is evaporated under vacuum (50 mbar) during rotation of the flask in rotary evaporator. Starting from atmospheric pressure, the 50 mbar vacuum is reached in about 5 minutes, lowering the pressure gradually to avoid the boiling of the chloroform solution. The flask is also partially immersed in a water bath at 40°C, which avoids the lipids to go below the phase transition temperature as the sample cools down due to the evaporative cooling of the solvent removal. Infact, if the dry lipid film is formed when the lipids are undergoing a phase transition or are in the solid phase, the successfull liposomes preparation is compromised. For a usual amount of 1 mg of lipids in 1 mL of chloroform, the rotary evaporation is run for 1 hour. The dry lipid film is also known as "lipid cake", as it is composed of a multiple layers of lipids ordered in bilayers.

PBS buffer is added to the flask to a lipid concentration of 2 mg/mL. To help the formation of unilamellar vescicles of lipids in buffer, the sample is undergoing several (5 to 10) cycles of freeze-thawing. This is accomplished by immersing the flask in liquid nitrogen, waiting for the solution to be completely frozen, and then immersing it in a stirred water bath at 40°C. When thawed, the sample is shortly vortexed and the freeze/thawing cycle is started again. Both AzoPC and DSPC might not get homogeneously into solution, appearing as flakes even after the 10th cycle. Then the sample gets sonicated with a tip sonicator, which ensures unilamellar vescicles in solution. To select for a distribution of sizes around a specific value, in this case 100 nm, the unilamellar vescicle solution is filtered with an extruder (7 to 13 cycles). The turbidity of the solution should visibly decrease over the extrusion cycles, finally becoming very clear.

To reconstitute MscL in the membrane of the LUVs, the same protocol as for the micelles is followed, but necessarily the protein:lipids ratio has to differ and a 1:500 molar ratio (for the pentameric oligomer, corresponding to 1:100 for the monomer) is adopted in our case. A lower lipid content does not allow for stable proteoliposomes. The correct relative amount of MscL in DDM (at CMC) is added to the LUVs solution, it is left for 1 hour shaking at room temperature and then the biobeads are added in two steps while shaking at

4°C overnight.

Nanodiscs

The reconstitution of MscL in nanodiscs was done by Antreas Vorkas, who provided me with the readily reconstituted sample in PBS buffer. The procedure to prepare it can be breafly described as follows: detergent solubilised MscL, MSP1D1 scaffold proteins and lipids get mixed in molar ratio 0.5 : 1 : 50 for 1 hour a 25°, then the detergent is removed with the help of biobeads during another hour at 25°. Finally, the sample is run through size exclusion chromatography and the wells where the elute absorbs at 280 nm are collected. We remind the reader that this absorption comes from the scaffold proteins, since MscL does not show any visible absorption (*cf.* "Quantification of protein sample" in the previous section). In order to confirm both the presence of MscL and the scaffold proteins, the sample is checked with an SDS-page.

The result of this preparation are nanodiscs: circular patches of lipidic bilayer containing one MscL protein. These patches are surrounded by α-helical scaffold proteins that run around the circumference. From the molar ratio of the protocol, about 100 lipids are expected to surround the membrane protein. Since the sample has been also submitted to cryo electron microscopy by Antreas Vorkas, the size has been confirmed to be about 10 nm in diameter and 5 nm in thickness. For the control measurements the same preparation has been followed, but MscL has been omitted.

The lipid mixtures used were the followings: pure POPC in the case of nanodiscs used in the electrophysiology experiment (whose results are in section 3.2.1), 50:50 mol of AzoPC and POPC for the MscL reconstituted sample used in the FTIR spectroscopy on the ion channel activation (section 3.2.4), and 20:80 mol of AzoPC and DPPC in the nanodiscs used to investigate the conformational changes happening to the lipids in nanodiscs (section 3.2.5).

2.2 Functional tests on MscL

Two functional tests were run to confirm the correct folding and activity of MscL and to explore to which extent this mechanosensitive ion channel could be activated when pulled by the photo-sensitive membrane: electrophysiological readings recorded with a Nanion Orbit Mini setup and a classical calceine efflux fluorescence experiment, adapted to a light trigger. Electrophysiological readings of the opening of the channel induced by local osmotic stress show the correct physiological function of MscL in non-light sensitive lipids. Then, the single channel activity of Mscl, recorded together with Antreas Vorkas,

occurring upon blue light illumination when the protein is reconstituted in light sensitive lipids, is adopted as proof of the ion channel activation *via* light illumination. The calcein efflux test reports on the ability of the photo-lipids to gate the channel in liposomes: MscL opens with the tension generated by the light-induced isomerization of AzoPC from *cis* to *trans* and releases the calcein enclosed in the liposomes, which then emits a detectable fluorescent signal.

2.2.1 Electrophysiological measurements

A single channel current signal across a free standing lipid bilayer, in which MscL has been reconstituted, is recorded. The setup is a commercial Orbit Mini workstation from Nanion. It is a miniaturized and basic version of a black lipid membrane electrophysiology setup. The free standing bilayer is built on a chip inserted into the body of the machine, which contains the amplifier and an electronic unit needed to transfer the signal to the computer. Every Orbit chip has four channels to run four experiments in parallel. What is reported in this section is the description of one of the four channels. A schematic representation of the measuring cell can be found in figure 2.2.
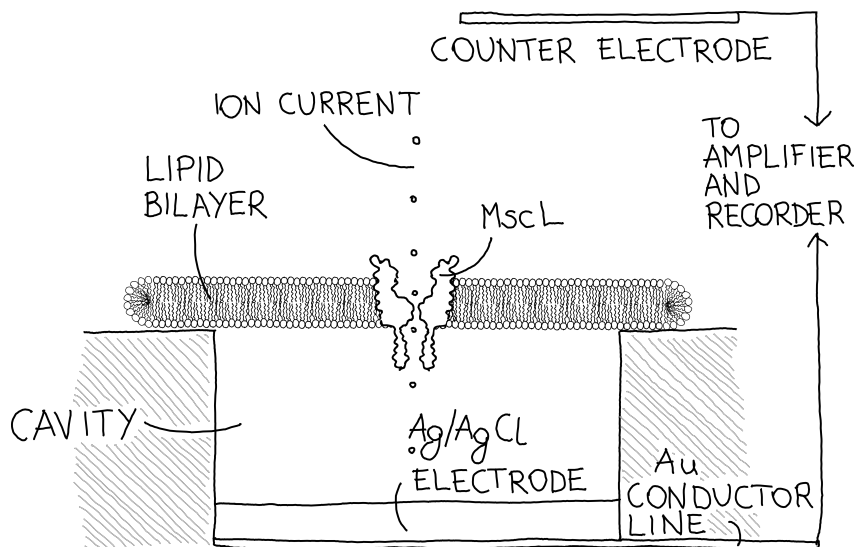
FIGURE 2.2: SKETCH OF ONE ELECTRICAL CELL OF THE ORBIT MINI SETUP USED FOR ELECTROPHYSIOLOGY. A lipid bilayer is built on top of a cavity filled with buffer. MscL is reconstituted in the membrane. A current passing through the ion channel can be measured when the ion channel opens, upon voltage application.

A Ag/AgCl electrode sits at the bottom of an insulating cylindrical cavity, whose diameter is 100 µm. The cavity and the whole volume above it, about 200 µL, are filled with PBS buffer, pH 7.2. The cavity gets then sealed with a free standing bilayer of pure 1,2-diphytanoyl-sn-glycero-3-phosphocholine

(DPhPC), in case of the control measurement where MscL gets activated by osmotic pressure. A mixture of 80:20 mol DPhPC:AzoPC was then used when testing the light-triggered activity of MscL. DPhPC is a commonly used lipid for free standing bilayers as its branched structure builds very stable bilayers. With its PC headgroup, it is well-mixable with other PC lipids.

The lipidic bilayer is formed by painting it on the top of the cavity as follows: a small amount of lipid solution, 10 mM in hexane, is taken up in a micropipette tip by capillarity, without applying any suction; then an air bubble is formed right above the cavity in the buffer solution by carefully pushing on the pipette piston; finally the bubble is swiped on top of the cavity to form the free standing lipid bilayer. As the air is pushed out of the tip and the bubble is inflated, the lipids will self organize in a thin film at the air/water interface, favoring the interaction between the hydrophilic headgroups and water. When the bubble touches the hydrophobic polymer in which the cavity is photolitographycally carved, the alkyl chains of the lipids interact with the plastic material and the lipids rearrange themselves self-assembling in a bilayer[100,101] (figure 2.2).

The existence, quality and stability of the bilayer can be tested running voltage cycles, each cycle being a sequence of patterns of applied voltages that allows the software to calculate a value for the resistance and the capacitance of the membrane from the current response. As per the Nanion device instructions, values indicative of an actual bilayer are a resistance of about 1 GΩ or higher and a capacitance of about 7 pF or higher.[101]

The reconstitution of MscL into the bilayer is then mediated by nanodiscs: 10 µL of MscL in nanodiscs at a concentration in the order of 10 µg/mL is released and mixed into the upper solution. After some time, indicatively in 10 to 30 minutes, a protein is spontaneously transferred from its nanodisc to the free standing bilayer[102].

To induce the opening of MscL in a DPhPC bilayer, we exploited the osmotic pressure that gets created across the bilayer if one side of the membrane is replaced by pure water. To do so, 10 µL of very pure deionized water (Milli-Q) is gently pipetted close to the top of the cavity. The difference in osmolarity between the inner ion-rich buffer and the outer pure water creates an osmotic pressure that bends the bilayer. Usually, inducing an osmotic gradient across the membrane is not recommended, as it leads to membrane rupture. But because of the presence of MscL, whose physiological role in bacteria is exactly to prevent cell lysis, the ion channel is opened instead and an ion current is let through the channel. The system is probed in voltage-clamp at 20 mV.

The ability of a photoactive membrane to gate the ion channel was tested

with a bilayer containing 20% mol AzoPC and 80% mol DPhPC. The lipid mixture in hexane was exposed to UV light for 10 minutes prior to building the bilayer on the electric cell, as to set the AzoPC lipids in the *cis* conformation. The bilayer was then bubble-painted in the dark. MscL was reconstituted from nanodiscs with the same procedure as for the non-active bilayer. Turning on the continuous blue light was then used as a trigger for membrane contraction.

The data analysis of the current traces was done together with Antreas Vorkas. The single channel recordings were filtered with -3 dB cutoff at 600 Hz and analyzed using Clampfit 10.4 software (Molecular Devices, United States).

2.2.2 Calcein efflux from liposomes

To test in proteoliposomes the light-induced opening of MscL, caused by the tension from the AzoPC isomerization, the triggered release of calcein upon illumination has been observed in a Cary Eclipse fluorescence spectrometer (Agilent) with a 90° geometry between a triggering blue LED light (for details on the LED-emitted light see appendix B.10) and the detector.

The sample form for this experiment consists of a PBS buffer solution of proteoliposomes loaded with 50 mM calcein. At such high concentration the dye is self-quenching,[103] therefore the observable fluorescence is low. The outer buffer is calcein-free. For details on calcein excitation-emission spectra and expected efflux-induced dilution, see Appendix C.2.

As soon as the proteoliposomes are illuminated with blue light, the isomerisation from *cis* to *trans* is induced in the photo-lipids. As a consequence of the reduction in steric hindrance of every lipid molecule, the tension of the liposome membrane is increased. The increase in lateral tension triggers the opening of the channels and the consequent release of calcein from the vescicles. As the calcein gets diluted by the exchange with the outer buffer, a strong fluorescent signal is observed increasing.

For the preparation of proteoliposomes for the calcein efflux experiment, the experimental protocol is modified as to include the dye at a high concentration inside of the liposomes, leaving the outer buffer clear. The liposomes were loaded with a 50 mM calcein solution. This was done by adding calcein to the usual PBS buffer and readjusting the pH to 7.2, as the calcein lowers the pH and its solubility in water is strongly pH-dependent, and using this solution to make the LUVs, as already described. The whole proteoliposomes preparation, from drying the lipid cake to removal of biobeads, is being done in the darkness with intermittent UV light illumination (about 10 min every half an hour of darkness) of the sample, to keep the AzoPC lipids in the *cis*
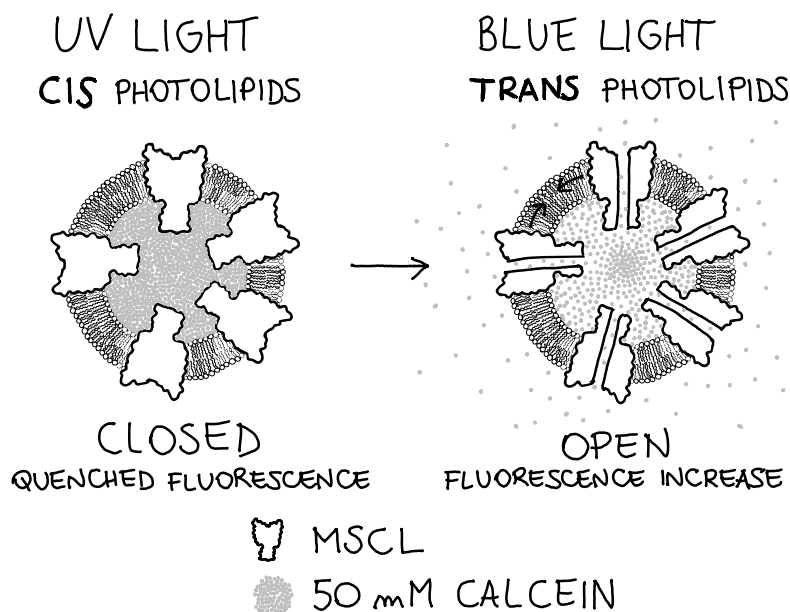
FIGURE 2.3: CONCEPT OF THE CALCEIN EFFLUX EXPERIMENT. Proteoliposomes containing calcein, 50 mM in PBS buffer, pH 7.2, do not emit fluorescence due to the self-quenching of the calcein at high concentrations. The AzoPC lipids are set in the *cis* configuration *via* UV light illumination during the whole sample preparation. When illuminated with blue light, AzoPC isomerizes to *trans*, the lateral pressure in the bilayer drops creating a tension, and the ion channels are opened. The released calcein is diluted in the external buffer and a fluorescent signal can be detected.

form. The external buffer is then to be exchanged with calceine-free PBS buffer through size exclusion chromatography: a Sephadex pd-10 column is first washed with water and PBS buffer, ph 7.2. It is then equilibrated with the same buffer with 0.5 M sucrose. The sucrose is necessary to equilibrate the osmotic pressure from the inside of the calcein-containing liposomes, to avoid premature opening of the MscL. The column is loaded with 500 µL of proteoliposomes solution and 2 mL of sucrose PBS buffer. The following 12 mL of elution is then collected in 1 mL samples.

The first four collected fractions are separately analysed in the UV-vis spectrometer, to check for the absorption from AzoPC lipids, and measured on in the FTIR spectrometer, to check for the AzoPC lipid marker bands. The 3rd sample is the one containing the calcein-loaded proteoliposomes in calceine-free buffer and 0.5 mL of it are diluted with 2.5 mL of sucrose PBS buffer, pH 7.2, and used for the experiment. This calcein efflux protocol is derived from the description of Powl *et al.*[104] and the pd-10 instruction manual.

2.3   Rheology of a photo-lipid monolayer

It has been demonstrated that MscL opening is triggered by lateral tension in the membrane.[21] A threashold tension of 10-12 mN/m is needed to open MscL.[105–107] To check if AzoPC is able to induce such a tension when photoiso- merised from the *cis* to the *trans* conformation, we measure the light-induced lateral pressure change in the monolayer.

A convenient setup to measure the rheological properties of a lipid mono- layer is the Langmuir-Blodgett (LB) trough. The setup (figure 2.4) is simple: a monolayer of lipids floats on an aqueous substrate contained in a teflon baseplate, two teflon barriers can compress the monolayer to a desired lipid density and a hanging dynamometer measures the tension of the film.
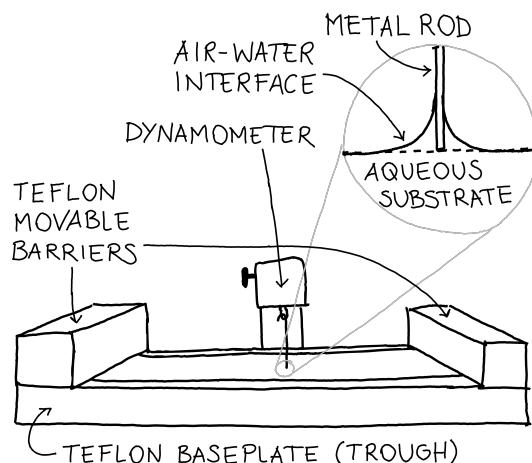

FIGURE 2.4: LB TROUGH SETUP A teflon baseplate contains the water substrate. At the air-water interface a monolayer of lipids is deposited. Two movable barriers can restrict the available area, effectively controlling the lipid density. A metal rod measures the lateral pressure at the interface.

Due to the amphiphilic nature of the lipids, to build the monolayer it is sufficient to deposit a small amount of lipids in a volatile organic solvent and they will distribute themselves homogeneously, covering the whole air/water interface. When the lipid density is low and the hydrophobic tails of the lipids are not strongly interacting, the monolayer is in the so-called gas phase. At a fixed temperature, which can be kept constant *via* a thermal bath, by compressing the barriers and reducing the available area per lipid, it is possible to draw the pressure-area isotherm of the specific lipid or amphiphilic molecule. A general scheme of it is represented in figure 2.5. The exact shape of the curve depends on the specific lipid-lipid interaction. Second-order phase trasitions, such as the main liquid ordered to liquid disordered transition of phospholipids, are characterized by a plateau in the isotherm.[108] AzoPC does not show such

plateau, as its transition temperature is expected to be below zero and therefore unaccessible with a LB trough experiment.
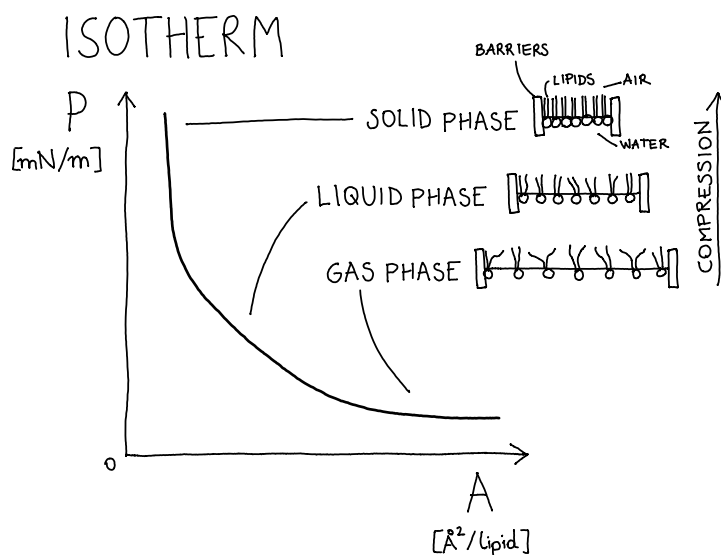

FIGURE 2.5: GENERAL SKETCH OF A LB ISOTHERM. Lipids are deposited at a low density (gas phase). The density can be increased by compressing the monolayer with the movable barriers. Depending on their specific structure, the lipid molecules rearrange themselves in specific condensed phases (falling under the more general terms of liquid and solid phases), characterized by a higher packing and increased lipid-lipid interaction.[108]

The amount of lipids to be deposited on the water surface has been determined to be low enough to leave the surface pressure reading unaltered after the deposition, an indication that the lipidic monolayer is in the gas phase. On the other hand, it should be high enough to reach 40 mN/m when the barriers compress the monolayer fully, to allow setting it in similar lateral pressure conditions to the ones of a single leaflet of a membrane bilayer. An initial lipid density between 100 and 200 Å^2/lipid fulfills both conditions. The results of a test to compare different starting densities are provided in appendix C.1.

The solution of lipids in chloroform was prepared with a concentration of 2 mg/mL. Since the precision syringe used for the deposition releases 1.32 µL/revolution, the deposited volume is limited to integer multiples of this amount. 12 revolutions, corresponding to 15.84 µL, were used. The molecular weight differences between different lipids did not affect the number of revolutions to best approximate the desired density, which then resulted is a slightly different effective initial lipid density. The available trough area is a rectangle with dimensions of $80 \times 350 \text{ mm}^2$.

2.4   UV-vis spectroscopy of photo-lipids

The absorption of AzoPC in the UV-vis range between 250 and 600 nm has been measured in a commercial single monocromator spectrophotometer, a Shimadsu UV-2600, for both isomerization states. Two different sample conditions have been tested: lipids solved in chloroform and LUVs in PBS buffer, pH 7.2. The concentration of AzoPC in chloroform is 2 mg/mL. The LUVs have been prepared as described in section 2.1.2 and diluted down to a concentration of 0.1 mg/mL.

2.5   IR spectroscopy

IR spectroscopy is an effective technique to answer structural questions at the atomistic level, in gas or condensed matter. It has been proven extremely valuable in the context of the the study of membrane proteins, advancing knowledge on their conformation and dynamics.[109–111] The method is sensitive to dipole moment changes associated to molecular vibrations and it is based on the analysis of the infrared light absorbed by the sample. The relative absorption is recorded for each frequency in the mid-infrared range, which is usually expressed in wavenumbers unit ($4000 - 1000$ cm^{-1}), corresponding to $2.5 - 10$ µm wavelegth. These two kinds of information revealed - the frequency at which vibrating bonds in a sample absorb light and with how much intensity - are directly related to the strength and polarity of the bonds, which are subject to changes depending on the molecular environment. Chemical structure and bond parameters, protonation events and hydrogen bonding strength, secondary structure and conformational freedom are examples of properties that can be investigated with FTIR spectroscopy.

In the following paragraphs the relevant aspects of this technique will be covered in relation to the study of biological samples, in particular proteins and lipids. The knowledge acquired by the community in the application of IR spectroscopy to this specific field has been condensed in some extremely helpful literature[112–115] of which this chapter is just a selective overview. Rather than introducing the technique as a whole, this section is meant to enable the reader to have a good understanding of the experiments and to better follow the discussion of the results in the later chapter.

2.5.1   IR spectroscopy of lipids and proteins

When looking at a spectrum of membrane proteins there are some absorption bands that are immediately recognizable and others whose interpretation requires a more in-depth look. The following paragraphs are a summation of

established spectroscopic characteristics of lipids and proteins. In particular, they focus on dialkyl glycerol phosphatidylcholine (PC) lipids, as these are used in this work for the reconstitution of MscL, and on membrane proteins, with a focus on the predominantly α-helical ones, such as MscL. In figure 2.6, a sketch of the two chemical structures can help the reader visualise the vibrational modes described.
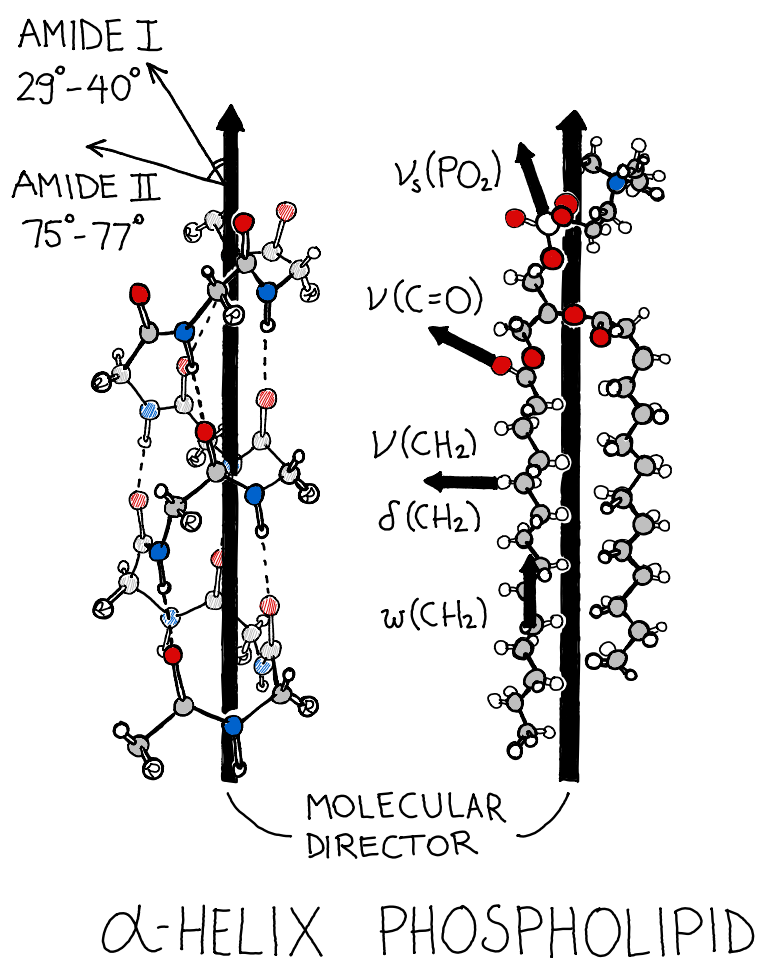

FIGURE 2.6: SKECTH OF THE STRUCTURES OF AN α-HELIX AND A PHOSPHOLIPID WITH THE RELATIVE DIRECTIONS OF THE MOST RELEVANT VIBRATIONAL MODES. Grey: carbon atoms; red: oxygen atoms; blue: nitrogen atoms; white: hydrogen atoms. Side chains of the amminoacids are indicated with 'R'. Protein backbone vibrations, amide I and amide II, are oriented as shown with respect to the molecular director in α-helices. The direction of the main vibrational transition dipole moments of phodspholipids are indicated by arrows next to the relative atoms.

Lipid absorption bands

The most characteristic absorption bands encountered when measuring a sample containing dialkyl lipids are the CH_2 stretching vibrations, $\nu_s(CH_2)$ and $\nu_{as}(CH_2)$. The symmetric and asymmetric modes appear respectively at 2849 cm^{-1} and 2917 cm^{-1} when the tails are ordered and increase to 2853 cm^{-1} and 2923 cm^{-1} when disordered. They are therefore good indicators of the alkyl chains packing order. Other modes of the CH_2 groups are also informative of the lipid phase: the scissoring mode, $\delta(CH_2)$, appears as two bands at 1463 cm^{-1} and 1473 cm^{-1} when in orthorhombic packing, but in the hexagonal packing they shift to different directions, respectively to 1468 cm^{-1} and 1470 cm^{-1}; the wagging, $\omega(CH_2)$, appears as a progression of bands between 1350 cm^{-1} and 1180 cm^{-1} that changes features when going from ordered to liquid-crystalline state, where the exact frequencies depend on the kinks introduced by the insaturations in the alkyl chains.

The carbonyl stretching vibration, $\nu(C{=}O)$, is a very distinct intense band at around 1733 cm^{-1}, for fully hydrated diacyl phosphatidylcholines. The two ester groups that generate the signal are situated at the interface between the hydrophobic tails and the headgroup. Their absorption frequency is sensitive to hydrogen bonding and to the interfacial environment in general and the peak frequency increases in case of an anhydrous sample. Indeed the band can be deconvoluted into two components, a higher one at 1742 cm^{-1} and a lower one at 1728 cm^{-1}, which have been assigned respectively to the dehydrated and the hydrated esters.[116,117]

The phosphate group at the head of the lipid molecule can also be affected by hydrogen bonding: its asymmetric stretching vibration, $\nu_{as}(PO_2^-)$, absorbs at 1260 cm^{-1} when hydrated and at $1220 - 1240$ cm^{-1} when anhydrous. The symmetric stretching vibration, $\nu_s(PO_2^-)$, is not affected and absorbs at 1090 cm^{-1} instead.

Protein absorption bands

Due to its higher level of complexity, the protein signal is usually harder to interpret. The range below 1500 cm^{-1} is referred to as the "fingerprint region", since it is highly characteristic of the protein, but of difficult interpretation since the absorption bands arise from complex vibrational modes. However, several modes where only fewer atoms are involved are indeed well assigned. Most protein side chains absorb in the range $1400 - 1800$ cm^{-1} and the specific frequencies can be altered depending on the local environment of the residue. Due to the large amount of amino acids in a protein, it is usually hard to discern from which residue comes a certain absorption. There are

techniques to identify specific residues, such as site-directed mutagenesis or isotopic labeling. These are rather advanced for the stage we are now with the spectroscopic study of MscL, but will surely be part of the future of its investigation. For a table and analysis of the side chain bands, the reader is invited to read the review from Andreas Barth,[113] among the many available.

What we can monitor, and can give us a readout on the gating status of an ion channel, are the amide bands. These come from the absorption of the protein backbone and are therefore relevant to probe the overall structural changes. The amide I band is a prominent band around 1650 cm^{-1}. It arises mostly from the absorption of the C=O stretching vibration, but it has some contribution also from the CN stretching, the CCN deformation and the NH in-plane bend. This mode is coupled between neighbouring amide groups and therefore it is influenced by the secondary structure of the peptide: α-helices absorption is centered between 1660 and 1665 cm^{-1}, while β-sheets are found between 1640 and 1615 cm^{-1}. The exact absorption frequency tends to be lower for longer helices, coiled coil structures or because of solvent exposure; hydrogen bonding of the helices can result in a lower absorption frequency for the amide I band of 10 to 30 wavenumbers. The amide II band is usually found at about 1550 cm^{-1} and it arises from the combination of NH bending and CN stretching modes. The amide bands have a well defined orientation with respect to the molcular director of the α-helix (figure 2.6) and are therefore useful in determining the orientation of α-helical segments (a recent example from Ataka and colleagues in reference[118]).

Liquid water absorbs MIR radiation in two spectral regions:[119] the OH stretching vibrations absorption results in a broad band centered at about 3400 cm^{-1}, while the water bending mode in a sharper band peaked on 1645 cm^{-1}. Since biological samples are often in acqueous solution, a good method to avoid the overlap between the water bending absorption with the amide I band is to replace the H_2O with D_2O. The increased mass of deuterium shifts the absorption maxima of heavy water to 2500 cm^{-1} and 1200 cm^{-1}, from the stretching and bending modes respectively. The H/D exchange affects all hydrogen bonds between the solvent and the protein as well. The amide I band is shifted of $\sim$ 10 cm^{-1} towards lower wavenumbers, the amide II to $\sim$ 1475 cm^{-1}.[120]

Difference spectroscopy

To understand a mechanism it is useful to look at what changes between an initial state and a new state. By comparing the system in the two states it is possible to highlight the differences and to isolate only the desired information related to the change, especially if what we are interested in is very little with

respect to the whole system. In FTIR spectroscopy of complex biological systems this is often achieved by difference spectroscopy:[121] simply, the spectrum of a pre-trigger state is used as a background for the after-trigger spectrum. This means subtracting one absorption spectrum from another. The resulting difference spectrum will show bands relative to the initial state as negative and bands from the final state as positive. Often the spectra are crowded with absorption bands and positive and negative bands get summed up. In figure 2.7 there are some examples of how typical band shapes can arise in a difference spectrum.
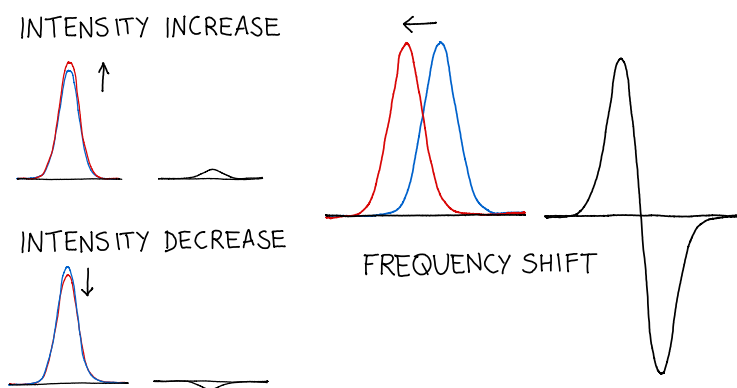

FIGURE 2.7: EXAMPLES OF THE MOST COMMON DIFFERENCE SPECTRAL FEATURES. Left: A change in intensity of an absorption band between two states of the sample (from blue to red lines) appears in the difference spectrum as a positive or negative band (black lines) depending if it is respectively an increase or a decrease of the absolute absorpion. Right: Another common feature is the 'derivative-shaped' band with two lobes, one negative and one positive (black line), resulting from a shift in absorption frequency (spectral change from the blue line to the red line).

2.5.2   The FTIR spectrometer and the sample geometries

The basic necessity behind IR absorption spectroscopy is to be able to detect which frequencies in the MIR range from a broadband emitted light have been attenuated by going through the sample and of how much. Originally, a classical dispersive IR spectrometer would have had a monochromator to select monochromatic light from the source and the frequencies would have been swept sequentially.

Instead, in a FTIR spectrometer, the attenuation in the full frequency range is measured simultaneously, with the advantage of using the entirety of

the power from the emitted light. To accomplish that, the light passes through a Michelson-Morley interferometer and for each movable mirror position a light intensity is recorded, giving rise to the interferogram. To obtain a spectrum in the frequency domain, the interferogram is then Fourier transformed from the spacial domain. The spectrum obtained this way is usually called "single channel spectrum" and, if the light has not passed through any sample, it shows the black body radiation emitted from the Globar source. A sketch of the beampath of the Bruker Vertex 70v spectrometer used for this work is shown in figure 2.8.
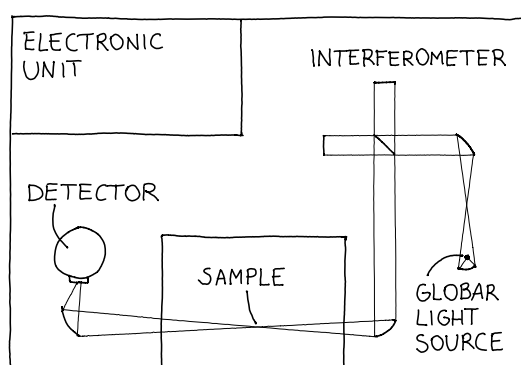

FIGURE 2.8: BRUKER VERTEX 70V SPECTROMETER BEAMPATH. The MIR light emitted by a globar light source passes first in a Michelson-Morley interferometer, then through the sample, which will absorb some radiation, and then it reaches an Mercury-Cadmium-Telluride (MCT) detector.

The sample transmission spectrum can be calculated as the ratio between the single channels recorded with and without sample: $T = I/I_0$. The absorbance is then defined as follows:

$$A = -\log(\frac{I}{I_0})$$

where I_0 is the single channel reference spectrum and I is the single channel spectrum of the light transmitted through the sample. Absorbance and transmittance are unitless quantities, but in the field absorbance is often referred to as optical density, although the term is deprecated. A base 10 logarithmic relation links absorbance and transmittance, which can then also be expressed as $T = \frac{1}{10^A}$. It is easy to notice that, if the sample does not absorb any photon, $A = 0$ and $T = 1$. To have an idea of what absorbance means in terms of photon count, usual absorbance values for a FTIR experiment are in the order of $A = 10^{-3}$, which means that the absorbed photons are in the order of 1 every

1000 irradiated. The changes in absorption that we detect in the difference spectra are in the order of $A = 10^{-6}$, corresponding to a difference in photon absorbed of 1 every million.

In a IR absorption experiment, the absorbance follows what is known as the Lambert-Beer law:

$$A = \varepsilon c l$$

which means that it is proportional to the molar extinction coefficient ε, the concentration c and the pathlegth l. To maximize the absorption signal from the sample, whose ε is fixed, we would have to increase the other two quantities. This might not always be the best approach and different solutions have been found to increase the desired signal. Moreover, liquid water has a strong absorption peaked at 1645 cm^{-1}, the H$_2$O bending mode, overlapping with the amide I frequency range, an important spectral region for protein. This is an unfortunate fact very well known to bio-spectroscopists, since most samples are in acqueous solution or need some degree of hydration. To solve this issue there are several possibilities, both regarding sample preparation (higher concentration, isotope labeling, using heavy water), measuring technique (selective enhancement, such as Surface Enhanced InfraRed Absorption Spectroscopy, SEIRAS) or data analysis (water spectrum subtraction, difference spectroscopy).

Sample geometries: Transmission and Attenuated Total Reflection (ATR)

The most straight-forward geometry to measure an absorption spectrum of a substance is in transmission (left sketch in figure 2.9). The sample is sandwiched between two IR-transparent windows (usually BaF$_2$ or CaF$_2$) and the probing IR beam crosses the sample from one side to the other. If the sample is deposited as a dry film, rehydration is possible by addition of small droplets of glycerol/water mixture on the sides of the sample. The specific ratio between glycerol and water determines the humidity of the atmosphere on top of the sample and therefore the sample hydration.[122] The chamber is sealed with a silicone-greased O ring.

The Attenuated Total Reflection (ATR) configuration (right sketch in figure 2.9) allows for easy access to the sample from the top (in transmission, modifications to a condensed sample during measurement can only be obtained for fluid samples in a flow cell). Also in the case of an ATR configuration, the sample can be enclosed in an atmosphere with stable humidity. The ATR configuration offers the possibility of selecting a light polarization, as exploited in this work, or to implement other techniques such as Surface Enhanced InfraRed Absorption Spectroscopy (SEIRAS).[86] Moreover, adopting the ATR

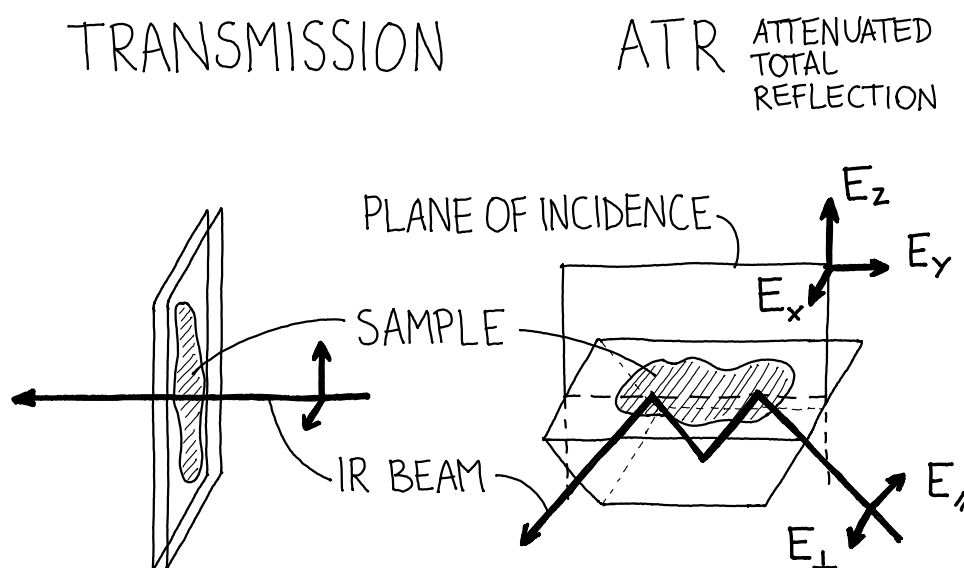TRANSMISSION   ATR ATTENUATED TOTAL REFLECTION

FIGURE 2.9: ATTENUATED TOTAL REFLECTION (ATR) AND TRANSMISSION GEOMETRICAL CONFIGURATIONS FOR FTIR MEASUREMENTS. Two different ways to probe the sample with an IR beam. In transmission, the sample is placed in the IR beam path, sandwitched between two IR-transparent windows. In ATR, the sample is dried on top of a crystal with a high refractive index, and it is probed by the evanescent wave resulting from the total internal reflection at the interface with the sample. This configuration, known as Kretschmann configuration, allows for linearly polarised measurements. The vectors perpendicular to the IR beam show the linear polarizations that can be selected by adding a polarizer on the incoming beam, in both geometries. $E_\parallel$ and $E_\perp$ are the field components parallel and perpendicular to the plane of incidence, corresponding respectively to p-polarized light and s-polarized light. E_x, E_y and E_z show the laboratory/sample reference system to which the ATR polarized spectra are converted (see section 2.5.3).

geometry minimizes the water contribution to the spectrum, requiring a smaller amount of sample of higher concentrations.

Called attenuated total reflection, it takes advantage of the phenomenon of total internal reflection. This takes place when light encounters an interface from one medium of higher refractive index to another medium with a lower refractive index at a higher angle to the normal to the interface than the critical angle. Snell's law gives the general relation between the angles of the incoming and outcoming light at an interface, depending on the materials, and

it is the following:

$$n_1 \sin \theta_1 = n_2 \sin \theta_2$$

For the case where θ_2 is 90°, the critical angle, θ_1, equals

$$\theta_c = arcsin(n_2/n_1)$$

where n_1 is the higher refractive index and n_2 the lower.

Due to their transparency to IR and having a high refractive index compared to water ($n = 1.33$) and membranes (n between 1.44 and 1.70)[123], common materials for the refractive element are diamond ($n = 2.38$)[124], germanium ($n = 3.97$)[125], silicon ($n = 3.42$)[126] and zinc selenide ($n = 2.41$)[127]. The material of the crystal used in these measurements is silicon.

When the IR beam gets totally reflected at the interface between the crystal and the sample, an evanescent wave decays exponentially with the distance z from the interface:

$$E = E_0 e^{-\frac{z}{d}}$$

The penetration depth d depends on the angle of incidence θ_1 and the refractive indices of the media, n_1, n_2:

$$d = \frac{\lambda/n_1}{2\pi\sqrt{\sin \theta_1{}^2 - (n_3/n_1)^2}}$$

where n_3 is the refractive index of the medium above the sample. Regarding our experimental conditions, the sample is hundreds of µm thick, enough not to consider what is above it and apply the thick film approximation where then $n_3 = n_2$.

2.5.3 Linearly polarized FTIR spectroscopy

When measuring with unpolarized light an oriented sample in transmission, the vibrational modes aligned to the Poynting vector, here coinciding to the normal to the windows (see left sketch in figure 2.9), are not getting excited and therefore they would not appear in the absorption spectrum. Moreover, selecting any linear polarization direction which lies in the frontwave plane of the IR beam does not make a difference, if the ordered sample is isotropic for rotations around the axis normal to the plane. Conversely, probing the sample with polarized light in ATR configuration allows for selection of specifically oriented vibrational modes, by adding a linear polarizer before the sample.

The absorption A depends on the transition dipole moment M and the projection of the IR electric field E on M:

$$A \propto |ME|^2 \cos \zeta^2$$

where ζ is the angle between M and E. Therefore the closest the direction of the transition dipole moment associated to a vibration is to the selected polarization direction, the higher the absorption.

The measurements are carried out with either p-polarized or s-polarized light, respectively parallel and perpendicular to the plane of incidence, as shown in the right side of figure 2.9. In the laboratory coordinates, the XY plane where the membrane lies coincides with the interface between the ATR crystal and the sample, the Z coordinate is the normal to it.

In case of our lipid deposition, either from chloroform or from vesicles, we obtain a highly oriented sample, as reported by the measured dicroism (see the results chapter, section 3.1.4). From the rock-and-roll deposition, the method of sowly drying the sample under a dry air flow with circular motions, we expect to have a multibilayer[128] with the alkyl chains of the lipids oriented on average along the Z axis and the membranes spanning the XY plane.

In order to obtain the spectra in the coordinates frame relative to the membrane orientation, the measured absorption must be corrected projecting the electric field amplitudes onto the new reference frame. The electric field amplitudes E_x, E_y and E_z are calculated as follows:[123]

$$E_x = \frac{2\cos\theta(\sin^2\theta - n^2)^{1/2}}{(1-n^2)^{1/2}\left[(1+n^2)\sin^2\theta - n^2\right]^{1/2}}$$

$$E_y = \frac{2\cos\theta}{(1-n^2)^{1/2}}$$

$$E_z = 2\cos\theta\sin\theta/(1-n^2)^{1/2}\left[(1+n^S2)\sin^2\theta - n^2\right]^{1/2}$$

Using these, the spectra with polarization in the xy plane A_{xy} and along the x axis A_z can be calculated from the measured spectra $A_\perp$- and $A_\parallel$[129,130]:

$$A_{xy} = \frac{A_\perp}{E_y^2}$$

$$A_z = \left(A_\parallel - \frac{A_\perp E_x^2}{E_y^2}\right)\frac{1}{E_z^2}$$

Since the effective penetration depth in the two polarizations differs and it is dependent on the angle of incidence, it is possible to determine the angle

from the dichroic ratio of an isotropic sample. The angle of incidence θ has been therefore determined from the intensity ratio of the water bands:

$$R_{ATR} = \frac{2\sin^2\theta - n^2}{(1 + n^2)\sin^2\theta - n^2}$$

The obtained value is 45 deg. For the calculation based on water spectra, see section B.5 in Appendix B.

2.5.4   InfraRed Reflection Absorption Spectroscopy

Infrared external reflection absorption spectroscopy, also commonly known as InfraRed Reflection Absorption Spectroscopy (IRRAS), is a method to get structural insight about monolayers of amphpathic molecules at the air-water interface.[131–134] It conveniently combines the LB technique, which gives qualitative information on the mechanics of the monolayer, with IR spectroscopy, which can non-invasively monitor changes in conformation and configuration of bonds absorbing in the MIR range. Here we applied it to the study of pure AzoPC.

Based on the phenomenon of external reflection, IRRAS was originally developed to characterize thin films deposited on metal substrates,[133,135] but, since Dluhy's pioneering experiments in the 80s,[136–139] it was clear that it would have benefited the research on pulmonary surfactants or, even more broadly, the studies on protein-lipid interaction happening at the membrane interface, which are at the core of many enzymatic activities.

The monolayer at the air-water interface can be modeled with a three-phase system: air, thin lipid film, water. The optical properties of any and each absorbing medium is represented by a complex refractive index $\tilde{n} = n + ik$, where n is the real refractive index and k the absorption constant. IR polarized light, either p-polarized or s-polarized (respectively parallel or perpendicular to the incident plane), is shined at the interface and it hits the surface at a specific incident angle. A detector at the same angle, but on the opposite side, collects the reflected light.

When light crosses an interface between two media of different refractive indices, it is partially reflected and partially refracted, as described by Fresnel equations. The fraction reflected depends on the mismatch between the refractive indices and its intensity is what is detected. This quantity is called reflectance absorbance (RA) and it is measured as follows:

$$RA = -\log\left(\frac{R}{R_0}\right)$$

where R is the reflectivity of the monolayer on the aqueous subphase and R_0 is the reference reflectivity of the subphase without monolayer. The RA intensity depends on the incident angle of the light, the polarization of the light, and the orientation of the absorbing transition dipole moment, other than the optical constants of the monolayer and the subphase. Being the real part n of the refractive index of water dominant with respect to k, RA can assume both positive and negative values or show derivative-shaped bands. The current formalism to describe and simulate IRRAS was developed by Kuzmin and Michailov[140–142] and it is not going to be treated here. The simulated spectra of AzoPC presented in the results were calculated with a custom MATLAB script from Christian Schwieger, implementing the Kuzmin-Michailov equations.

The reflectivity of the interface in the two polarizations, p and s, changes with the angle of incidence and differs between the two (figure 2.10). The reflectivity of s-polarized light increases with the incident angle, while for the p polarization it has a minimum where it reaches the value of 0 at the Brewster angle $\theta_B = \arctan\left(\frac{n_2}{n_1}\right)$, where n_1 and n_2 are respectively the index of refraction of the medium of the incoming light and of the medium after the interface. Around the Brewster angle though, the reflectance absorbance of a deposited monolayer has a positive and a negative maxima (figure 2.10), therefore it is advisable to measure around the Brewster angle to maximise the signal.[131] In the case of an air-water interface, where $n_{air} = 1$ and $n_{water} = 1.33$, the Brewster angle is at 53°.

When investigating lipids, the absorption bands of the methyl groups on the alkyl chains, the CH_2 stretching vibrations, are usually considered. Their frequency change reflects qualitatively a change in the packing of the lipids. In general, a lower wavenumber for the reflectance absorbance corresponds to a higher packing. For certain monolayer compositions, a direct correlation between a specific wavenumber and a lipidic phase could be drawn confirming it with other methods such as ellipsometry or X-ray techniques.[131]

The generally high intensity of these bands makes them easily identifiable. Other bands, overlapping with the water vapour absorption, are of harder analysis. The problem of water vapour in IRRAS is well known and several expedients have been found to increase the signal to noise ratio as much as possible.[134] First, H_2O can be substituted with D_2O, therefore shifting the absorption bands of liquid water and water vapour to lower frequencies, freeing the desired amide frequency range. Then, in order to minimize the time between the reference spectrum and the sample, a double trough system can be adopted. In addition to the main trough containing the deposited monolayer, a second smaller trough is set next to it. Both troughs are slowly shuttled between two positions to easily repeat the measurement multiple times
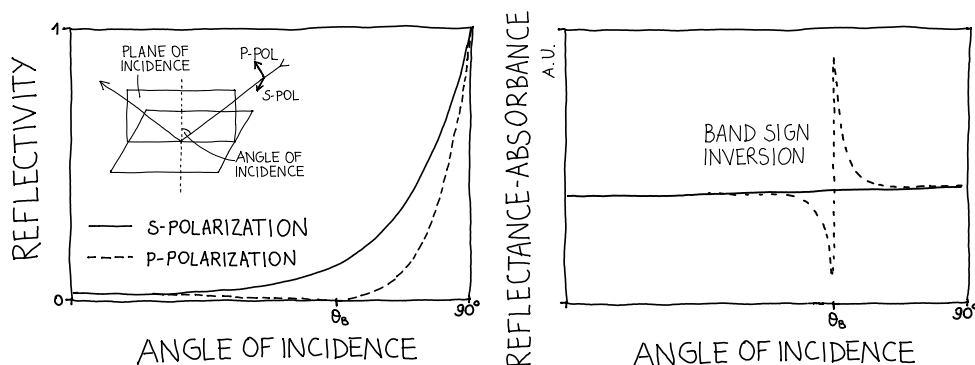
Figure 2.10: Reflectivity and reflectance-absorbance (RA) as functions of the angle of incidence In the inset, the visualization of the s- and p-polarized light with respect to the plane of incidence. For p-polarized light, the reflectivity reaches 0 at the Brewster angle (θ_B), where the band sign inversion happens due to the change of sign in the RA. In a IRRAS experiment, it is convenient to set the incidence angle close to, but not exactly at the Brewster angle, where the RA has its extremes.

and to reduce the time between the reference and the sample spectra recordings.

Last, another method to remove the presence of unwanted water vapour bands was developed: using a photoelastic modulator (PM), and alternating the polarization of the IR light, makes possible to separate the isotropic absorption of water from the polarization-dependent absorption of the monolayer. This technique is known as PM-IRRAS, but, differently from the previous two workarounds, it was not implemented in the setup used for the measurements presented in this work.

The setup used for the recording of the data presented here was self-built by Christian Schwieger in the laboratory of Prof. Hinderberger. We modified it to add the illumination sources necessary to the AzoPC switching on top of the trough and to automate the light triggering/recording process. As sketched in figure 2.11, the setup comprises a Vertex 70 FT-IR spectrometer from Bruker

Optics, Germany, equipped with a globar source and a liquid nitrogen-cooled Mercury-Cadmium-Telluride (MCT) detector. The IR beam is guided to the monolayer, and after reflection to the detector, with an automated arm system (A511 reflection unit, also from Bruker Optics) which can be set at a precise incident angle. A KRS-5 polarizer allows to select for p or s polarization of the beam. The monolayer was built on a pure D_2O subphase in a teflon trough (Riegler and Kirstein, Germany) with an area of 30×6 cm^2.

AzoPC was dissolved in chloroform in a concentration of 1 mg/mL, and deposited on the D_2O with a high precision Hamilton syringe in order to have an initial density on the surface of 100 Å^2/lipid. About 10 minutes were left for the chloroform to completely evaporate. The compression is exerted by bringing closer two teflon barriers and the lateral pressure can be monitored from a paper Wilhelmy plate attached to a pressure sensor. A secondary smaller round trough, also in teflon and with a radius of 3 cm, was filled with D_2O and used for the reference reflectivity. The subphase level was kept equal and constant at all times with a laser-reflection feedback pumping system connected to a D_2O reservoir.

The two troughs can be shuttled back and forth to record the two single-beam reflectivity spectra (R_0 from the small reference trough, R from the larger trough with the monolayer) necessary to calculate the RA. A 365 nm UV lamp and a 450 nm LED array, the same used in the LB light switching experiment and whose emission spectra can be found in Appendix C, were mounted 16 cm above the trough. The whole setup was enclosed in a transparent acrylic box which was purged with nitrogen. A sketch of the setup can be seen in figure 2.11

The angle of incidence was tested between 50° and 70° to check for band inversion and to select the best intensity: all spectra were then recorded at 60° of incidence. For each absorption spectrum in the s polarization, 1000 coadditions were averaged, while 2000 for the p polarized. Spectral resolution is 4 cm^{-1}.

2.5.5 Density Functional Theory calculations

The DFT simulations have been run by Rubén Cruz in Gaussian with the method BP66 and the basis set 6-311G with polarization and diffuse functions (bp66/6-311+g*). For the data treatment on the output of the calculations, discussed together and implemented by Rubén Cruz, see section B.4 in Appendix B.

In order to obtain orientational information from the calculated vibrational modes, all coordinates of the obtained dipole moments have been expressed on a base of vectors relevant to the lipid molecular structure. In particular,
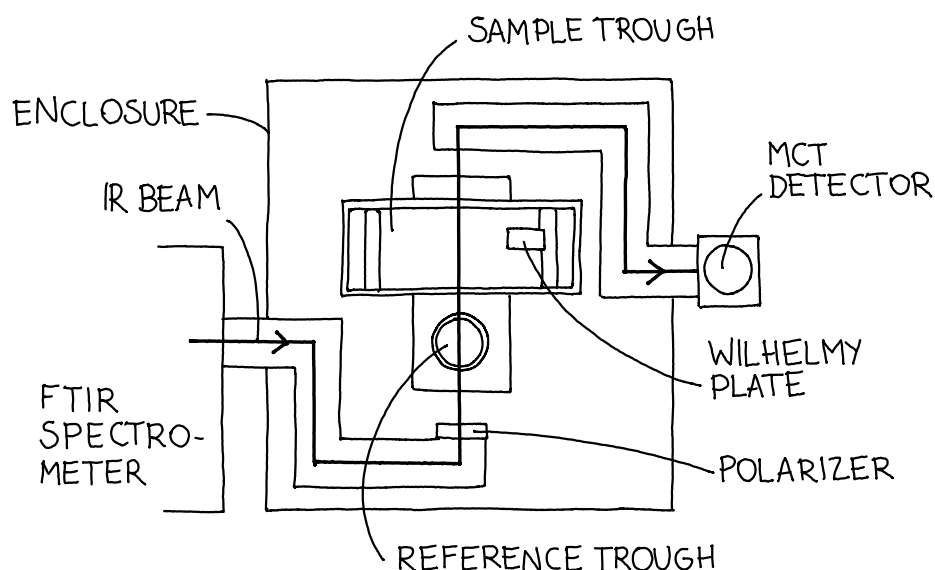
Figure 2.11: Sketch of the IRRAS setup as seen from the top. The IR beam comes from the interferometer in the FTIR spectrometer. It is conducted inside a movable arm through a polarizer, and it is reflected on the trough aqueous surface. Collected by the opposite movable arm, it then reaches the MCT detector. The angle of incidence of the beam to the water surface can be modified by changing the position of the two movable arms. The sample trough and the reference trough can be shuttled back and forth to meet the reflection point on one or the other surface. The water level is kept constant with a feedback system connected to a small water pump (omitted from the sketch for visual clarity). The setup is enclosed in an acrylic box to be purged, and it is accessible from some windows. The UV lamp and the array of blue LEDs used to illuminate the trough were attached to the ceiling of the enclosure, 16 cm above the sample trough.

the Z axis was chosen to best align with the main axis of the molecule, and it has then been defined to be parallel to the vector between the carbon atoms C3 and C17 of the $sn-1$ all-aliphatic alkyl chain. The Y axis was searched to be perpendicular to the Z axis and it has been identified as parallel to the vector between the hydrogen atoms H20 and H21. The X axis must then necessarily be orthonormal to the X and the Y axes. This basis set should ideally coincide with the lab framework used for the ATR polarized spectra, to allow for direct comparison of the calculated and the experimental spectra. We must be aware that, although the lipidic multibilayer dried from chloroform on the ATR crystal is expected to be highly oriented,[115] the two reference frames
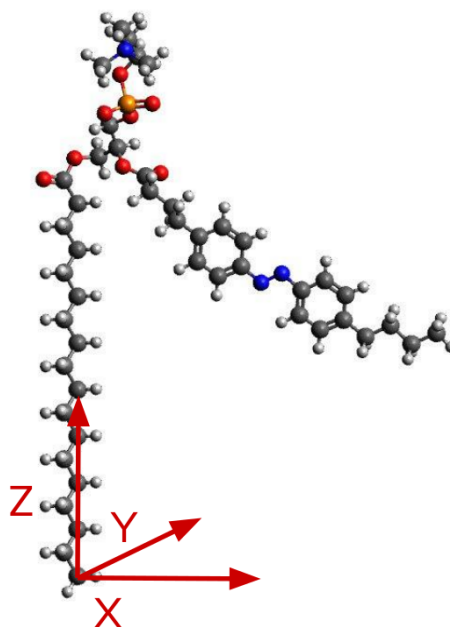
might differ.

FIGURE 2.12: REFERENCE FRAME FOR THE DFT COORDINATES. The Z axis has been set along the molecular director, defined by the carbons C3-C17. The perpendicular Y axis was set on the bisector between the directions of hydrogens H20 and H21. The X axis is then univocally determined.

Results 3

3.1 AzoPC lipids

3.1.1 UV-vis absorption

The absorption in the UV-visible range of AzoPC lipids was measured in two conditions: the lipids were either solved in chloroform, the form used for the deposition of the monolayer on the LB trough, or assembled in 100 nm unilamellar vescicles (LUVs) in water, prepared as described in the sample preparation section (2.1.2) of the Materals and Methods chapter.

The spectra in Figure 3.1 show a difference in absorbance between the two conditions: when the lipids are solved in chloroform the absorption peaks appear at longer wavelengths than when the lipids are arranged in a bilayer. The absorption band of the *trans* state is at 337 nm in chloroform and 319 nm for the LUVs. The bands of the *cis* state are centered at 310 nm and 440 nm in chloroform and at 295 nm and 440 nm for the LUVs.
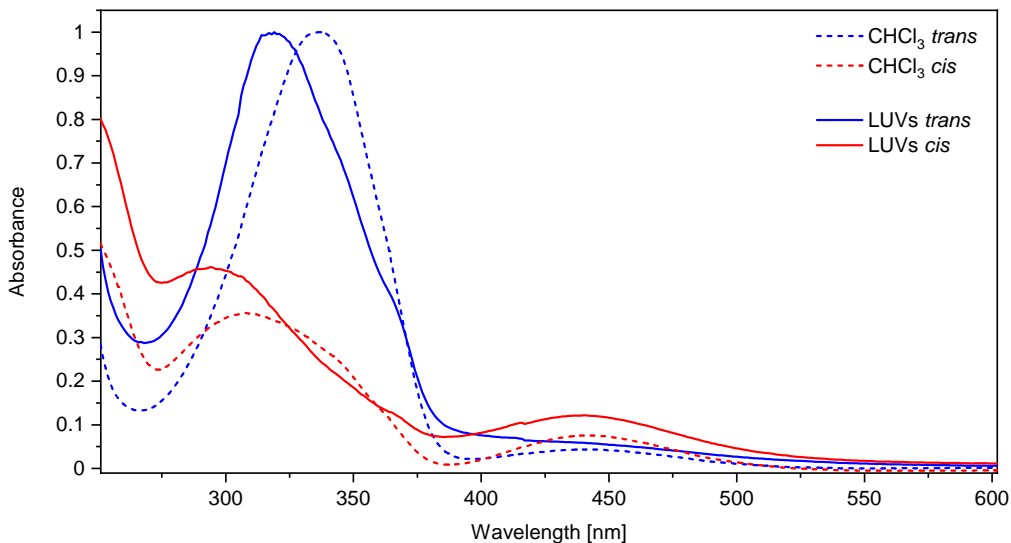
Figure 3.1: UV-vis absorption spectrum of AzoPC. UV-vis absorption spectrum of AzoPC in the *trans* (blue) and in the *cis* (red) isomers. The dotted line indicates the chloroform solution while the continuous line the LUVs in water.

3.1.2 Rheology changes induced by photo-switching the lipid monolayer

The lipids, deposited from a chloroform solution at a low surface density (here 100 Å^2/lipid), get compressed by the LB trough barriers to cover a smaller area. As the available area per lipid decreases, the lateral pressure increases until a monolayer is formed. This plot is a pressure-area isotherm of the lipid monolayer. A final lateral pressure of 30 to 40 mN/m is comparable to the one of a single leaflet of an average planar bilayer, but any measured effect of light switching cannot be transposed quantitatively to other bilayer systems, as we would have to neglect any interleaflet interaction. The qualitative observations are nevertheless valid.
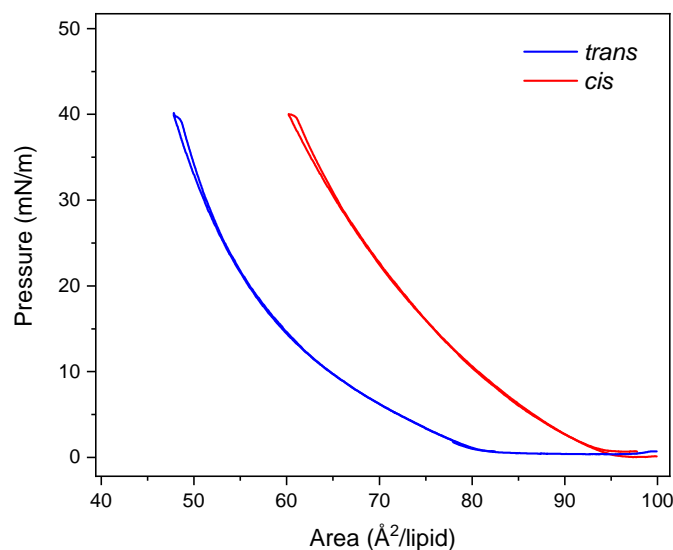
FIGURE 3.2: ISOTHERMS AT 25°C OF AZOPC IN THE *TRANS* OR IN THE *CIS* STATE. In red (blue), the compression/expansion isotherm under UV light (blue light) illumination.

Depending on the desired initial equilibrium condition for the monolayer, if it is in the *trans* or in the *cis* state, the compression is executed under blue or UV illumination (Figure 3.2). Both isotherms exhibit no knee, meaning that no evident phase change is happening during the whole compression/expansion cycle. Although it has not yet been measured, we expect the transition temperature for AzoPC, in the range of lateral pressures we take into consideration, to be much lower than the 25°C at which the isotherm was recorded, similarly to asymmetrical unsaturated dialkyl phospholipids[143].

In the *trans* state, each lipid molecule has a smaller footprint than in the *cis* state, as the lipid packing is favoured by the *trans* geometry of the azobenzene.[81,144,145] From the isotherms of Figure 3.2, we can extrapolate values for the potential expansion/contraction as a percentage of the molecular footprint, for pressures in the range of 30 to 40 mN/m (Figure 3.3) In this range, the difference in footprint for a single AzoPC molecule is around 27% with a decreasing trend towards higher pressures.
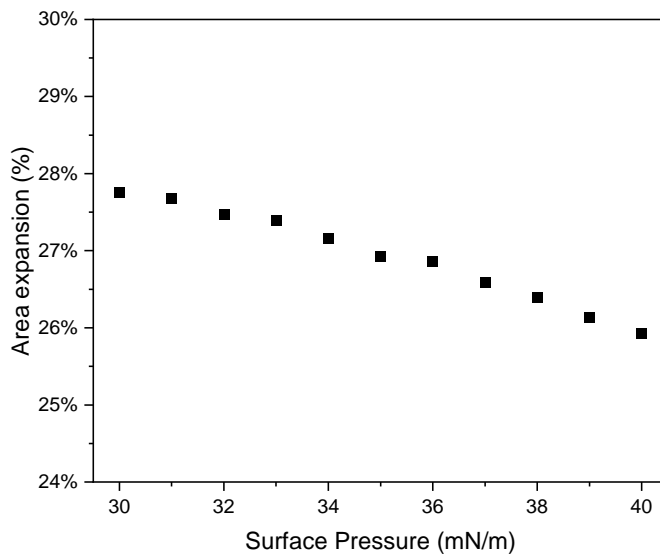
Figure 3.3: Difference in the footprint of an AzoPC lipid molecule between the two isomerization states. From the values of Figure 3.2, the area expansion is calculated for several surface pressure values as $\frac{area(cis)-area(trans)}{area(trans)}$, where *area* stands for area *per* lipid.

Blocking the barriers in place determines a fixed value for the available area *per* lipid. The corresponding lateral pressure at a specific area *per* lipid depends on the isomerization state of the lipids. To any given area *per* lipid would correspond a higher lateral pressure in the *cis* state (in Figure 3.2 the red line is always higher than the blue one, for any value of the abscissa). If we keep the barriers in place, therefore fixing the area *per* lipid, and we illuminate the monolayer intermittently with UV and blue light, the lateral pressure will change cyclically. This can be observed in Figure 3.4, where the monolayer was prepared under ambient light conditions, then isothermically compressed to 30 mN/m and the switching started with a UV light illumination. The lateral pressure difference between the initial *trans* and the *cis* state is 48 mN/m and it is reversible: when switching back from the *cis* state to the *trans* state with blue light, an equal tension is created, with respect to the equilibrium lateral pressure reached in the *cis* state.
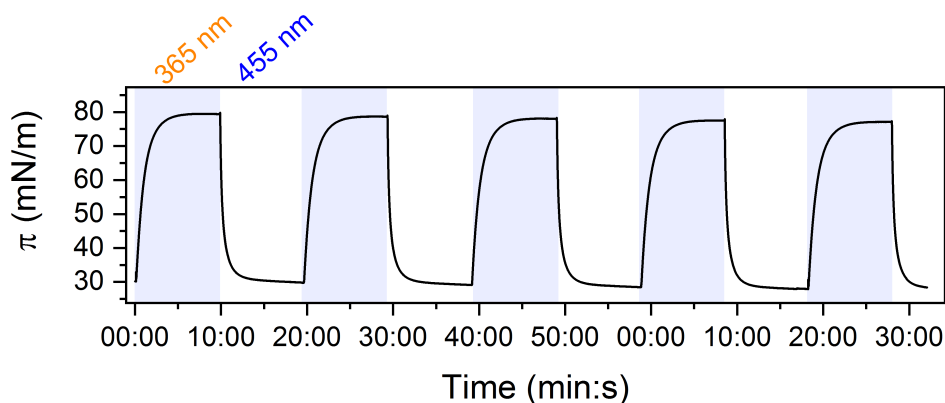
FIGURE 3.4: LIGHT SWITCHING OF AN AZOPC MONOLAYER, STARTING IN THE *TRANS* STATE. The lateral pressure in the monolayer changes due to alternating UV/blue light illumination. Equilibrating the *trans* monolayer at a starting lateral pressure of 30 mN/m, the pressure change obtained from light switching is of 48 mN/m. Published figure.[146]

The intensity of this lateral pressure changes depends on the starting lateral pressure. In Figure 3.5 it is shown that higher pressure jumps are achieved for monolayers compressed to higher pressures.
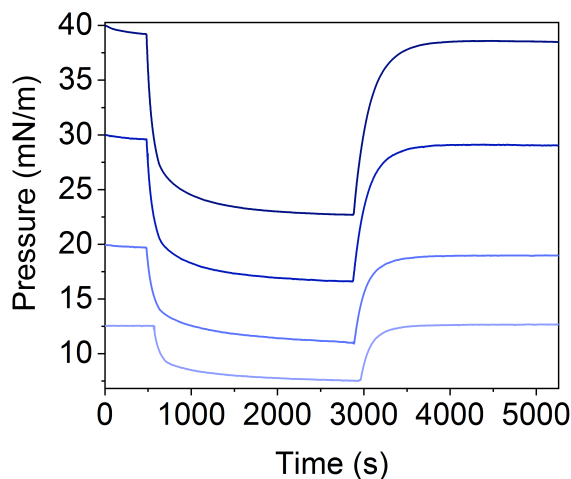

FIGURE 3.5: STARTING PRESSURE DEPENDENCE OF THE LATERAL PRESSURE CHANGE. The difference in lateral pressure that is created in the monolayer upon illumination depends on the starting conditions: a higher starting lateral pressure leads to a higher tension exertable.

Also, it is relevant in which state the lipid film is initially compressed. Having in mind an application where the photolipids could be used to pull on a mechanosensor, we want to equilibrate the membrane in the highest

lateral pressure state, the *cis* state, and then illuminate to decrease the lateral pressure, effectively applying a tension. In Figure 3.6, we show the cyclical switching, starting from a *cis* state and applying a tension with blue light first. The lateral pressure difference obtained in this case is 13 mN/m. Even if in both cases (Figure 3.4 and 3.6) the monolayer lateral pressure is brought to 30 mN/m by the isothermal compression, the potential change upon light switching is very different, as an equal initial pressure in the two isomerization states correspond to two different trough areas and therefore lipid densities.
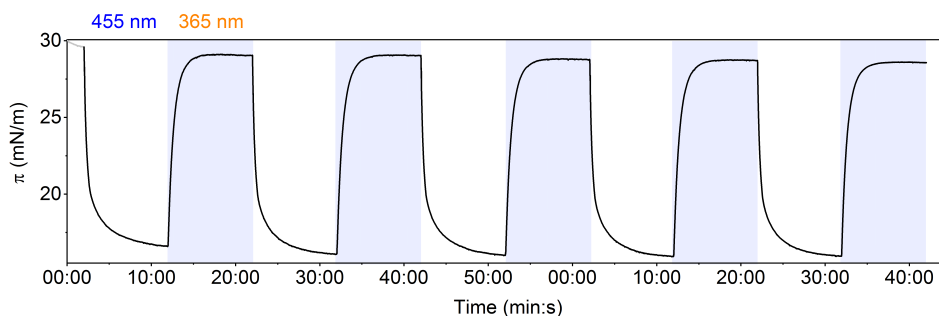

FIGURE 3.6: Light switching of an AzoPC monolayer, starting in the *cis* state. The lateral pressure in the monolayer changes due to alternating UV/blue light illumination. Equilibrating the *cis* monolayer at a starting lateral pressure of 30 mN/m, the pressure change obtained from light switching is of 13 mN/m. Published figure.[146]

3.1.3 IR band assignment of AzoPC

An assignment of the absorption bands of AzoPC is necessary to correctly interpret what happens during light switching of the photolipids. Two ways have been developed in parallel, to then be able to cross check the assignment. The absorption spectrum of AzoPC in the *trans* state, its ground state, is first compared with the one from the natural lipid it is derived from, 1,2-distearoyl-sn-glycero-3-phosphocholine (DSPC), whose band assignment is known (*cfr.* section 2.5.1), and then with the DFT calculated frequencies.

IR spectral comparison of AzoPC and DSPC

Figure 3.7 shows the ATR FT-IR absorption spectrum of the photolipid in the ground state, the *trans* state, compared to the one of DSPC, the corresponding non-photoactive phospholipid. The two lipid structures differ in one of the two alkyl chains: DSPC has two 18:0 fatty acid tails, while in AzoPC one of the chains has an azobenzene moiety substituting the carbons C6-C13 (chemical
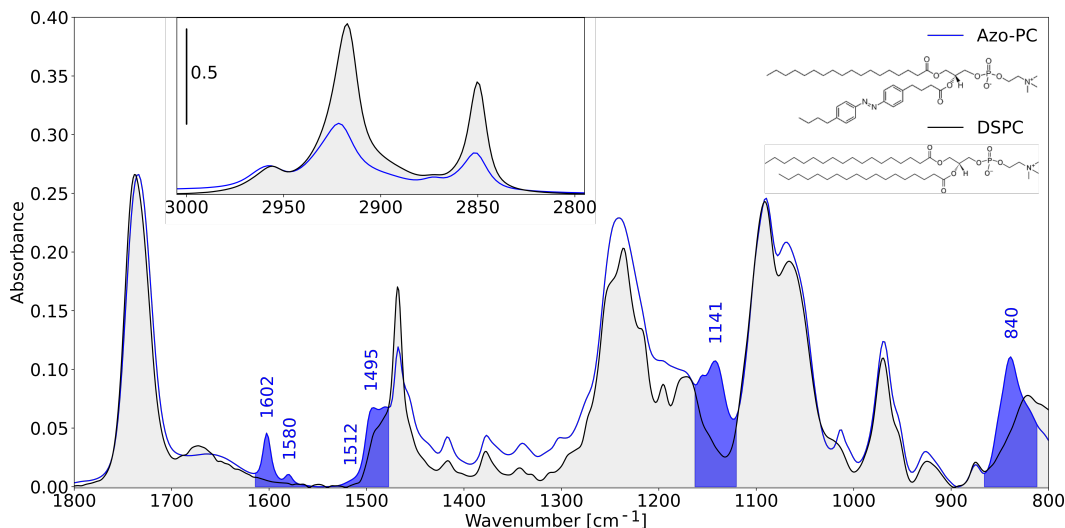
structures in the legend of Figure 3.7).

FIGURE 3.7: AzoPC (blue) and DSPC (black, gray-filled) infrared absorption spectra overlayed to highlight the differences. Blue-filled are the modes of the azobenzene rings, present only in the AzoPC sample. In the legend, a chemical structure of the two lipids is provided.

In the methylene stretching region, $3000 - 2800$ cm^{-1}, the absorption frequency of the asymmetric and symmetric CH$_2$ stretching are respectively at 2917 and 2850 cm^{-1} for DSPC and 2922 and 2852 cm^{-1} for AzoPC in the ground state. The higher frequencies of the photoactive lipid seem to indicate a reduced degree of organization in the tails,[147] as it would be expected from the presence of the azoswitch. The absorption frequencies of the asymmetric and symmetric CH$_3$ stretching are better overlapping, respectively at 2956 cm^{-1} and 2873 cm^{-1} for DSPC and 2957 cm^{-1} and 2873 cm^{-1} for AzoPC.

The strong absorption of the carbonyl stretching within the ester groups of the alkyl chains gives rise to the intense band at 1738 cm^{-1} in the DSPC spectrum and at 1735 cm^{-1} in the AzoPC one, which do not differ significantly. An analysis of the anhydrous and and hydrated ester absorptions contributing to this band can be found in Appendix B.3.

The absorptions of the azobenzene moiety stand out, as they appear as positive bands (highlighted in blue in Figure 3.7) present only in the AzoPC spectrum and not in the DSPC. The assignment has been done by comparison with literature on azobenzenes[148,149] and it has been confirmed by comparison with the DFT calculation. They are the ring C-C stretching modes at 1602, 1580 and 1495 cm^{-1}, the C-H scissoring mode at 1141 cm^{-1} and a mode of the choline headgroup coupled to a ring breathing mode at 840 cm^{-1}. Another

49

ring mode at 1512 cm^{-1} is barely visible in the *trans* spectrum, but rather recognizable in the *cis* spectrum (*cfr.* Appendix B.2 for a comparison between the absorption spectra of the two isomers of AzoPC.)

The methylene groups are more abundant in DSPC, since some of the carbons of the sn-2 alkyl chain of AzoPC are replaced by the azobenzene. This matches with the higher intensity of the methylene stretching bands, the main CH$_2$ scissoring band at 1468 cm^{-1} and terminal CH$_2$ rocking at 720 cm^{-1}. On the other hand, the intensity offset in the range $1450 - 1300$ cm^{-1} between the signal from AzoPC and DSPC is not yet explained, although it could be an artifact arising from the baseline correction (*cfr.* Appendix B.1 for a description of the baseline correction).

DFT calculated IR absorption bands

The DFT calculation can be very helpful in supporting the assignment of the absorption bands to the correct groups. With programs such as Gaussian, Avogadro or Molden, it is possible to animate the calculated vibrational modes responsible of every absorption line to recognize which group is involved in each mode. This allows us to confirm tentative assignments made by comparison with literature values.

It has to be considered that there are important differences in conditions: while the ATR lipids were measured in the condensed phase, assembled in a semi-hydrated bilayer, the DFT calculation was run on a simulation of a single lipid molecule in vacuum. Therefore all the inter-molecular interactions, the environmental effects and the steric constraints are ignored and will not contribute to the calculated vibrational modes. Nevertheless, the overlap and correspondence between the simulated and experimental spectra is striking. In Figure 3.8 the DFT calculated spectra are compared to the AzoPC spectrum of a dry film measured on the ATR. The frequency positions have been corrected as described in the Methods chapter, and more in detail in the Appendix B.4. The absorbance scale for the DFT calculated frequencies is arbitrary and therefore the intensities have been collectively scaled to match the C=O peak intensity at about 1740 cm^{-1}.
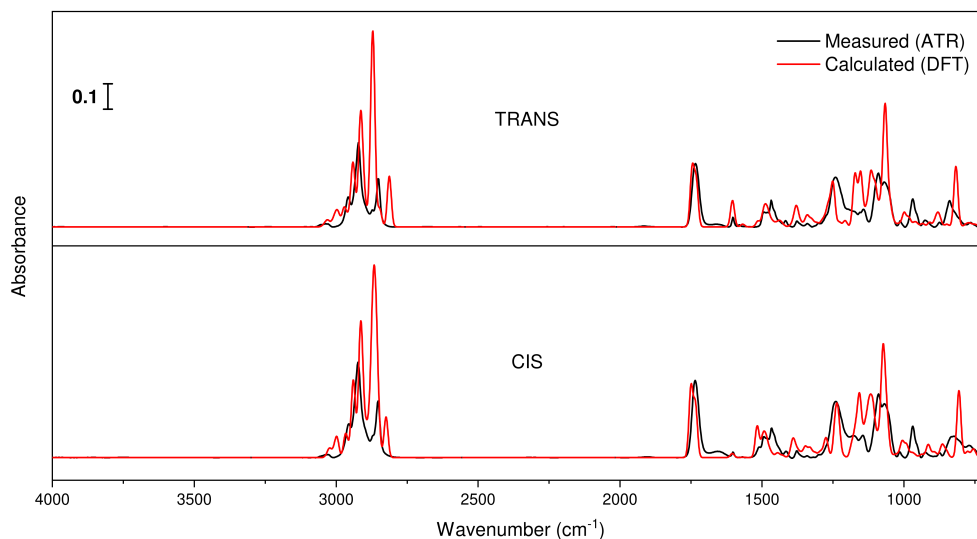
FIGURE 3.8: COMPARISON BETWEEN THE MEASURED AND THE CALCULATED SPECTRA OF AzoPC IN THE TWO ISOMERIZATION STATES. Overall, the agreement between the calculated and the measured spectra is satisfactory. In order to use the result of the DFT calculation to support our band assignment, each of the main calculated frequencies assigned from Gaussian was matched to a measured band. For details on the data analysis and the assignment, see Appendix B.4.

In the zoomed-in comparison (Figure 3.9) between ATR and DFT spectra in the amide I/amide II range, which will be relevant when treating the protein conformational changes, we can better identify the marker bands of AzoPC and their differences in the two conformational states. Around 1740 cm^{-1} two components of the C=O stretching vibration are clearly distinguished. It is important to notice that, while for the measured sample the two components come from the anhydrous and the hydrated populations of the esters as already discussed, the two modes calculated from a single AzoPC molecule in vacuum originate from the $sn-1$ (fully aliphatic) and the $sn-2$ (azobenzene-substituted) alkyl chains, respectively for the highest and the lowest wavenumbers.

The ring breathing modes at 1604 and 1514 (1516 for the *cis* state) cm^{-1} are matching very closely the experimental values. It is noticeable how, as recognised for the experimental spectra, the 1604 cm^{-1} band is more prominent in the *trans* state, while the 1516 cm^{-1} in the *cis* state. In fact, the latter is hardly detectable in the FTIR data of the *trans* state.

The band at 1488 (1492) cm^{-1} comprises two bands overlapped. One corresponds to the ring breathing mode found at 1496 cm^{-1} in the experimental spectrum, while the other one is the CH_2 scissoring mode found at 1468

51

cm^{-1}. The other two bands marked in Figure 3.9 at 1436 (1444) and 1379 (1390) cm^{-1} are coming from the CH$_2$ wagging absorptions. We notice how the CH$_2$ bands result upshifted in frequency with respect to the experimental values. We can expect such difference since these bands are sensitive to alkyl chain conformation and packing, which cannot be compared between the single simulated molecule and the real multilayer.
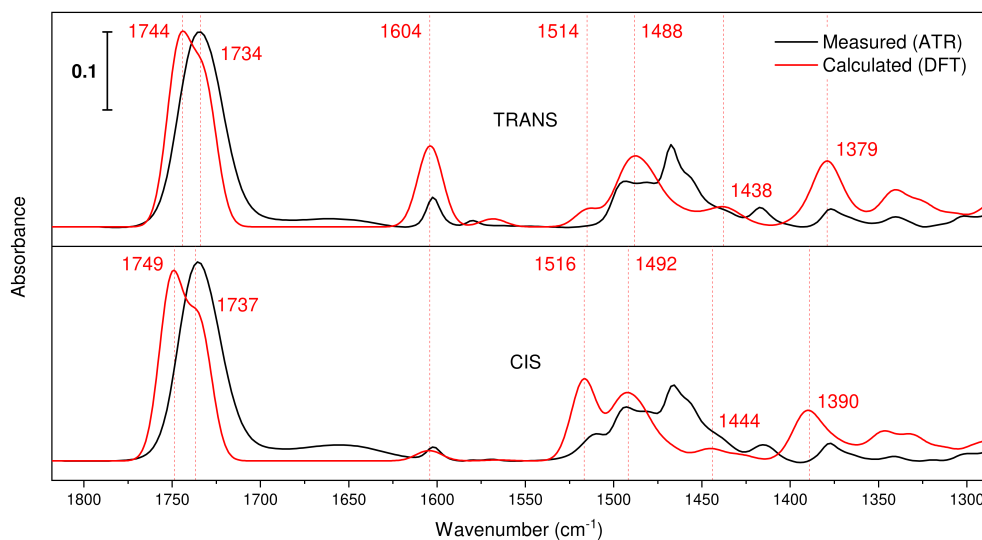

FIGURE 3.9: ZOOM-IN OF THE RANGE OF INTEREST $(1800-1300$ CM$^{-1})$ FOR THE MEASURED AND DFT CALCULATED SPECTRA OF AZOPC IN THE TWO ISOMERIC STATES. The DFT frequencies assigned to the marker bands of AzoPC are highlighted for easier comparison with experimental values from Table 3.1.

The assignment for all relevant bands is summed up in Table 3.1, cross-checked between literature values and DFT calculated frequencies.

Table 3.1: *Assignment of the main infrared absorption bands of AzoPC.*

ASSIGNMENT	FREQUENCY
$\nu_{as}(CH_3)$	2957 cm^{-1}
$\nu_{as}(CH_2)$	2922 cm^{-1}
$\nu_s(CH_3)$	2873 cm^{-1}
$\nu_s(CH_2)$	2852 cm^{-1}
$\nu(C=O)$	1735 cm^{-1}
N=N + ring $\nu_s(CC)$	1602 cm^{-1}
ring $\nu(CC)$	1580 cm^{-1}
N=N + ring $\nu_{as}(CC)^*$	1512 cm^{-1}
ring $\nu(CC)$	1496 cm^{-1}
$\delta(CH_2)$	1468 cm^{-1}
$\omega(CH_2)$ progression	$1200 - 1400$ cm^{-1}
$\nu_{as}(PO_2^-)$	1237 cm^{-1}
ring $\delta(CH)$	1140 cm^{-1}
$\nu_s(PO_2^-)$	1090 cm^{-1}
$\nu_{as}N^+(CH_3)_3$	970 cm^{-1}
$\nu_s N^+(CH_3)_3$	920 cm^{-1}
ring $\omega(CH)$	840 cm^{-1}
$\rho(CH_2)$	720 cm^{-1}

[*] It appears mostly in *cis* state, almost absent in *trans*.

3.1.4 Sample orientation on the ATR crystal

Using ATR-FTIR, it is possible to measure separately the absorption of the sample on the membrane plane or along the axis normal to it. Absorption bands that show dichroism, appearing with different intensities in the two polarizations, reveal a specific orientation of the dipole moment change associated with that absorption. To then extract meaningful information regarding the orientation of specific bonds in the sample, the relative direction of the dipole moment vector with respect to the lipid molecule coordinates is calculated with the DFT.

Experimentally, with the use of a polarizer as described in section 2.5.3, we can select a linear polarization of the probing IR light, recording the absorption spectra of the vibrations parallel and perpendicular to the plane of incidence separately. The intensities are then combined and rescaled, as explained in section 2.5.3, to adjust for the different electromagnetic fields in the lab frame (XY plane corresponding to the ATR surface, Z axis normal to it). For the DFT calculation the axes are defined with respect to the lipid molecule (see

Figure 2.12) and might diverge from the lab frame.

In Figure 3.10 we can compare the DFT spectral prediction with the experimental spectra. The calculated spectra show that the C=O stretching vibration at ~ 1740 cm^{-1} is almost completely ortogonal to the Z axis, defined as the sn-1 alkylchain main axis, in both isomers, as the band is absent in both Z polarized spectra. This is not the case for the spectra of the real membrane where the band is clearly present in both polarizations. The 1602 cm^{-1} band from the ring breathing mode is clear in both polarizations with almost a double intensity along the Z axis, only for the *trans* isomer. In the ATR spectra it seems to have a much clearer orientation along the Z axis for both states. The marker band characteristic of the *cis* isomer, the ring breathing mode at 1512 cm^{-1}, in the simulated spectra shows a major Z axis component.
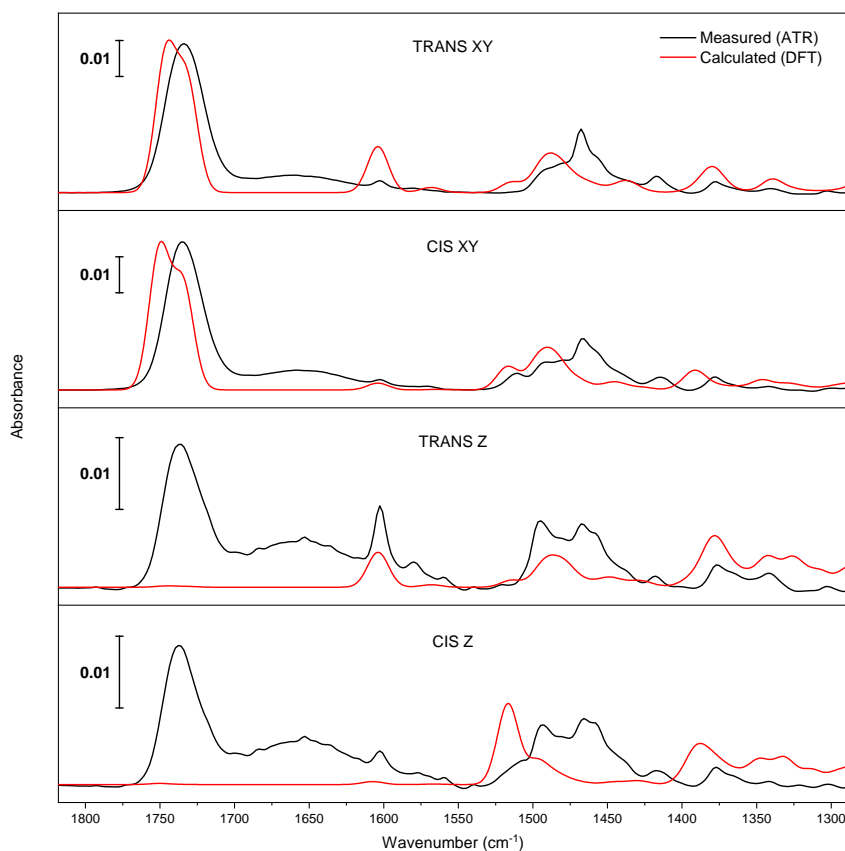

FIGURE 3.10:

We can then analyze the experimental data of the multilayer by overlaying the spectra in the two polarizations for each state. In the ATR polarized spectra (Figure 3.11), the AzoPC marker bands show a strong dichroism, indicating an oriented sample. In particular we can recognize the orientation of lipids in the multilayer as described in literature[115] for chloroform dried samples: the C=O band at 1734 (1738) cm^{-1} has a larger XY plane component than a Z axis one, as the ring breathing mode characteristic of the *cis* state at 1511 cm^{-1} and the CH$_2$ scissoring at 1468 cm^{-1}, whereas the ring breathing modes at 1603 and 1495 cm^{-1} have a larger Z component, particularly visible in the *trans* state. The reorientations happening upon isomerization are then better analyzed from the polarized difference spectra.
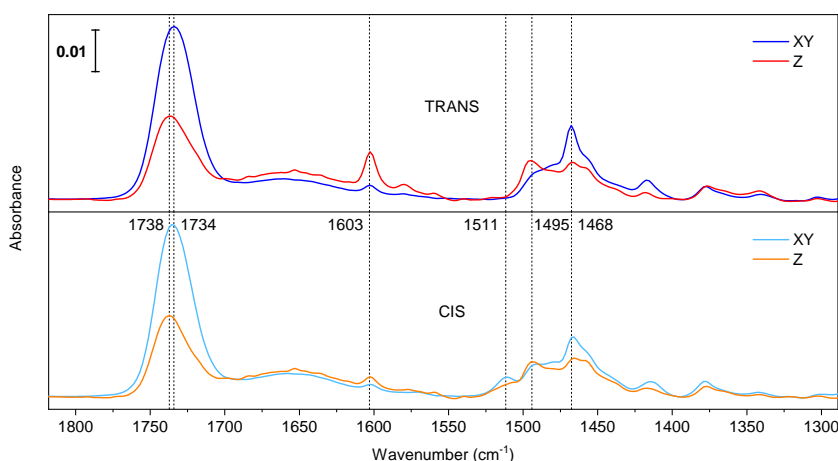

FIGURE 3.11: DICHROISM OF AZOPC ON THE ATR IN THE TWO ISOMERIZATION STATES. ATR absorption spectra of AzoPC in the *trans* and in the *cis* state comparing the two polarizations: XY for the plane parallel to the ATR surface and Z for the direction normal to it. The marker bands of AzoPC are highlighted with dashed lines.

3.1.5 Photo-switching the lipids: difference IR spectra between *cis* and *trans* isomers

The difference spectra between the two isomerization states of the photolipid reveal the changes in conformation occurring upon UV or blue light illumination. Combining several sources of information - our previous assignment, the orientation of the dipole moments from DFT and the comparison between the two polarizations - we are able to speculate how specific groups reorient during switching.

Reorientation of the lipid during photo-switching

In order to interpret the difference bands arising from the light-switching of AzoPC, it is convenient to consider the polarized difference spectra. In Figure 3.12 are reported the DFT-optimized structures for the *cis* and the *trans* form, to help the spacial visualization of the group rearrangements described in this section.
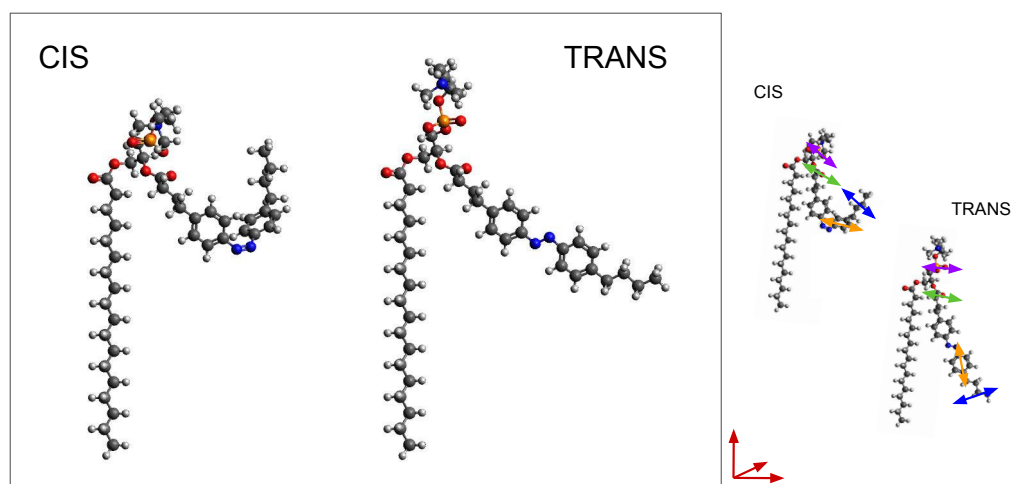

FIGURE 3.12: DFT-OPTIMIZED GEOMETRIES OF AZOPC AND HYPOTHESIZED REORIENTATIONS. In the frame on the left side, DFT-calculated geometries for a single AzoPC molecule in vacuum in the two isomerization states, *cis* and *trans*. In the right side, the modified structures as imagined for a lipid molecule sitting in a membrane with the arrows indicating the dipole moment orientations of the marker bands. Purple: PO_2^- asymmetric and symmetric stretching; Green: C=O stretching; Orange: phenyl ring breathing mode; Blue: CH_2 asymmetric and symmetric stretching. The left figures are just a help for the reader to visualize the reorientations described in the text, as the calculated structures are for single lipid molecules, but the measured spectra from condensed lipid matter. The arrows are based on the coordinate values of the dipole moments vectors calculated with the DFT.
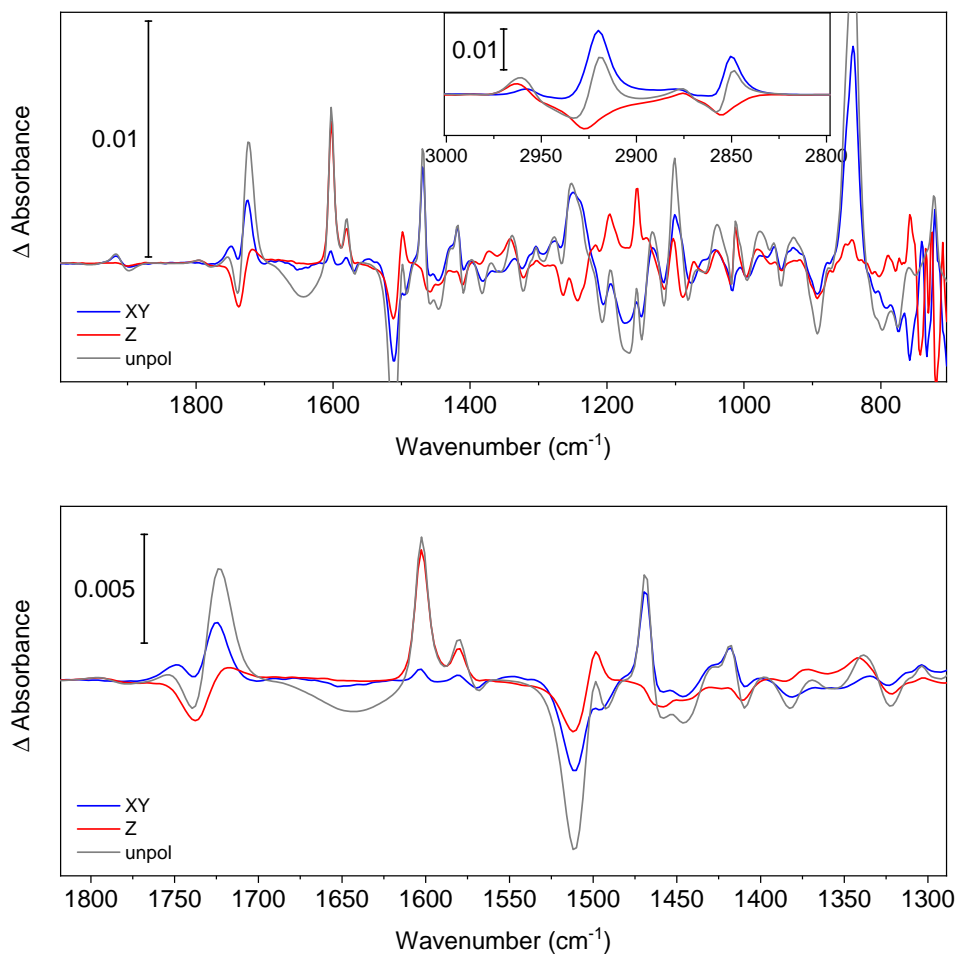
FIGURE 3.13: POLARIZED DIFFERENCE SPECTRA OF AZOPC. ATR difference spectra of AzoPC of the transition from *cis* to *trans*. In gray the non-polarized difference spectrum, in red the Z polarized and in blue the XY polarized. The lower panel is a zoom in the range of interest.

Starting form the methyl bands in the range 3000 - 2800 cm^{-1} (inset in the upper panel of Figure 3.13), we can already see some indirect signs of the azobenzene conformational change. Going from *cis* to *trans*, we observe positive bands for the XY component at 2919 and 2850 cm^{-1} and negative bands for the Z component at 2922 and 2852 cm^{-1}, previously assigned to asymmetric and symmetric CH$_2$ stretching. The dipole associated with these vibrations has a component along the Z axis for the *cis* state, since the sn-2 chain is bent and tilted with respect to the sn-1 chain, while it is laying almost entirely in the XY plane in the *trans* state. Therefore a loss of the Z component is appearing as negative bands, while the gain in XY as positive bands. The small shift to lower frequencies that can be observed in the XY polarization is compatible with a higher degree of order in the *trans* state than in the *cis*, where the packing is disrupted by the bent azobenzene.

Zooming in between 1800 and 1300 cm^{-1} (lower panel of Figure 3.13) we can focus on the AzoPC marker bands. The C=O band which was at 1735 cm^{-1} in the absolute spectrum shows some interesting shape in the difference spectrum. Going from *cis* to *trans*, a negative-positive differential shape appears in the isotropic spectrum. Following the assignment already discussed, such profile represents an increase in hydrogen bonding, since there is a clear decrease in the higher frequency component and an increase in the lowest. When this spectrum is decomposed into the two polarizations, it is clear that the negative band is coming from a larger part from the Z component, while the positive band almost completely from the XY component. We can therefore associate the reorientation of the C=Os during the *cis* to *trans* transition to a local hydration increase.

This is supported also by a comparison with data from the switching of a rehydrated sample measured in transmission (Figure 3.14). The difference spectra of AzoPC are overall very similar in the two hydration conditions and in the two geometries, air-dried and exposed to the ambient humidity, measured in ATR configuration, or rehydrated and sealed in a transmission cell. The major difference is the C=O band. When AzoPC is rehydrated (blue line), this band is positive, as for the ATR-measured dry sample, and it is still showing two components, but not showing the negative-positive shape. If we consider, from what can be learned from the ATR polarized spectra, that the higher frequency component is due to the reorientation of the C=O from a direction that had both XY and Z components to a position in the XY plane only, it is expected to see a positive band only, in transmission. This because an oriented sample in transmission would not absorb along the longitudinal axis, but in the transversal plane. Due to the orientation of the lipid, these correspond respectively to the Z axis and the XY plane, therefore the reorientation of the C=O groups is a net increase in signal in the transmission spectrum.
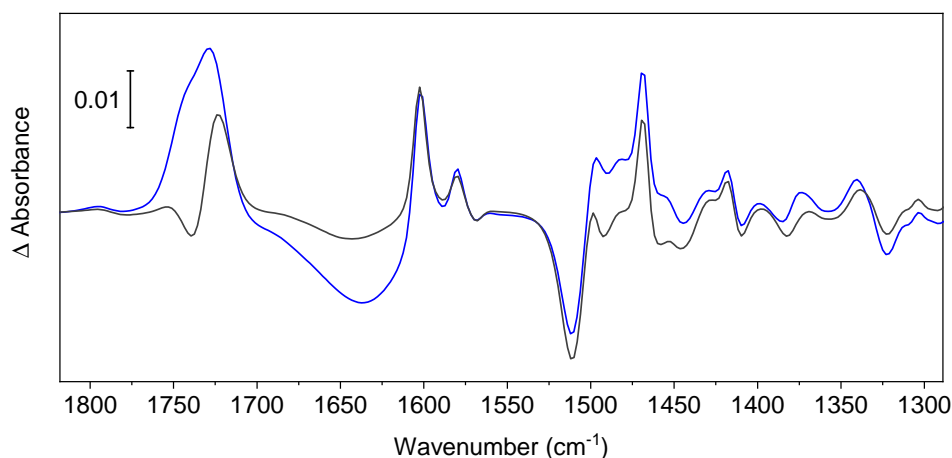
FIGURE 3.14: COMPARISON BETWEEN DIFFERENCE SPECTRA OF HYDRATED AND DRY AZOPC. Difference spectra of AzoPC switching from *cis* to *trans* measured in transmission for the hydrated sample (blue) *vs.* measured in ATR for the dry sample (black). The spectra are baseline corrected, keeping the liquid water signal intact, and the hydrated spectrum is normalized to the dry one at 1602 cm^{-1}.

About the phenyl rings of the azobenzene, we see an increase of the 1602 and 1580 cm^{-1} for both polarizations. From a comparison with the DFT calculation of the *trans* state, it is clear that each of these bands is actually an overlap of two normal modes very close in frequency, each band arising from one mode laying mostly along the Z axis and the other one having also a XY component. This is recognizable in the much larger increase in the Z spectrum in comparison with the XY. In the *cis* state the same modes are distributed differently and appear at different frequencies, 1512 and 1496 cm^{-1}, whose bands are in fact depleted in the *cis* to *trans* transition and appear as negative.

The band composition in terms of dipole orientations in the *cis* state is not simply shifted in frequency as a bloc: the first band arises from a vibration whose dipole has components along all axes, but the second one is laying purely in the XY plane. The relative negative bands are larger in the XY-polarized spectrum and are of lower intensity in the Z-polarized spectrum. In addition, the Z spectrum shows a positive band at 1498 cm^{-1} stronger than in the XY spectrum, an absorption of the *trans* conformation which has both XY and Z components. The overlap of these two effects gives rise to the observed band shape.

As for the mechanistic interpretation, we have to check how the dipole direction of these modes compares with the position of the rings in space. From the coordinates calculated with the DFT, all dipoles of the ring breathing modes observed here are in-plane. We can therefore describe the reorientation of the benzene ring in the *cis* to *trans* transition as going from an inclined

position with both XY and Z components, to an almost completely vertical position. This model is compatible with the dynamics described for the azobenzene substituted alkyl chain alone[145] and it would promote the H-aggregates in the *trans* state already hypothesized in literature.[144,150,151]

The band at 1468 cm^{-1} shows also a strong dichroism: in the *cis* to *trans* difference spectrum the XY polarized light shows a positive band, while this is absent from the Z spectrum. The vibration is well assigned to the scissoring mode of the CH$_2$ groups of the alkyl chains. Its relative dipole in the *cis* state for the sn-1 chain is fully oriented in the XY plane, which corresponds to the plane of the motion, and it does not change during switching.

Going back to the wider view (upper panel of Figure 3.13) to continue to lower frequencies, the head group reorients as well: we can see it from the dichroism of the difference spectra at the frequencies assigned to the PO$_2^-$ asymmetric and symmetric stretching vibrations, respectively at 1237 and at 1090 cm^{-1}. As calculated from the DFT, the Z component of the PO$_2^-$ stretching vibrations associated dipole is non-zero only for the *cis* state. When the lipid is in *trans* state, the dipole lays on the XY plane, coincident to the plane of motion of the vibration. Therefore in the *cis* to *trans* transition we observe a negative band for the Z component and a positive band for the XY component. Similarly to the CH$_2$ scissoring mode with respect to the molecular axis, the PO$_2^-$ stretching vibrations are perpendicular to the main headgroup axis. The loss of the Z component therefore signifies a verticalization of the headgroup. This is also visible in the framed part of Figure 3.12 as a change of angle between the headgroup axis and the molecular director of the single AzoPC molecule in the two states, being more aligned in the *trans* configuration.

Reversibility and reproducibility of the photo-switching

The switching is totally reversible: AzoPC, dried from chloroform on an ATR crystal, can be illuminated alternatively with UV or blue light for many times (> 50) without loss of signal and the difference spectrum in one switching direction is the mirror image of the one in the opposite direction (Figure 3.15). Being the switching totally reversible, the analysis on one switching direction can be transposed for the opposite direction. The analysis in this work was done on the *cis*-to-*trans* direction, since this transition corresponds to an increase in lateral tension and therefore also to the putative trigger for the opening of MscL.
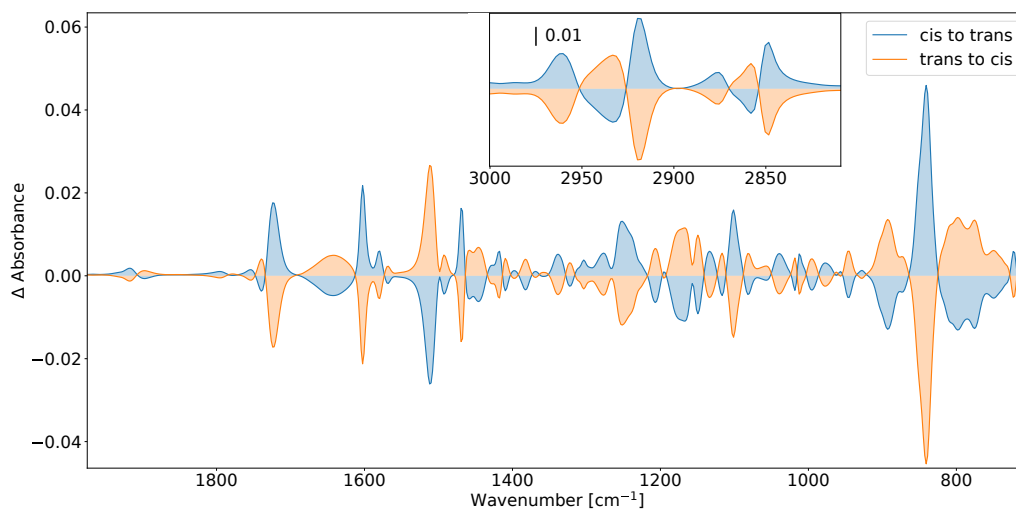
FIGURE 3.15: REVERSIBILITY OF THE SWITCHING. ATR difference spectra of AzoPC switching from *trans* to *cis* and viceversa. To be noticed is the reversibility of the switching, demonstrated by the mirroring shape of the difference spectra in the opposite switching directions.

The reproducibility of the switching is also confirmed: all spectra taken in the same conditions (lipids dried on ATR crystal from chloroform at room temperature) were averaged and the variance was calculated (Figure 3.16). The difference spectrum is extremely well reproducible.
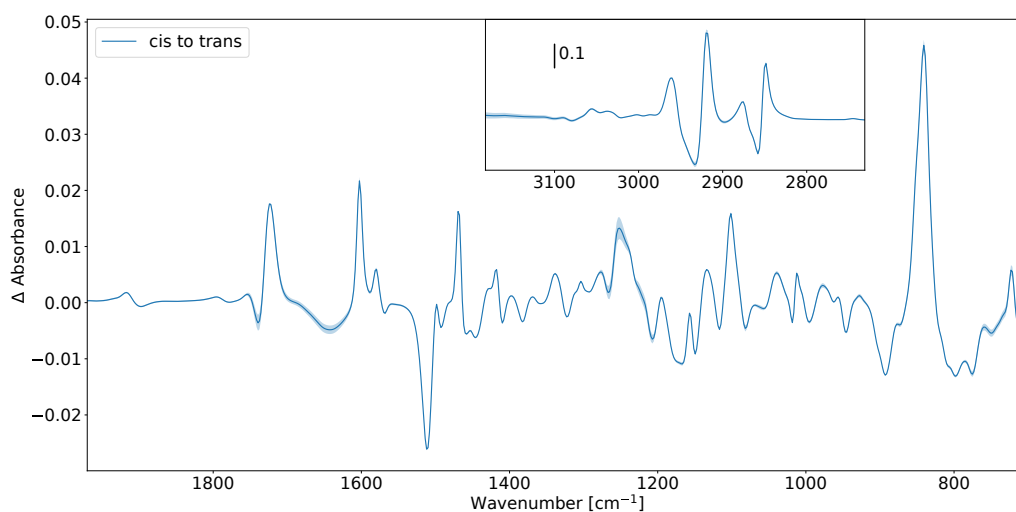

FIGURE 3.16: REPRODUCIBILITY OF THE SWITCHING. ATR difference spectrum of AzoPC switching from *cis* to *trans*, averaged over 7 switching cycles. The shaded area around the curve represents the variance. The azo-lipids were dried on the ATR crystal from chloroform at room temperature, in ambient conditions.

3.1.6 Infrared Reflection Absorption Spectroscopy

IRRAS offers the possibility to combine the monolayer rheology with the IR spectroscopy. Unfortunately, the sample on which the measurements were conducted was later revealed to be degraded and could not be repeated timely, therefore these data cannot contribute to this thesis' arguments. Nevertheless, something could be learned from the application of the method and therefore it is valuable to report the results on the degraded sample anyway.

Several parameters concur to determine the sign of the RA bands, as described in section 3.1.6 in the Materials and Methods chapter. Predicting the RA spectrum is helpful not only to more easily recognise characteristic features in the absolute spectrum, but also to correctly evaluate the difference bands: if a RA band is negative in the absolute spectrum, because of the already discussed band inversion, its behaviour in the difference spectrum should be interpreted accordingly (a negative difference band would mean an increase in intensity for that specific absorption, opposite to what we are used to understand from a usual FT-IR spectrum). The results of the simulation for the two polarizations is shown in Figure 3.17.
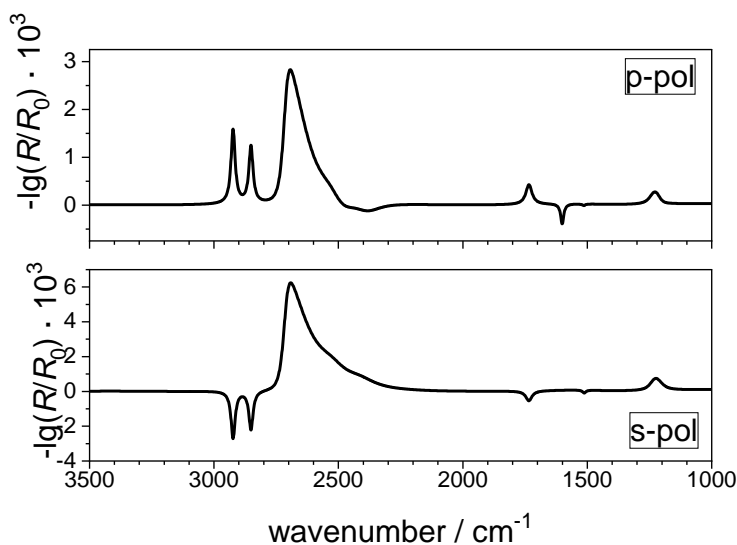

FIGURE 3.17: SIMULATED IRRAS SPECTRA OF AZOPC IN THE *TRANS* STATE. Results of a simulation run by Christian Schwieger of the RA spectrum of AzoPC in the *trans* state at $60°$ incident angle with *s*-polarized and *p*-polarized light. To be noticed is the sign inversion for some of the RA bands.

The expected absorption frequency, the transition dipole moment expected orientation, the extinction coefficient, the refractive indices, and the angle of incidence were given as parameters. In the *p*-polarized spectrum we expect

the AzoPC marker band from the ring breathing mode at 1603 cm^{-1} to be negative. In the *s*-polarized spectrum this band is not visible because we set the relative dipole moment orientation to be completely aligned with the Z axis, but the minor band at 1511 cm^{-1} set at an angle to the axis is visible and negative. For this polarization we notice that also the methyl bands and the ester stretching vibration would be inverted.

We designed the IRRAS experiment to investigate two main questions: what happens to AzoPC at different lateral pressures and how, starting from a lateral pressure of 30 mN/m, AzoPC reacts to the light-switch. To answer the first question, we recorded RA spectra of pure AzoPC during compression isotherms in the two isomeric states. The isotherms (Fig. 3.18) are very much comparable with what could be measured in Heberle's LB setup (*cfr.* Figure 3.2). The differences are attributed to the fact that the sample measured in IRRAS was probably different due to an unknown level of degradation that might have caused different packing dynamics.
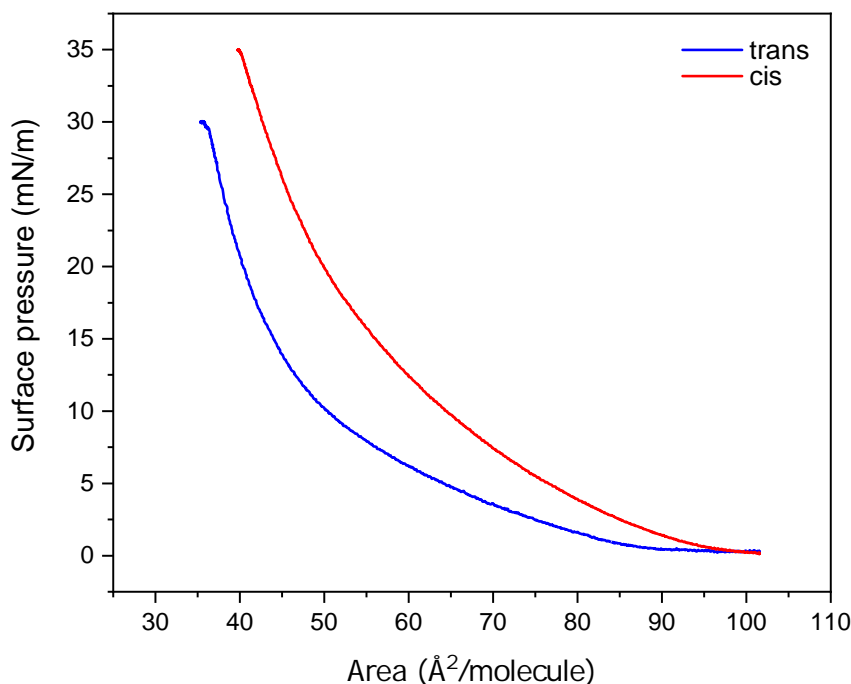

FIGURE 3.18: ISOTHERMS OF THE AZOPC MONOLAYER FROM THE IRRAS SETUP. Compression isotherms of AzoPC in the two isomeric states, taken under continuous illumination, UV for the *cis* state, blue for the *trans* state.

The RA spectra obtained at increasing lateral pressures are presented in

Figure (3.19). During compression of the monolayer, the lipid density increases and therefore increasing amounts of lipids are detected by the IR beam, so the RA signal of all bands increases. Even after data correction for the baseline and for the water vapour signals (see Appendix B.1), the spectra look very noisy in the amide region. The methyl bands though are well distinguishable and they are shown in more detail in Figure 3.20.
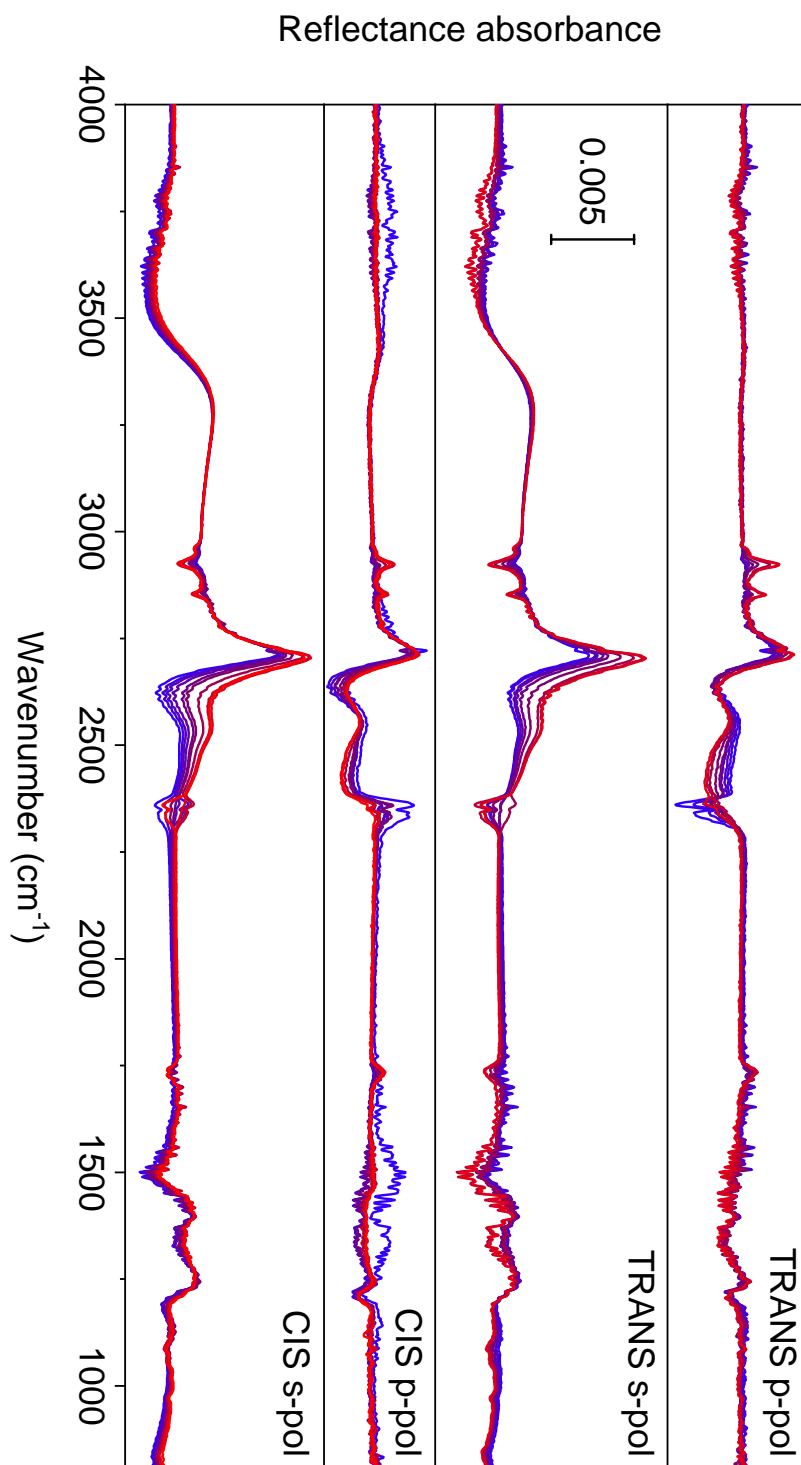
FIGURE 3.19: IRRAS SPECTRA OF AZOPC DURING FILM COMPRESSION. The spectra were taken starting from 0 mN/m (blue line), to 35 mN/m (red line), equally spaced in the area/lipid parameter. The corresponding lateral pressures are the same as the x axis coordinate of the data in Figure 3.21.
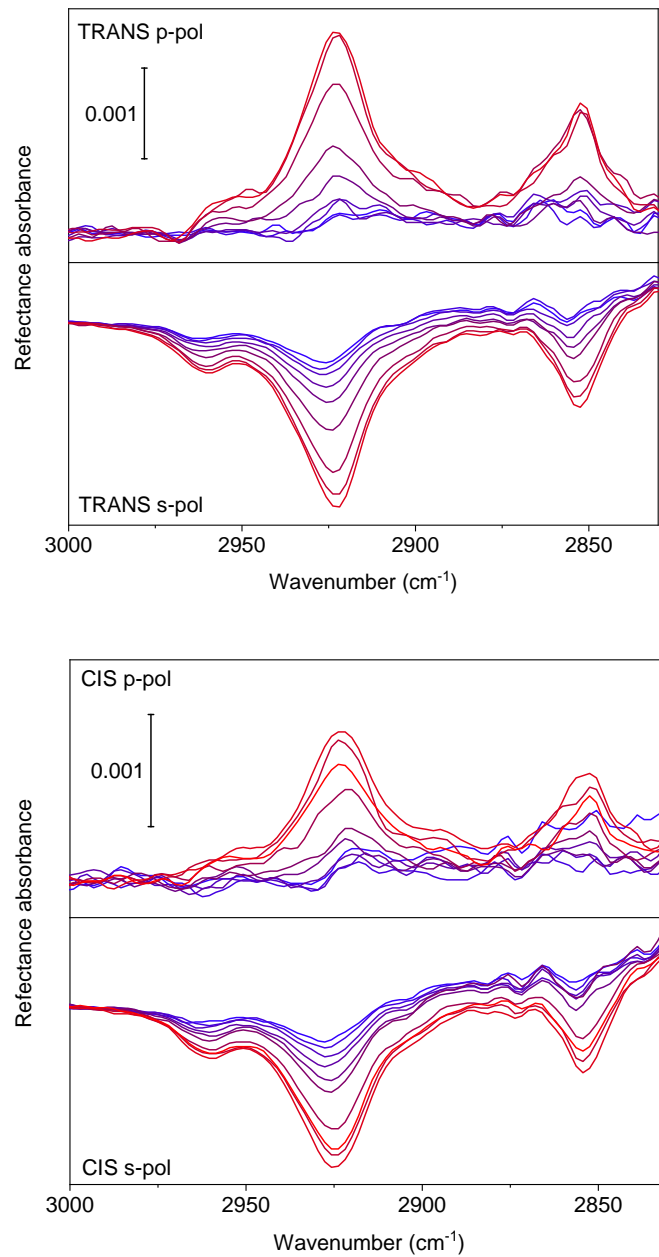
FIGURE 3.20: IRRAS SPECTRA OF THE METHYL BANDS OF AZOPC DURING FILM COMPRESSION. Zoom in of Figure 3.19 in the methylene region of the spectrum. The s-polarized data are inverted, as predicted from the simulation (3.17) based on the Kuzmin-Michailov equations.

For the CH_2 asymmetric stretching vibration bands, the increment in intensity is combined with a peak shift (Figure 3.21). From the data of the *s*-polarized light, as the lipids gets pressed together and pass from a 2D gas phase to a more ordered condensed phase, the increase in packing density is

reflected in a decrease of the wavenumber. Moreover, at higher lateral pressures, the *trans* state shows to reach higher packing than the *cis* state, reaching lower wavenumbers when compressed. The noise in the p-polarized data does not allow for the same analysis as the error on the peak positions of the fitting gaussians is larger than the potentially observable shift.
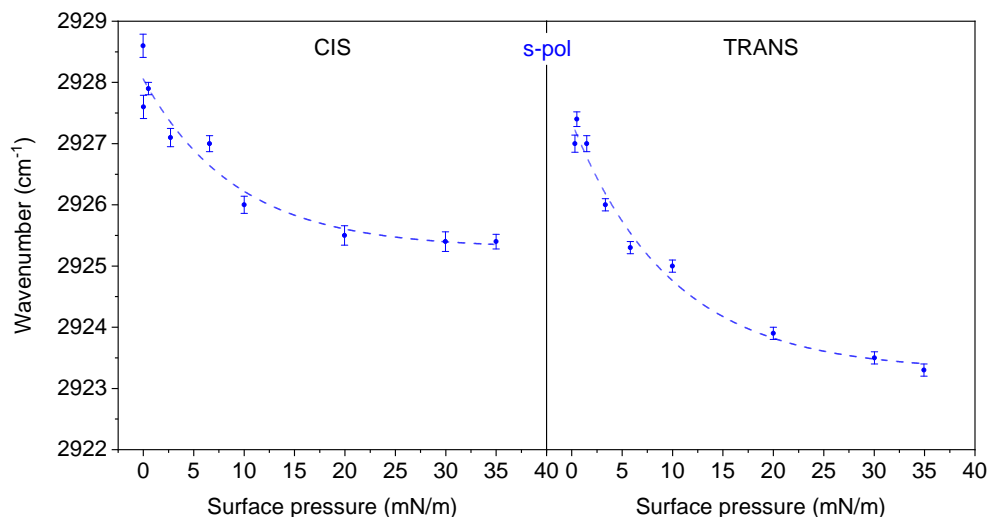

FIGURE 3.21: FREQUENCY SHIFT OF THE CH_2 ASYMMETRIC STRETCHING PEAK WITH COMPRESSION. During compression, with increasing lateral pressure and packing density, the absorption wavenumber of the CH_2 asymmetric stretching maximum shifts to lower energies. This is very clear for the *s* polarization (the dashed lines are just a guide for the eye), but it cannot be observed for the *p* polarization. The error bars represent the error of the peak position in the fit of a gaussian curve to the CH_2 asymmetric stretching absorption bands.

Even though the absolute RA spectra could not clearly show the marker bands in the amide frequency region, by calculating difference spectra between the *trans* and the *cis* states it was possible to recognize some familiar features that could hint to an answer to our second question, regarding the AzoPC response to light-switching. This was achieved by repeatedly switching UV and blue light in cycles of 10 minutes and recording the spectra to be subtracted in the two pressure extremes. Experimentally, it was done as follows: to prepare the film with AzoPC in the *cis* state, first a compression isotherm was run during UV light illumination; the barriers were then locked when 35 mN/m were reached; by alternating blue and UV light illumination, the AzoPC monolayer was switched between the two states. The lateral pressure was monitored and single-beam spectra were recorded at each cycle in the conditions indicated by black dots in Figure 3.22.
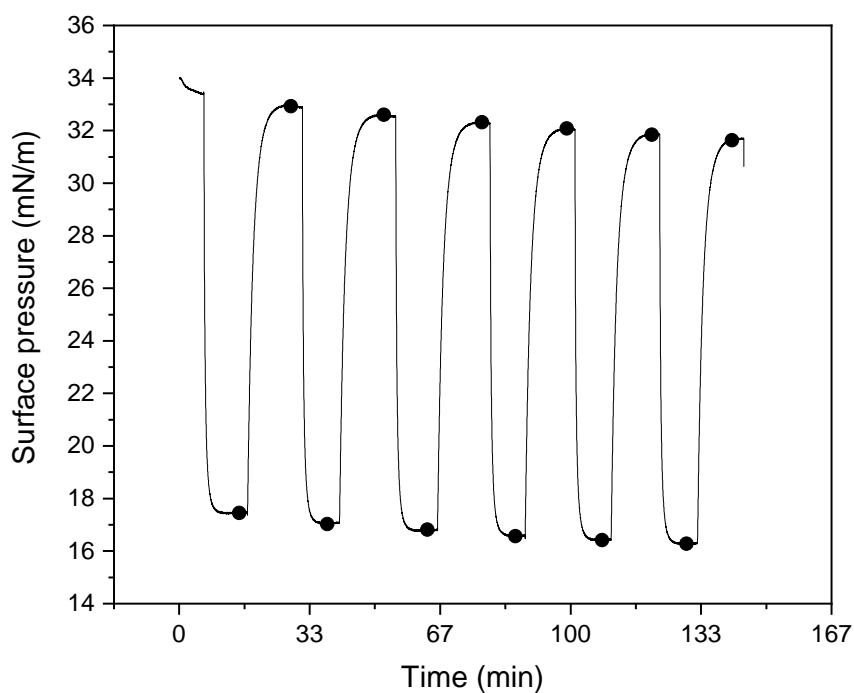
Figure 3.22: Lateral pressure changes during the light-switching of an AzoPC monolayer. The isomeric state of the AzoPC monolayer was switched by cycles of alternating UV and blue light illuminations of 10 minutes. The black dots represent the conditions in which the single-beam spectra were recorded, in order to calculate difference spectra of the switching behavior.

RA difference spectra were calculated by taking the single-beams pairwise for the *cis*-to-*trans* transition and pairwise but shifted by one spectrum for the opposite transition. A very strong background due to the D$_2$O substrate distorts the spectra. In the difference spectra of the *s* polarization (Figure 3.23) we could not witness any mirrored signal when comparing the two light-induced transitions.

FIGURE 3.23: S-POLARIZED DIFFERENCE SPECTRA OF AzoPC MONOLAYER LIGHT-SWITCHING. The difference spectra of the light-switching of the A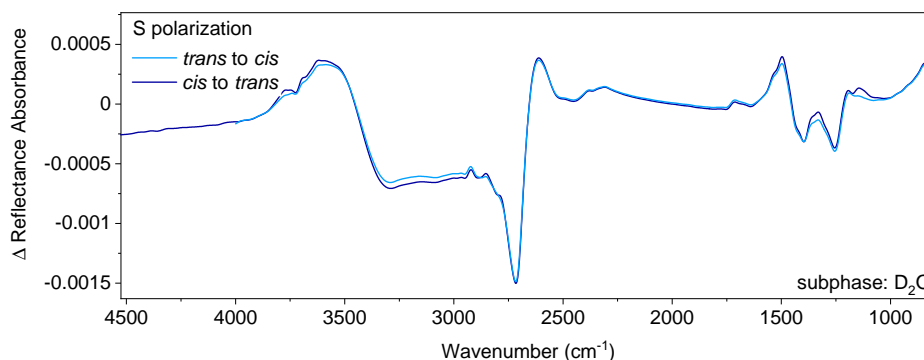zoPC monolayer in the s polarization are extremely distorted from the baseline due to the D_2O substrate and residual H_2O absorptions. No mirroring signal can be observed in the opposite transitions. No baseline correction was applied, as the inclusion of some spectral features in the baseline would have been an arbitrary choice, without improving the data.

For the *p* polarization (Figure 3.24), although the noise is visibly stronger, the methyl bands show some mirrored behaviour as well as the AzoPC marker bands. If we compare these spectra to the ATR polarized difference spectra, we would expect some similarity between the IRRAS *p*-polarized and the ATR Z-polarized. The CH_2 asymmetric and symmetric stretching bands, respectively at 2924 and 2852 cm^{-1}, and the ring breathing mode at 1603 cm^{-1} appear inverted with respect to the relative (*cis*-to-*trans*) ATR difference spectrum. In the case of the ring breathing mode the inversion is to be expected: the band was inverted in the absolute reflection absorption spectrum *per* simulation and therefore it appears as behaving oppositely in the difference spectrum.

3.2 Light-induced gating of MscL

The activation of MscL with light through the action of AzoPC has been investigated under different conditions and with several methods. The opening of the ion channel upon illumination has been confirmed by electrophysiology and through fluorescence detection (section 3.2.1) and the effects of light-switching the membrane on the protein were observed in a bilayer system *via* IR spectroscopy (section 3.2.2). Spectroscopic knowledge on the light switching of the system and of its consequential effects on the protein could provide relevant details on the protein-lipid interaction and the gating mechanism. Together with the extensive structural and functional information available on MscL, we could build a working model of the system. Here we present the seminal work on MscL light-activation.
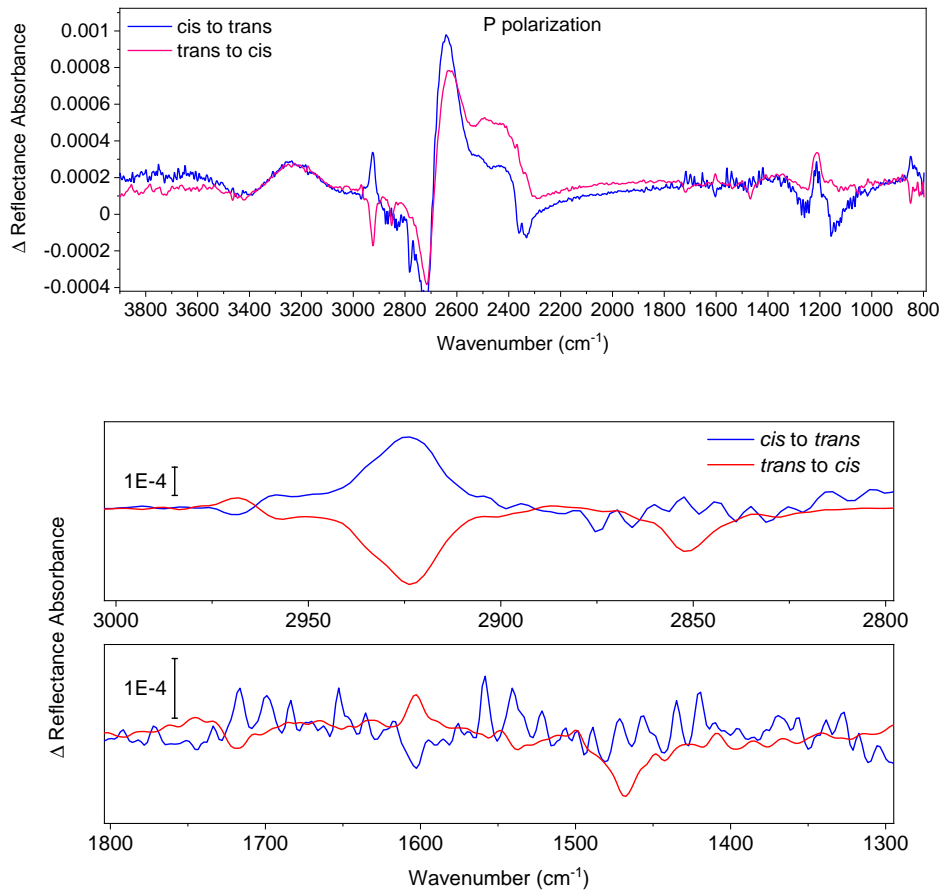
FIGURE 3.24: P-POLARIZED DIFFERENCE SPECTRA OF AZOPC MONOLAYER LIGHT-SWITCHING. The difference spectra of the light-switching of the AzoPC monolayer in the p polarization are extremely distorted from the baseline due to the D_2O substrate and residual H_2O absorptions. A mirrored signal can be observed in the opposite transitions for the main methyl band at 2923 and at 1603 cm^{-1}, enlarged in the two lower panels. No baseline correction was applied to the full spectrum, as the inclusion of some spectral features in the baseline would have been an arbitrary choice, without improving the data. A baseline correction was applied locally in the two zoomed-in ranges.

3.2.1 Functionality tests on MscL

Electrophysiology

Before including MscL in the free standing lipid bilayer, the photo-sensitive membrane was tested for stability and permeability under switching blue/UV light. A mixture of 20:80 mol of AzoPC:DPhPC in hexane was used to paint the bilayer on the cell. A costant voltage of 20 mV across the bilayer were applied. As shown in Figure 3.25, no current is recorded upon light-switching of the photo-sensitive membrane. This means that not only the mixed lipid bilayer is stable under such voltage, but also that the light switching does not induce any leakage current.
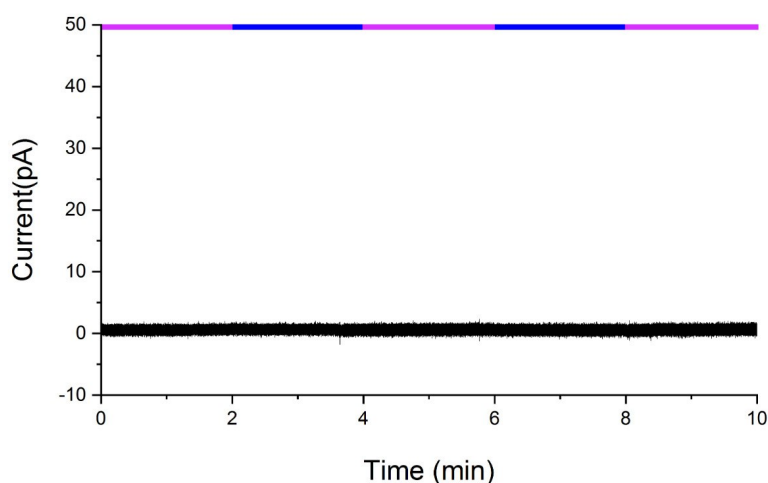
FIGURE 3.25: PERMEABILITY TEST OF A PHOTOSENSITIVE FREE STANDING BILAYER UPON LIGHT SWITCHING. Applied voltage: 20 mV.

We could then proceed with the insertion of MscL in the photoswitchable bilayer, safely assuming that any current signal we might observe would be related to the presence of the ion channel in the bilayer. MscL was transferred to the same free standing lipid bilayer with the help of nanodiscs. The ion channel was reconstituted in POPC nanodiscs and the solution was added to the pre-formed bilayers. The bilayer is exposed only to UV light during the painting process and for the following 10 minutes. The AzoPC is then in the *cis* state, corresponding to the highest lateral pressure, or the lowest tension conditions for the membrane.

The incubation then happens in the dark and it takes about half an hour. The ion channel, if not subject to tension, is in its closed state and it does not show any current by insertion. The only way to know if MscL correctly

71

inserted into the free standing bilayer is to activate the channel, either by osmotic shock or with light. We cannot exclude that the protein was not yet inserted when the triggering osmotic shock or blue light illumination started, and that maybe it is the alteration of the lipid membrane what facilitates the protein insertion. On the other hand, we have never witnessed a current without any trigger, which let us exclude an insertion of MscL in the open state.

First, and as a control, the gating of the ion channel can be induced by local osmotic shock, similarly to what triggers MscL in nature. Induced by the strong difference in osmolarity between the two sides of the bilayer, the channel opening is obtained by gently pipetting 10 μL of pure water close to the upper side of the bilayer. Immediately after the water addition and for some seconds afterwards, channel activity is observed, until an equilibrium is reached again in seconds and the current stops.

Similarly, the activity can be induced with light. When the membrane containing AzoPC in the *cis* state is illuminated with blue light, the isomerization to *trans* reduces the footprint of AzoPC lipids, increasing the lateral tension in the bilayer. After 5 to 10 seconds, activity from the channel can be observed as current flowing across the membrane. Two examples of such current traces are in Figure 3.26.
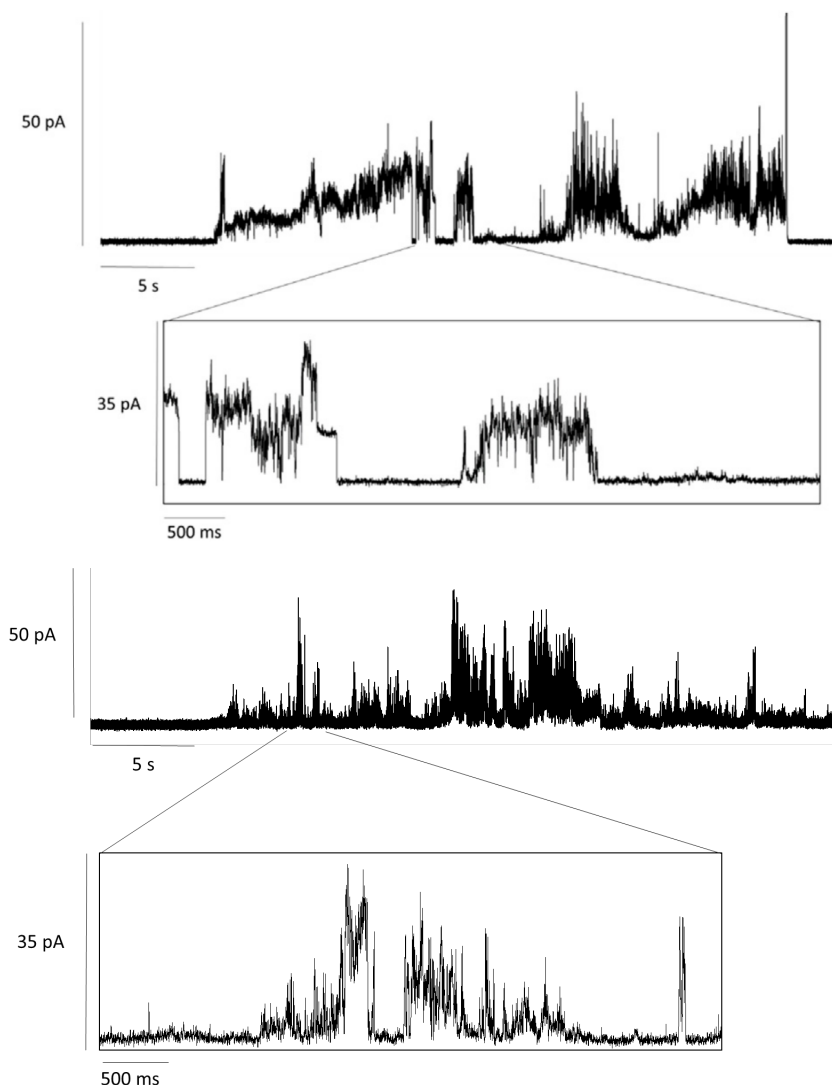
FIGURE 3.26: CURRENT TRACES OF MSCL LIGHT ACTIVATION. Single channel recordings of MscL light activation in a free standing lipid bilayer containing 20% AzoPC and 80% DPhPC. Closed MscL was reconstituted from POPC nanodiscs while the AzoPC component of the bilayer was in the *cis* state. From the beginning of the traces and for all shown duration, a continuous blue light was turned on to induce the channel opening. A tension of 20 mV was constantly applied.

The opening events do not show one clear-cut current level for a well defined conducting state, but more of a distribution of current intensities. In the statistical analysis we reported in our publication[146], we identified the presence of a single protein per electric channel, with a first conducting state at 16 pA. Following the simple Ohm's relation $V = I \cdot R$, where $V = 20$ mV is the applied voltage and $I = 16$ pA is the measured current, we can calculate a resistance $R = 1.25$ GΩ, corresponding to a conductance $C = 1/R$ of 0.8 nS. From the same principle, for a fully open state of 3 nS, when applying 20 mV,

we would expect to see a current of 60 pA.

Calceine efflux

The system, MscL in AzoPC, was investigated at work in proteoliposomes. With the calcein efflux assay it could be demonstrated that calcein can be realeased from proteoliposomes of AzoPC and MscL by illumination with blue light.

Calcein loaded proteoliposomes were carefully prepared in the dark or under intermittent UV illumination to maintain the photolipids in the higher lateral pressure state, the *cis* state. After recording a baseline fluorescence for some seconds, the proteoliposomes were illuminated with blue light and the intensity of fluorescence was tracked over time. Finally the liposomes were disrupted by addition of Triton X-100, a detergent. The recording of the experiment is reported in Figure 3.27, compared to a control run done in the same conditions but with natural non-photoactive lipids, DOPC.
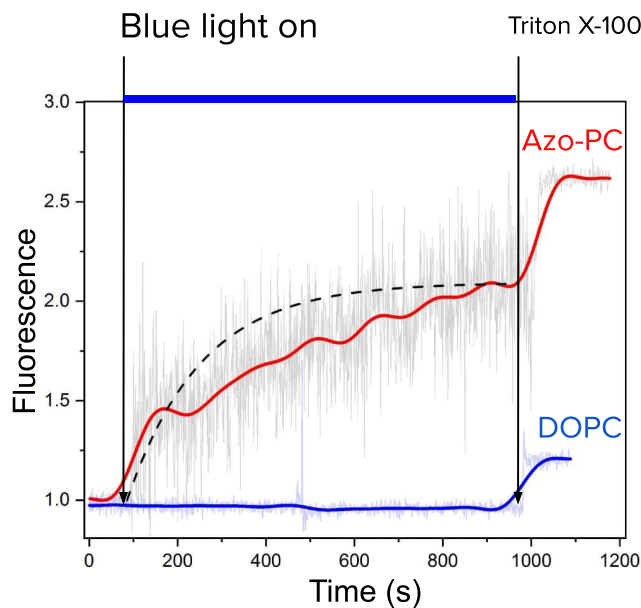
FIGURE 3.27: CALCEIN EFFLUX ASSAY. Fluorescence intensity over time: in red AzoPC sample of MscL proteoliposomes, overlayed in black the exponential fit, in blue the control experiment with natural lipids instead, 1,2-dioleoyl-sn-glycero-3-phosphocholine(DOPC). At $t = 100$ s the blue light is turned on, at $t = 1000$ s the liposomes are dissolved with a detergent, Triton X-100.

When the sample is exposed to the blue light, the absorption of the azoben-

zene induces the isomerization from *cis* to *trans* in the photolipids, then the lateral pressure in the bilayer drops and the generated tension pulls MscL open, releasing the calcein. The control experiment with MscL in DOPC show that the liposomes are intact until addition of detergent, therefore *azo*-lipids definitely play a role in the calcein release. Two major controls are still missing: to exclude that the lipids itself do not create pores in the membrane, the same experiment should be run on AzoPC liposomes in absence of MscL; and even if that control shows no leakage upon illumination, another control experiment should be run substituting MscL with a non-mechanosensitive membrane protein. It could as well be that, even in the case the bilayer itself does not create pores, the membrane detaches from the protein creating some ruptures at the lipid-protein interface.

Due to the technical challenges posed by this experiment, reproducing these results is difficult (further results of repetitions of the same experiment can be found in section 2.2.2 in Appendix C.2) and only with more control experiments it would be possible to claim with confidence that the blue-light-induced tension in the membrane lets the calcein out of the liposomes through the MscLs, excluding other interpretations of the data, such as pore formation between the protein and the bilayer.

3.2.2 IR spectra of MscL

The FT-IR spectroscopy on MscL was carried out in different environments for the ion channel. After expression, for the purification process, the membrane protein gets solubilized in the aqueous buffer by addition of a detergent, dodecyl maltoside (DDM) in this case. This substitutes the natural lipids that were encircling the protein and it provides an alternative form of hydrophobicity/hydrophilicity mediation to keep the membrane protein in solution.[98,152] In order to measure MscL in an environment closer to its natural one and to allow for the light-triggering, the ion channel was reconstituted back into lipidic systems, as described in the Materials and Methods chapter. It is known that membrane protein functions can be altered depending on their environment.[153,154] The systems considered for this work are micelles, liposomes and nanodiscs. In Figure 3.28 we can see the comparison between the absolute spectra of MscL in all reconstitutions, where a nominal 50:50 molar ratio between AzoPC and POPC were used.
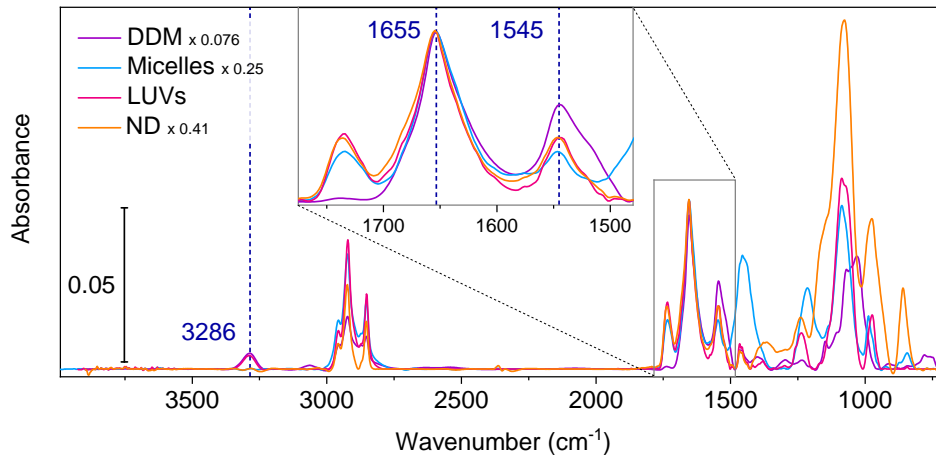
Figure 3.28: FT-IR spectra of MscL in different reconstitutions. Absolute spectra of MscL reconstituted in detergent (DDM) or in 50:50 AzoPC:POPC lipidic systems: micelles, large unilamellar vesicles (LUVs) and nanodiscs (ND). All spectra were normalized to the amide I band of the LUVs reconstitution by multiplication with the factors indicated in the legend. The inset shows a zoom in the amide I and II spectral range. The highlighted bands are respectively the amide A, the amide I and the amide II absorption bands.

All spectra are measured in transmission and they are all baseline corrected. The baseline correction removed the liquid water contribution between 3500 and 3000 cm^{-1} of the OH stretching mode, but not the sharper band of the O-H-O bending mode at 1640 cm^{-1} overlapping with the amide I band. LUVs and nanodiscs retained enough water after drying to avoid rehydration. Micelles instead were rehydrated with D_2O, as it's clearly visible from the shifted bending mode at 1454 cm^{-1}, which was also not eliminated by the baseline correction.

The presence of MscL is very clear from the amide bands, amide I at 1656 cm^{-1} and amide II at 1545 cm^{-1} (inset of Figure 3.28). These two bands confirm the α-helical nature of the secondary structure of MscL. Interestingly, also the amide A band is visible in the DDM and the LUVs reconstituted samples; it appears at 3286 cm^{-1}. It is probable that its presence in the other two spectra was hidden by the large OH water band and that it got removed by the baseline correction. This band corresponds to the absorption of the NH stretch and it is mostly uninfluenced by the protein backbone conformation, but it is sensitive to hydrogen bonding.[155,156] The position and shape of the amide bands is a good indicator of the folded state of the protein in the analysed sample. We must remember that, in the case of the nanodisc-reconstituted MscL, the scaffold protein contributes to the spectrum. Being the scaffold protein α-helical as well, its amide bands sum up indistinguishably to the ones from the MscL absorption.

Other distinctive bands are the CH_2 and CH_3 symmetric and asymmetric stretching vibrations, which here exhibit the characteristic absorption profile of alkyl chains, between 3000 and 2800 cm^{-1}. The lipids or the detergent are the molecules mostly responsible for this absorption, as presented in section 2.5.1.

In the range below 1300 cm^{-1} we can recognize the phosphate asymmetric stretching vibration at 1250 cm^{-1} from the glycerophspholipids, AzoPC and POPC. The last three bands at lower frequencies are coming from the absorption of the phosphate buffer (the spectrum of the buffer can be compared in Appendix B.6) and they obscure the fingerprint region.

The lipid composition in the micelle and liposome samples was varied: MscL was also reconstituted in 100% AzoPC and 100% POPC, the latter as a control. The absolute spectra can be found in Appendix B.7.

3.2.3 MscL isotropy on the ATR crystal

The main structural event occurring by the MscL gating is the tilting of the TM helices. It has been therefore hypothesized and then calculated that a channel opening of MscL would be visible with linearly polarized FTIR spectroscopy on a highly ordered sample.[157]

In an experiment from Arkin *et al.* in 1997, MscL reconstituted in DMPC vescicles, with a protein:lipid molar ratio of 1:100, was deposited on an ATR crystal and measured with linearly polarized FTIR.[40] They calculated an order parameter for the lipid bilayer and for the alpha helices and observed a net orientation of MscL in the dry lipid film. The order parameter, usually called S, is calculated as follows:[158]

$$S = \left(\frac{E_x^2 - R \cdot E_y^2 + E_z^2}{E_x^2 - R \cdot E_y^2 - 2E_z^2} \right) \left(\frac{3\cos\alpha^2 - 1}{2} \right)^{-1}$$

where E_x, E_y, E_z are the electric field amplitudes along the three axes already mentioned in section 2.5.3, $R = A_\parallel / A_\perp$ is the amplitude ratio for a specific band between the parallel and the perpendicularly polarized spectra with respect to the plane of incidence. The whole argument in the second brackets is the average tilt angle with respect to the membrane normal. In case of the calculation being applied to the amide I band, $\alpha = 38°$ is the angle between the main axis of the helix and the transition dipole moment.[158] To apply it to the CH_2 symmetric or asymmetric stretching mode of the lipids, whose vectors lay in the membrane plane, α is set at 90°. It must be noticed that the calculated S values are averages over the whole sample.

S ranges from 1, for an orientation along the membrane normal, to -0.5, for an orientation in the membrane plane. Reference values are $S = 0$ for isotropic samples and $S = 1$ for an ordered bilayer. They obtained a value of $S_{amideI} = 0.25$ for the amide I and $S_{CH_2} = 0.4$ for the CH$_2$ symmetric stretching mode of the lipids, corresponding to 45° and 39° tilt angle from the membrane normal respectively. They corrected the value for the amide I by assuming $S = 1$ for the lipids and obtained the new value of $S = 0.65$ for the α-helix. Albeit all this, they concluded to have observed a general net transmembrane orientation for MscL, admittedly not yet knowing how well this picture could represent all single helices in the protein. A year later the first X-ray structure of Mscl would become available.

With a very similar sample preparation, and with the strong dicroism observed for the pure AzoPC bilayer, we initally expected to have a similarly oriented sample. But, when looking at the absolute polarized spectra of MscL (Figure 3.29), the dichroism seems extremely reduced. The order parameter were computed as Arkin *et al.* did, calculating the intensity ratio from the parallel and perpendicular spectra (Figure 3.30), the electric field component as calculated for our setup and $\alpha = 38°$ for the amide I and $\alpha = 90°$ for the lipid band.[159] We obtained $S = -0.03$ for both the amide I and the CH$_2$ stretching, confirming a rather isotropic sample, as suspected from the XY and Z polarized spectra.

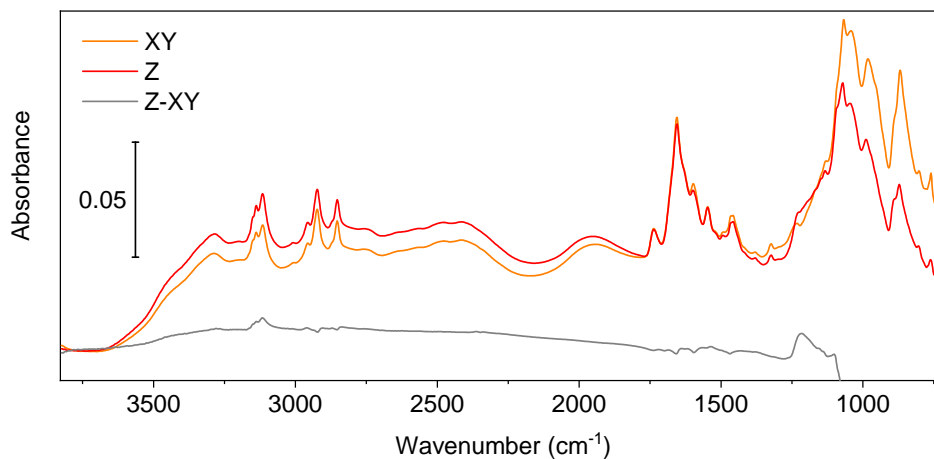FIGURE 3.29: XY AND Z POLARIZED SPECTRA OF MSCL IN MICELLES AND THEIR DIFFERENCE. Spectra in the XY and Z polarization have been computed from the raw perpendicular and parallel measured ones as described in the section 2.5.3 of the Materials and Methods chapter. No baseline correction was applied, not to alter the potential differences.

It is clear that a solution of multilamellar vescicles containing MscL, such

as the one used for the micellar sample, when dried on a surface, did not maintain an orientation. The presence of MscL did not allow for an ordered packing of bilayers, as observed from us for AzoPC and as it is known for other phospholipids instead.[123] The same results showing sample isotropy were obtained with the nanodisc sample. We therefore abandoned the idea of separating the MscL spectrum into the XY and Z components, at least for this work.
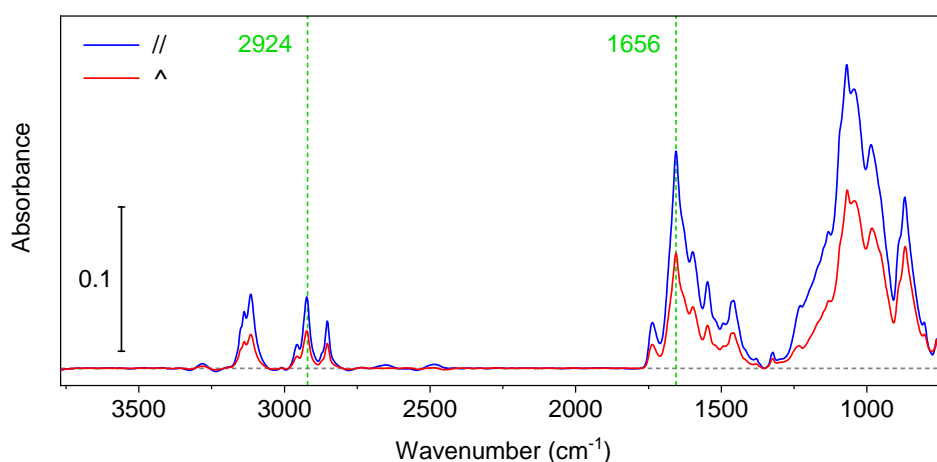
FIGURE 3.30: PARALLEL AND PERPENDICULAR POLARIZED SPECTRA FOR THE COMPUTATION OF THE ORDER PARAMETER. The spectra were baseline corrected to allow for a measure of the peak height, necessary to the calculation of the order parameter S. Highlighted in green are the two bands used: the asymmetric CH_2 stretching vibration and the amide I vibration.

3.2.4 Light-switching MscL: IR difference spectra

Finally, to all MscL reconstitutions introduced, light switching was applied and difference spectra were collected (Figure 3.31). In the amide I frequency range, a reversible spectroscopic feature appears in the spectra of all MscL samples containing AzoPC, although with some differences in each sample. This signal is absent in the non-light-sensitive samples containing only POPC lipids, or in the spectra of identical micelles and liposomes sample preparations, not containing MscL (data not shown).
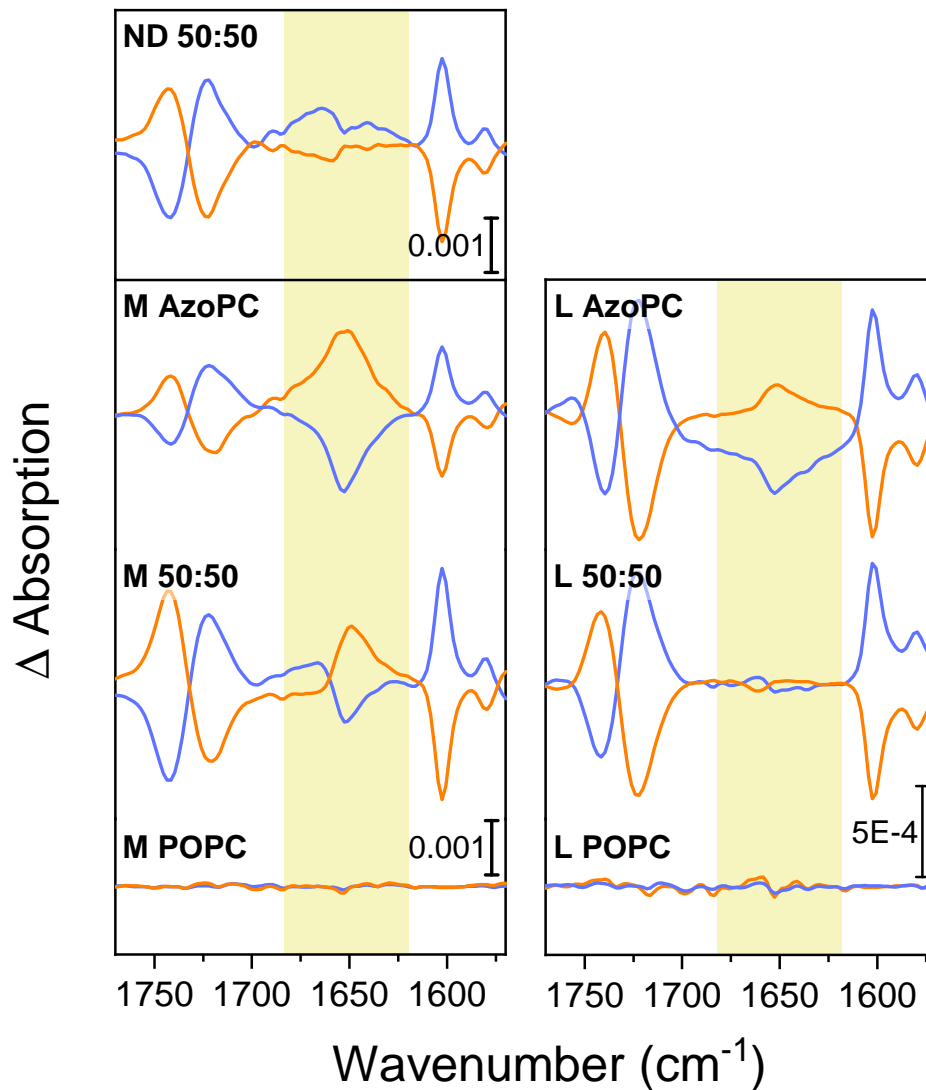
FIGURE 3.31: DIFFERENCE SPECTRA OF THE LIGHT SWITCHING OF MscL IN VARIOUS RECONSTITUTIONS. Blue lines indicate a *cis* to *trans* transition, orange the opposite, as it can be recognized from the sign of the AzoPC marker band at 1603 cm^{-1}. ND = Nanodiscs, M = Micelles, L = Liposomes. The lipid composition was varied between 100% AzoPC, 50:50 molar ratio AzoPC:POPC, and 100% POPC. The yellow region highlights changes in the amide I frequency range. Nanodiscs and liposome samples were dried and have not been rehydrated, since they retain water. Micelles have been rehydrated with D$_2$O. All spectra are the average of 7 switching cycles (more on the reproducibility of MscL light swtching can be found in Appendix B.9).

In correspondence with the *cis* to *trans* transition of AzoPC, this signature

of a change in the protein backbone structure is characterized by a negative dip at 1653 cm^{-1} and an opposite - more or less intense - knee at 1660 cm^{-1}. The signs are reversed for the opposite transition. The intensity of this signal depends on the portion of AzoPC lipids in the specific reconstitution, being larger in the 100% AzoPC samples and smaller in the 50%.

When compared to AzoPC (gray line in Figure 3.32), the pure lipid difference spectrum in the amide I frequency range shows a broad and smooth band, which we have seen depends on hydration (*cfr.* Figure 3.14), with the same sign as the main peak at 1653 cm^{-1}. Therefore, the amide I feature visible in the MscL samples is indeed a positive-negative differential shape, stretched in the direction of the 1653 cm^{-1} peak by the AzoPC broad band. In the nanodisc sample, where this AzoPC contribution seems to vanish, the differential shape is more pronounced. Such an amide I band shift could indicate, for α-helices, a stronger hydrogen bonding in correspondence of the higher lateral pressure state of the membrane, the *cis* state of AzoPC.
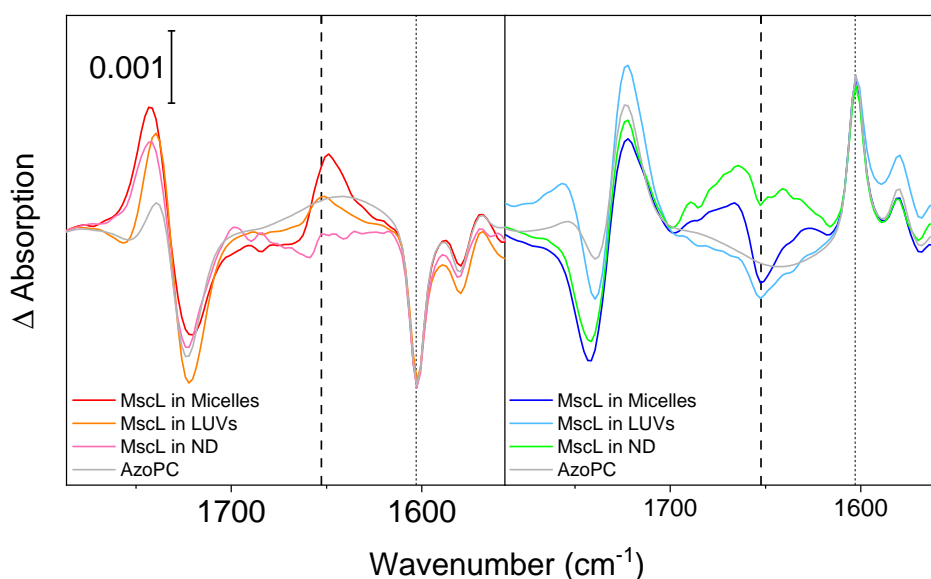
FIGURE 3.32: OVERLAY OF DIFFERENCE SPECTRA OF MSCL IN DIFFERENT RECONSTITUTIONS WITH THE DIFFERENCE SPECTRUM OF PURE AZOPC. Left panel: *trans* to *cis*. Right panel: *cis* to *trans*. All spectra are normalized to the AzoPC ring mode at 1603 cm^{-1} (dotted line) of the nanodisc with factors 1.85 for the micelles, 3 for the liposomes, and 0.1 for the pure AzoPC. The dashed line is a reference for the eye at 1653 cm^{-1}.

Differently from the micelles and liposomes controls, when testing the control sample for the nanodiscs, nanodiscs which do not contain any MscL,

we can also see a similar amide I differential shape (Figure 3.33), although not as clear, especially in the *trans* to *cis* direction of switching. When the empty nanodisc difference spectrum is subtracted from the MscL-containing nanodisc spectrum, we observe a clear large band, opposite to the one observed in pure AzoPC. This is the IR signature of MscL response to the light-induced change in lateral pressure in the nanodiscs.
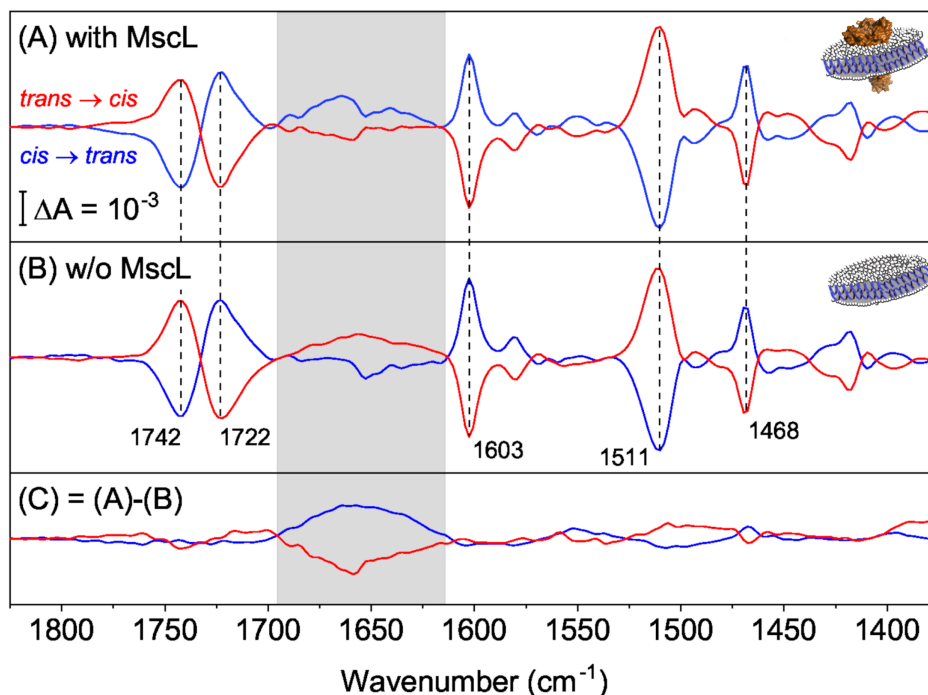
FIGURE 3.33: DIFFERENCE SPECTRA OF THE LIGHT SWITCHING OF MSCL IN NANODISCS. Difference spectra of nanodiscs with AzoPC:POPC in 50:50 molar ratio, in the presence (A) and in the absence (B) of MscL (blue for the *cis* to *trans* switching, red for the *trans* to *cis*). Vertical dashed lines indicate marker bands for the isomerization of AzoPC. In (C), double-difference spectra calculated by subtracting the difference spectrum of empty nanodiscs (B) from the one with MscL (A). The grayed area highlights the amide I range. Insets) A diagram of a nanodisc with (A) and without (B) MscL reconstituted. The ion channel is in orange, lipids are in white and the scaffold proteins in blue. Published figure.[146]

Nanodiscs contain the α-helical scaffold protein MSP1D1, which is also affected by the lateral pressure change in the bilayer. In order to confirm that the scaffold protein reacts to the light-induced lateral pressure change, my colleague Aoife Redlich has measured in the same conditions a sample of empty nanodiscs where the scaffold protein was isotopically labelled with ^{13}C. She could identify the contribution of the scaffold protein to the difference spectrum. The results (Figure 3.34) show a clear red shift from 1653 to 1613

cm^{-1}, compatible with the ^{13}C labelling.

FIGURE 3.34: SHIFT IN THE DIFFERENCE SIGNAL OF AMIDE I DUE TO ^{13}C LABELLING OF THE SCAFFOLD PROTEIN. ATR light-triggered difference spectra of labelled and unlabelled nanodiscs containing 80% DPPC and 20% AzoPC. The spctra were normalized at 1603 cm^{-1}, the AzoPC ring mode marker band. In black, the difference spectrum of nanodiscs with MSP1D1 scaffold protein, in blue with the ^{13}C labelled MSP1D1. Published figure.[160]

We are therefore confident that part of the smaller differential-shaped signal in the amide I range comes from changes to the backbone of the scaffold protein and part of it from MscL, as it is visible also in micelles and proteoliposomes, which do not contain protein other than MscL.

3.2.5 AzoPC as a lateral pressure light-induced trigger in nanodiscs

When looking at the difference spectra of MscL (Figure 3.31), left to the amide I range we find the carbonyl range with a symmetric bilobed differential shape. What could be observed from the pure AzoPC lipids light-induced difference spectra, was an asymmetric bilobed differential shape (*cfr.* Figure 3.13 in the section about AzoPC lipids). The direct comparison can be better appreciated in the overlay in Figure 3.32, where the intensity ratio between the two lobes is clearly in favour of the lower frequency lobe whereas the MscL reconstitutions have very similar intensities between the lobes.
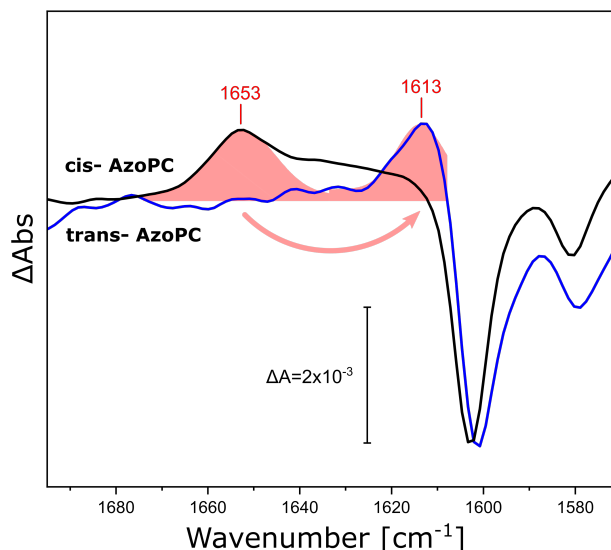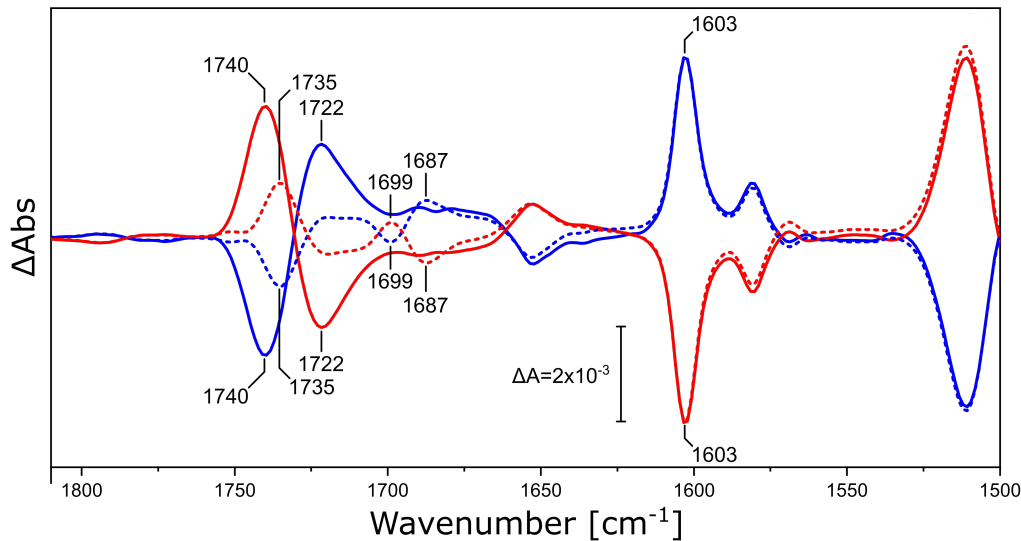
FIGURE 3.35: SHIFT IN THE DIFFERENCE SIGNAL OF THE ESTHER BAND DUE TO ^{13}C LABELLING OF THE LIPIDS. ATR light-triggered difference spectra of nanodiscs containing 80% DPPC and 20% AzoPC. The spectra were normalized at 1603 cm^{-1}, the AzoPC ring mode marker band. The solid lines are spectra of nanodiscs containing natural DPPC, while the dashed lines of nanodiscs whose DPPC content is ^{13}C labelled. In red, the transition is from *trans* to *cis*, in blue *vice versa*. Relevant bands are labelled. Published figure.[160]

This specific band was investigated in the context of a study designed by my colleague Federico Baserga about lipid response to conformational changes of target proteins reconstituted in nanodiscs.[160] AzoPC was used in a low amount, 20%wt in empty nanodiscs of DSPC, to create a change in lateral pressure which should simulate a generic protein conformational change. In particular, we were interested in the carbonyl band, because this had been observed anomalously in difference spectra of several nanodisc-reconstituted proteins. To disentangle the DSPC from the large AzoPC carbonyl signature, once again we used isotopologues.

Nanodiscs with ^{1}3C-labelled DSPC were built, containing 20%wt AzoPC and no protein other than the scaffold protein. The difference spectrum was compared to identical empty nanodiscs, with unlabelled DSPC. The results (Figure 3.35) shows a clear splitting of the carbonyl signal with a shift of the heavier labelled component's maximum/minimum towards lower frequencies.

In the case of MscL reconstituted in nanodiscs, we can expect that the carbonyl absorption change would contain also a contribution from the ion channel, which has a non-negligible content of aspartic (5.1%) and glutamic acid (5.9%), as well as asparagine (4.4%) and glutamine (2.9%), amino acids which present a carbonyl group in their side chain.

Discussion 4

4.1 Creating pressure by light-switching a lipid molecule

Structural reorganization of AzoPC

AzoPC lipids are able to switch with light: the azobenzene moiety photo-isomerizes and the lipid molecule can switch between two stable states corresponding to the *cis* and the *trans* configurations of the azobenzene.

This is visible in the change of UV-vis absorption, peaking at 365 nm when in *cis* configuration and at 450 nm when in *trans* (Results, section 3.1.1). From the FTIR absorption, there are also two spectrally distinguished states for the lipids, which are characterized by specific marker bands, the most visible being the phenyl ring breathing mode of the azobenzene at 1602 cm^{-1} for the *trans* state and the corresponding one at 1512 cm^{-1} for the *cis* state (Results, section 3.1.3).

The light-induced transition involves reorientations and hydration changes in the bilayer that could be tracked with polarized ATR FTIR. In particular, in the *trans*-to-*cis* transition where the azobenzene gets excited with UV light, it is possible to identify a reorientation of the C=O bonds which changes the population ratio between the hydrated and anhydrous oxygens and overall results in a hydration decrease at the hydrophobic/hydrophylic interface of the bilayer[160] (Results, section 3.1.4).

As resulting from the analysis of the polarized difference IR spectra, the structural reorientation involves also the PC headgroup and the phenyl rings.

The distal phenyl ring rotates from an almost vertical position along the main lipid molecular axis, to a more horizontal position, almost perpendicular to the axis. This qualitative, but crucial, observation of the ring reorientation is compatible with the current proposed models of azobenzene light-induced isomerization, whose dynamic details are at present still highly debated.[161–164]

Different lipid configurations determine different lateral pressures

This structural reorganization due to the light-induced isomerization increases the steric hindrance of each molecule. The change in footprint of a single AzoPC lipid can be quantified as about 30% of its initial *trans* footprint, and the consequentially expected increase in packing density during monolayer compression was confirmed from the LB isotherms (Results, section 3.1.2). Also the IRRA spectra showed the higher packing density for the compression in the *cis* state, even though on a possibly degraded sample (Results, Figures 3.20 and 3.21).

When the monolayer area is fixed in the LB trough and the UV light is switched on, the increase in footprint creates a macroscopic lateral pressure that can be measured. Cycles of light-switching the AzoPC monolayer on the LB trough showed that not only the light-switching is reversible, but also that the lateral pressure can be cyclically switched between two values. These two values depend strongly on the initial conditions of the monolayer, in particular on the starting lateral pressure, and the time constant of the change depends on the light intensity (Results, section 3.1.2). The lipid expansion was substantiated with the results from our collaborators in Potsdam who observed the same expansion in AzoPC GUVs[165].

4.2   The fundamental issue with the direction of the light switching

The isomerization in the two directions is not equivalent

The light-switching of the lipids appears macroscopically to be fully reversible and reproducible from the FTIR spectra: the switch between the two spectroscopically distinct states can be cyclically induced with no apparent fatigue from the pure AzoPC lipid system, even after > 1000 cycles (Results, section 3.1.5).

However, the stability of two states is not equivalent: the electronic ground states of the two isomers, in the pure azobenzene molecule, differ by 12.0

kcal/mol, the *trans* state being the lowest in energy, and the two transitions, *trans*-to-*cis* and *cis*-to-*trans*, follow different geometric and energetic paths.[166] At room temperature, the AzoPC lipids in the *cis* state will revert back to the *trans* state with a time constant of about 12 hours. In order to keep the photolipids in the *cis* state, the temperature must be decreased and the sample needs to be intermittently illuminated with the UV light. A continuous UV light illumination over hours will otherwise degrade the sample.

Moreover, in the condensed state, such as in the monolayer or in the membrane, the azobenzene moieties are able to interact intermolecularly. The flat geometry adopted by the azobenzene allows for coupling of rings from different adjacent molecules. Electronic coupling between stacked azobenzene molecules has been predicted by QM-MM simulations, resulting in a reduced photoisomerization yield.[167] The phenyl rings of the azobenzene moiety in AzoPC also tend to pair, forming H-aggregates.[81,144,150,151] These do not form if the lipids are single molecules solved in chloroform: the UV-vis absorption spectrum of AzoPC LUVs and of AzoPC lipids solved in chloroform are shifted (Results, section 3.1.1). We can thus interpret the higher energy requirement for the LUV AzoPC switching as a consequence of this intermolecular interaction.

In the monolayer, as reported from the LB trough, the amplitude of the lateral pressure change depends strongly on the initial conditions and it varies greatly between the two switching directions (Results, Figure 3.5 and *cfr.* Figure 3.4 with 3.6). This can be explained by the necessity of breaking the H-aggregates, that originate at higher packing densities or upon *cis*-to-*trans* switching, when switching in the opposite *trans*-to-*cis* direction.

On the contrary, as what is observed in the steady-state FTIR spectra is the absorption generating from an ensemble of AzoPC lipid molecules, the signals recorded from the two states do not report on the different pathways taken by the transition in the two directions and the possible intermediate interactions. In order to be able to see that, an ultra-fast time-resolved FTIR experiment would be necessary.

Opening MscL requires a *cis*-to-*trans* transition

Duly noted that the transition mechanism differs in the two directions, one must evaluate which direction is to be exploited when considering an application in conjunction with a mechanosensitive protein. The system is composed by two parts: the lipids - actuators that can effectively transform the light signal into a mechanical stimulus - and the mechanosensitive ion channel that reacts to the stimulus by gating.

When considering only the photolipids, it would be straight-forward to think of designing a system where the inactive state corresponds to the most stable state - the *trans* state - permanent under visible illumination. Then the activation occurs upon UV light illumination, inducing the transition to the *cis* state. Such a transition, *trans* to *cis*, induces in the monolayer or in the mebrane a lateral pressure increase or, in other terms, a loss of tension.

MscL, as most other mechanosensitive ion channels, naturally sits closed in the membrane. Its opening occurs when the tension of the membrane exceeds a threshold of about 10 mN/m, given its physiological role of emergency valve in the cell.[105–107] Therefore, in order to activate it, the membrane tension must increase. Such a condition requires the lipids to transition from the higher lateral pressure state, the *cis* state, to a state of lower lateral pressure, the *trans* state. This implies that when the ion channel is in the relaxed closed state, the photolipids must be kept in the less stable *cis* state.

This requires that the system assembly is carried out with the lipids in the *cis* state, which means that the protein reconstitution must occur in the darkness and under UV light illumination. One would think that, if it is technically challenging to set and keep the system in the *cis* state, it could be possible to prepare it in the *trans* state and then bring it to the *cis* state by illumination. The next blue light illumination would then be used for the activation. The problem with this is that, for the ion channel to gate, it is not a relative lateral pressure jump that it is necessary, but an absolute tension value. The system must be prepared in an initial state that can reach the desired activation state by a transition. The initial state is necessarily an equilibrium state where the channel is closed and the lipids - no matter in which isomerization state - arrange themselves at about 30 mN/m. Then, in order to reach the 10 mN/m required for the channel opening, a tension must be applied. Starting from a *trans* state and switching to *cis*, the lateral pressure can only increase. But most importantly, switching back to *trans* would bring the system back to the equilibrium state and no actual tension can be applied.

In a purely experimental setting, it is possible - although cumbersome - to prepare the sample with the AzoPC in the *cis* state. It would then become of hard applicability, though, when moving to biological organisms. It would be more convenient to have an initial stable state at equilibrium in visible light, and use UV light as a trigger instead. No such photolipid is available at the moment, but, exactly to remedy to this issue, such a photoswitchable lipid is currently under development by the same research group that synthesized AzoPC, the Trauner group (private communication).

Impact of the transition direction on the experimental design

Requiring the starting status of the system to be the closed MscL in a *cis*-AzoPC membrane imposes constraints on the design of the experiments.

In an efflux experiment, the excitation energy of the dye must overlap with the energy of the light used to trigger the channel opening. Calcein, the dye of choice in this work, has the excitation peak maximum at 495 nm. Given the broad overlap with the 450 nm LED light, calcein would get excited by the blue light used to isomerize AzoPC from *cis* to *trans*.

The reproduction of the calceine efflux experiment and the actual running of its controls has proven to be extremely difficult, even though the liposome efflux experiment is a rather standard test. The method requires for an exchange of the buffer external to the liposomes in order to remove all free clacein. This buffer exchange must be carried out timely and the experiment has to be run on the same day, due to the aforementioned time constant of the *cis* state, the whole procedure being carried out in the darkness or under intermittent UV light and exposing the sample to visible light only in the moment of the blue-light triggering during measurement.

As a method for the external buffer exchange, dialysis can be excluded due to the time required for this technique. The size exclusion columns, which have been used in this work, tend to get stuck with liposomes and interrupt the regular flow. Therefore, a possibly more successful approach to test the functionality of a light-activated MscL would be in GUVs rather than LUVs. In GUVs the same efflux experiment can be done under an optical microscope with a contrast gradient, without the use of a fluorophore, and with more effective buffer exchange methods.[168]

The protocol of the functional tests on the black lipid membrane in the electrophysiology setup is also influenced by the requirement of the transition direction. It is necessary to reconstitute the mechanosensitive ion channel in a membrane that holds the potential of increasing its tension, so where the AzoPCs are in the *cis* state. The reconstitution is therefore carried out in the dark and under intermittent UV illumination. When MscL sits in the membrane in its natural closed state, illuminating with blue light triggers the tension increase and opens the channel.

The activity starts after about 6 seconds, the time in which, under our experimental conditions, the blue light isomerizes enough AzoPC molecules to reach a gating tension. This activity has also a duration of about 30 seconds. After the activity stops, it is not possible to recover it by exposing the membrane to another illumination cycle (Results, section 3.2.1).

The termination of the activity of MscL in the free-standing bilayer can be explained by the presence of an annulus of lipids surrounding the cylinder that functions as structure for the black lipid membrane.[169,170] The annulus of lipids that encircles the free standing bilayer works as a pressure buffer: the tension generated in the membrane by the isomerization of AzoPC to *trans* pulls not only on the ion channel, but also on the lipids from the annulus, attracting them to the bilayer until the initial lateral pressure is re-established and the channel is back to its most stable condition, closed.

A subsequent illumination with UV light increases the lateral pressure in the membrane, but this state must necessarily differ from the initial *cis* bilayer built under UV illumination, because it does not respond anymore to blue light with any detectable current. Possibly, the escess lipids are pushed outside of the free-standing bilayer area back to the annulus, creating a reservoir of lipids that can easely enter or leave the free-standing bilayer depending on the illumination, without allowing for stable changes of tension in the membrane. With techniques such as small-angle X-ray scattering (SAXS) or small-angle neutron scattering (SANS), it would be possible to investigate the lipid density of the bilayer during consecutive blue/UV light switching cycles, and to confirm or disprove this model, which for the moment is only a conjecture.

4.3   Light-gating MscL

Orientation of MscL reconstituted in a light-switchable membrane

A membrane constituted by only lipids shows a strong orientation when dried from liposomes on an ATR crystal or a transmission window, allowing for polarized measurements and determination of ensemble readings of specific bond re-orientations. When MscL-reconstituted proteoliposomes are used for the sample deposition, the ordered multilayer structure is lost and the dried sample appears isotropic under polarized light (Results, section 3.2.3). A possible explanation could be the high protein:lipid ratio (1:500) which was chosen to maximise the protein IR signal. Too little lipids are present in the sample to help maintain the bilayer form during deposition.

An ideal technique to obtain IR spectra which are relative to a specific direction in the protein would be SEIRAS. In this method, the protein can be anchored to the ATR support with a desired orientation, and a lipid bilayer is reconstituted around it, effectively forming a single bilayer on the substrate. Because of the selection rules intrinsic to the physics of the enhancement necessary to this technique, only the modes whose change in dipole is aligned

with the normal to the support plain are enhanced. While this was the first method of choice, this technique comes with many challenges and it was only tentatively applied in the context of this thesis, therefore it is absent from this work. After some initial measurement giving too weak absorption signals, the bulkier ATR and transmission techniques have been preferred. Nonetheless, with the current knowledge acquired with the other methods, SEIRAS would now be a highly advantageous approach to revisit.

MscL is gated into a sub-conducting state

A clear channel activity is observed in the black lipid membrane experiment. Given the potential applied across the bilayer, the current observed corresponds to a conductance of 0.8 nS. A fully open state is characterized with a conduction of 3.0 nS. In the Nanion Orbit setup it is not possible to measure the lateral pressure *in situ*, but it can be inferred that the lateral tension generated by the photolipids is not enough to pull the channel completely open. From the intensity of the observed current signal, the observed state of MscL with the first non fully-conducting state of the Sukarev model, S1, is identified.[107] This is an intermediate state between the fully closed state and the fully open state, which is known in MscL for lower tensions than the threshold required for the channel opening of about 10 mN/m.

When constrained laterally, a monolayer of AzoPC switching from *cis* to *trans* can reach the tension necessary for a full opening of MscL. While the anchoring at the annulus around the black lipid membrane seems too fluid, nanodiscs can possibly offer the mechanical constraint needed. Analyzing the difference spectra of MscL in various lipidic environments, the spectral signature of light-swithing MscL in nanodiscs differs from all other reconstitutions. It clearly shows reproducible structural changes of the protein backbone characterised in the IR difference spectra by a broad band in the amide I region and an overlapping smaller and sharper negative-positive differential feature. Moreover, it could be proven that these are distinguished from the reaction of the MSP to the change in lateral pressure due to AzoPC alone.

Nevertheless, an effect of decaying switching capability is observed happening in nanodiscs as well, although not as rapid as in the black lipid membrane. Over 7 switching cycles, lipids are either expelled from the nanodics or they rearrange in such a way that the tension the bilayer can exert on the ion channel fades exponentially.

Conclusions 5

In this thesis, the light-induced structural reorganization of membranes through the photoisomerization of AzoPC molecules was explored. This reorganization leeds to changes in lateral pressure within the membrane, which has significant implications for applications such as light-gating mechanosensitive ion channels.

The results here presented reveal that the direction of the light-induced transition in AzoPC lipids plays a crucial role in determining the exercisable tension in the membrane. The presence of intermolecular interactions, such as H-aggregation, further complicates the behavior of AzoPC lipids in condensed phases, influencing their switching kinetics and energetics. The directionality of the azobenzene transition has repercussions on the design of the system, when considering to use the generated tension to activate MscL. The choice of the initial lipid configuration is thus fundamental for such an application. For MscL, which naturally sits closed in the membrane, the desired initial state of the membrane is the *cis* configuration of AzoPC lipids, as it corresponds to a lower tension of the membrane and it allows for a higher tension to conveniently build up upon illumination.

This work also highlights the interplay of different experimental techniques, presenting advantages and limitations, concurring to the investigation of a completely new biological assembly. A method such as steady-state FTIR difference spectroscopy provides valuable insights into the structural re-arrangements of lipid molecules as an ensemble. In combination with polarized optics and with the support of DFT simulations, it helped build an intuitive 3D model. To capture the kinetics of the transitions and the details of the protein structural changes, techniques such as time-resolved FTIR or SEIRAS could represent the next stage in the spectroscopy. The LB trough has provided important information relative to the potential of light-generated tension in the monolayer.

In combination with spectroscopy it develops into the excellent tool that is the IRRAS technique.

Moving forward, the development of photoswitchable lipids with more stable and reversible switching capabilities, as pursued by the Trauner group, holds promise for overcoming some of the limitations encountered in this study. Additionally, including methods based on the AzoPC-MscL combination in the form of GUVs and combining that potential information with the electrophysiology recordings, could help forming a more robust understanding. Exploring alternative lipid environments, such as varying the lipid mixtures, or using polymer-bound nanodiscs, may also offer new avenues for controlling membrane tension and studying the behavior of light-gated ion channels.

In conclusion, with this thesis the exploration of the AzoPC photoswitchable lipids and their interplay with the mechanosensitive membrane protein MscL was started. Further research in this field will undoubtedly continue to uncover new insights with implications for the design and optimization of light-gated ion channels for various applications in biotechnology and biomedicine.

Supporting Information on the Biochemical Methods A

A.1 MscL purification: Chromatogram and SDS gel

In Figure A.2 is shown an example of chromatogram and relative SDS gel, from an expression and purification of MscL done by Antreas Vorkas. The fractions indicated at the bottom of the chromatogram were collected. Grouped in four batches based on the chromatogram, the elutes are run on an SDS-PAGE. MscL-containing samples are identified from the band slightly above the 17 kDa.

A.2 Lowry assay for protein quantification

Lowry assay for protein quantification combines a Biuret reaction, which in alkaline conditions forms a Cu^+ complex with peptides, with the Folin-Ciocâlteu reaction, in which the copper complex is oxidised and the Folin reagent is reduced, producing a strong blue color.[171] Anyway, the absorption is best measured at 750 nm, since not many other compounds absorb at that wavelegth. Finally, in order to quantify the protein amount, the absorption at 750 nm of MscL-containing samples are compared to a calibration curve built on known concentrations of BSA.
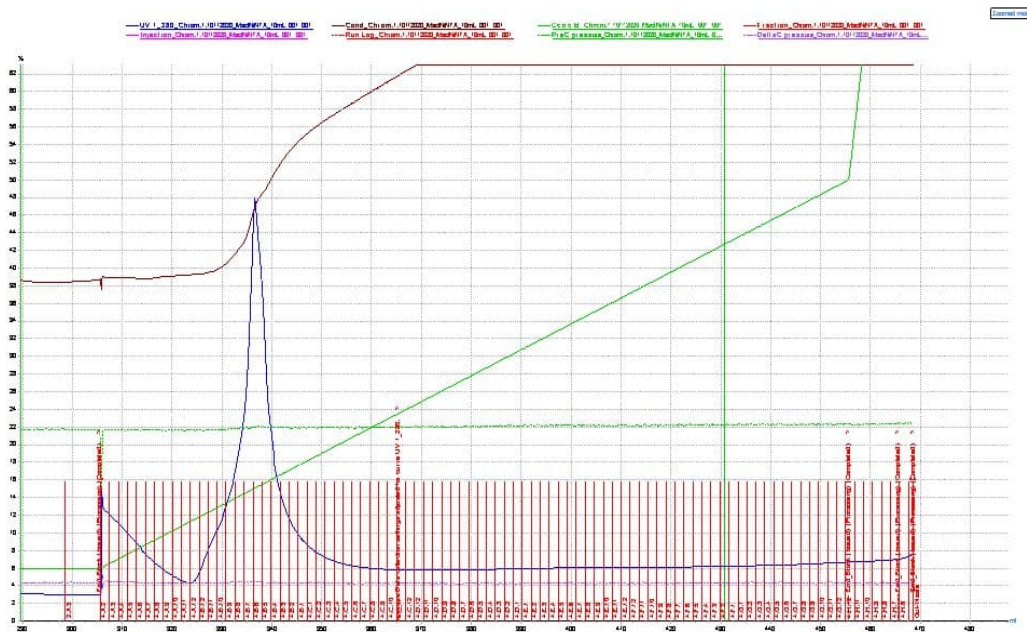
FIGURE A.1: CHROMATOGRAM OF MSCL PURIFICATION. The green line is the imidazole concentration in the elution solution. The blue line is the absorption at 280 nm. Since MscL does not absorb in the visible range, the large band is from impurities and the eluted MscL is undetectable. In red are marked all collected fractions. In order to collect the purified MscL, the fractions are grouped and run on an SDS-PAGE.
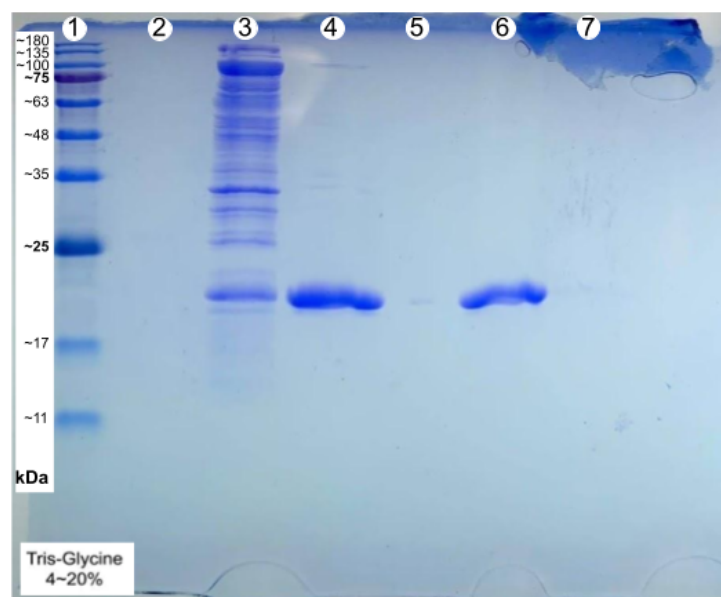
FIGURE A.2: SDS GEL OF MSCL PURIFICATION. Lanes: 1) Marker, 2) fractions A1-A11 from the chromatogram, 3) fractions A12-C1 (C1 corresponds to 180 mM imidazole), 4) fractions C2-D1, 5) empty well, 6) fractions D2-F1 (D2 corresponds to 430 mM imidazole), 7) fractions F2-H11. Elutes C2-F1 containing MscL are used for reconstitution and use. Sample running on lane 3 contains also MscL, but due to the high amount of impurities, it's discarded.
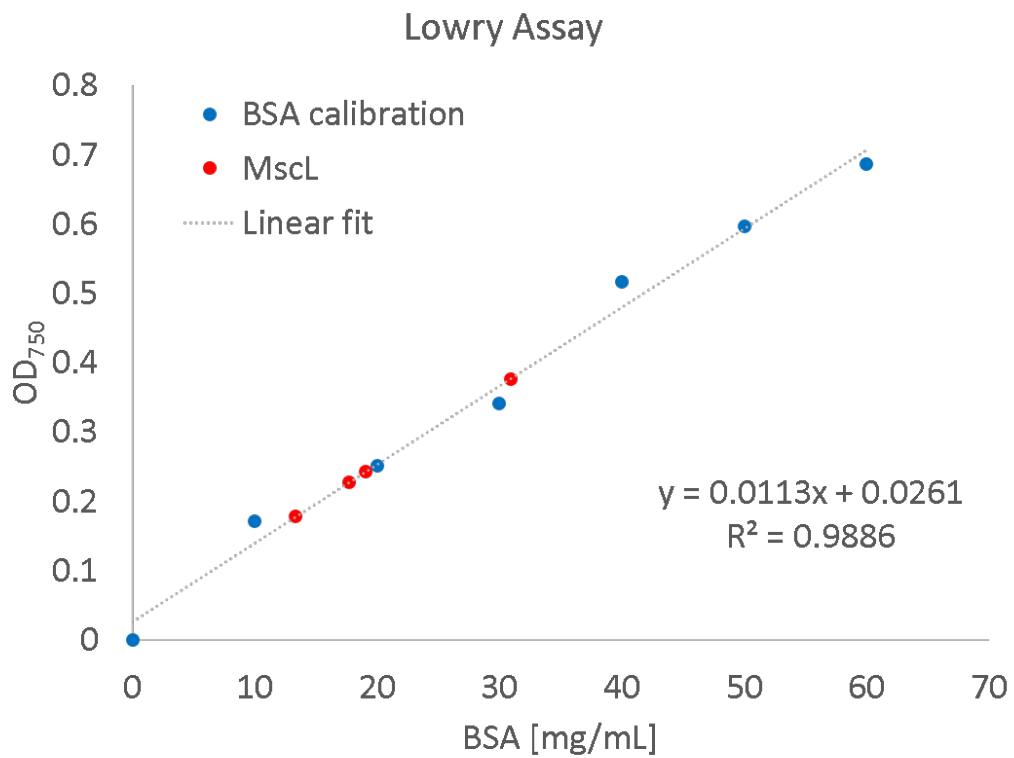
Figure A.3: Lowry assay on MscL. In blue, the calibration data from BSA, the dashed gray line is the corresponding linear fit. In red, the absorptions of purified MscL samples of different expression rounds (all expressions from Antreas Vorkas).
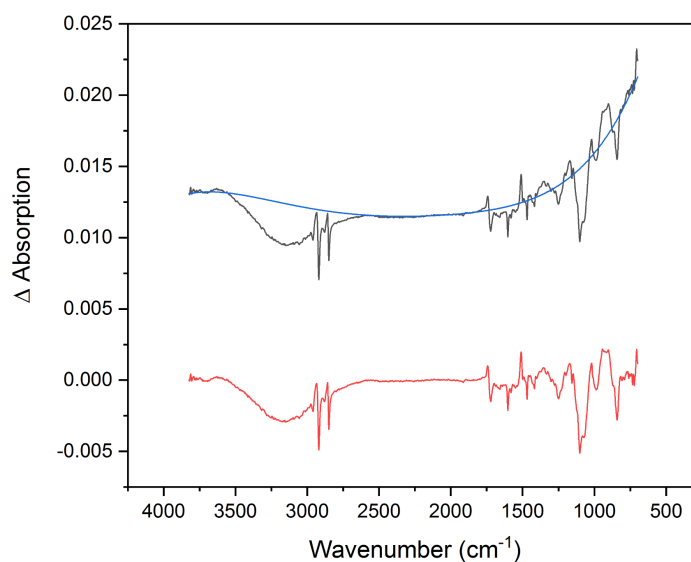
B.1 Baseline correction

FIGURE B.1: **Example of a polynomial baseline correction.** In black the original spectrum, a difference spectrum of MscL in nanodiscs; in blue, the fitted polynomial; in red, the corrected spectrum. In this example it was not corrected for the liquid water signal.

In Figure B.1 it is shown an example of the baseline correction applied to the data. A polynomial line is fitted through some points assumed to be on the zero line. The number of points and the position is determined for each spectrum *ad hoc*. A concious choice of removing or leaving the water signal is made depending on the desired analysis, and it is reported in the results. It is known and taken into consideration that, due to the arbitrariness of the fitting points, the corrected spectrum may vary. Nonetheless, given that the frequencies of the correction polynomial are much lower than the signals of interest, the variation between two different corrections applied to the same spectrum may vary by an offset at most.
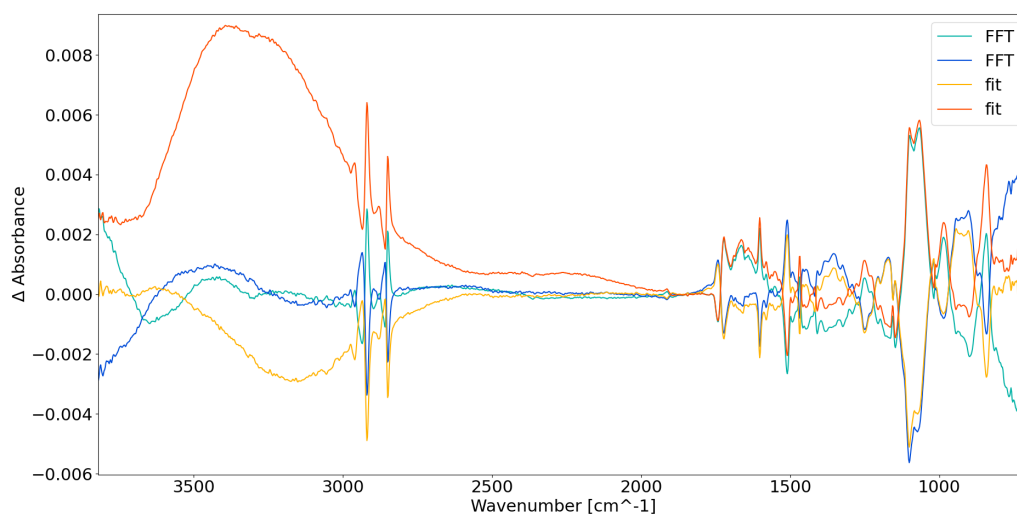

FIGURE B.2: **Example of FFT-corrected spectra compared to polynomial-corrected spectra.**

In Figure B.2 the spectra corrected with a polynomial fit are compared to a Fast Fourier Transform (FFT) baseline correction. The self-written FFT algorithm decomposes the spectral signal into its frequencies and the correction consists in the attenuation or deletion of some of the lower frequency components. The result does not differ significantly from the one obtained with the polynomial fit, but there is no control over the deletion of the liquid water absorption bands. As a consequence, all spectra shown in this work are polynomially corrected.

B.2 Additional AzoPC FTIR absorption spectra

In order to highlight and clearly see the absorption changes between the two isomerization states of the photolipids, in this thesis we make use of difference

spectra to analyse what happens during the switching. For completeness, a direct comparison over the whole MIR frequency range between ATR-FTIR absorption spectra of the lipids in the two states are reported here in Figure B.3. The spectra of the film of AzoPC dried from chloroform on the ATR silicon crystal show some dissimilarities after 2 minutes of illumination with either blue or with UV light. The differences that are evident also from the absolute spectra appear at the frequencies assigned to ring modes (see section 3.1.3), which are directly affected by the isomerization of the benzene ring.

The high reversibility (*cfr.* section 3.1.5) of the process can be appreciated also from these spectra, in fact, shown in Figure B.3, is the average spectrum of five different illumination cycles. The variance is shown as a shaded area around the line, but it is almost invisible, since its amplitude is in the order of the linewidth of the plotted lines and it appears almost imperceptibly only at the liquid water absorption frequencies (broad band around 3400 cm^{-1} in the figure inset), since the water content in the sample was not controlled.
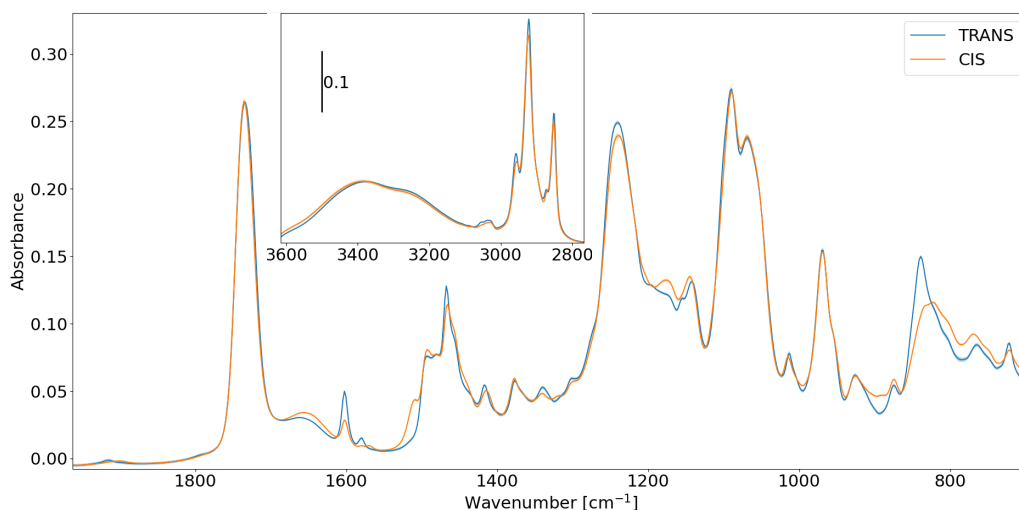

FIGURE B.3: **ATR absorption spectrum of AzoPC in the *trans* and in the *cis* state.** Comparison between the absorption spectrum of AzoPC in the two isomerization states. The ring modes are the most visibly affected by the isomerization of the azobenzene moiety of the azo-lipids.
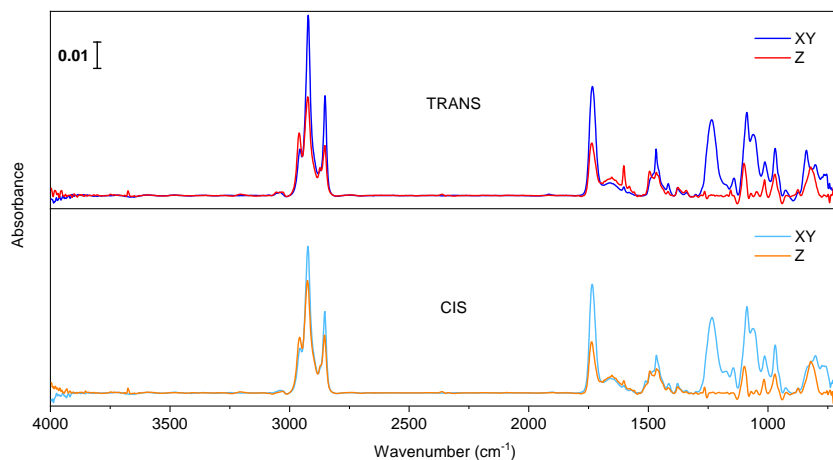
Figure B.4: AzoPC polarized spectra.

In Figure **??** are reported the polarized spectra of AzoPC over the whole measured MIR frequency range. It stands out that, in both *trans* and *cis* states, the methylene stretching vibrations ($\sim 3000 - 2800$ cm^{-1}), the C=O stretching (~ 1735 cm^{-1}), the methylene scissoring (1468 cm^{-1}) and the phosphate symmetric and asymmetric stretching (respectively 1090 and 1237 cm^{-1}) have a larger XY plane component. Only the ring breathing modes (1602 and 1512 cm^{-1}) are more oriented towards the Z axis.

B.3 AzoPC carbonyl band decomposition

An AzoPC lipid molecule, as all other glycerophospholipids, has two esters. Their carbonyl stretching vibration absorbs strongly at around 1740 cm^{-1} (*cfr.* the band assignment in section 3.1.3). The resulting band is a superposition of two absorption signals. It is possible to analyse the second derivative of the band and discern the two contributions. The highest in energy, at 1742 cm^{-1} in AzoPC, is assigned to the anyhdrous esters, while the lowest, at 1730 cm^{-1} in AzoPC, is assigned to the hydrated esters.[116,117] Examples of this band decomposition are shown in Figure B.5 for two indipendent measurements on the same sample.
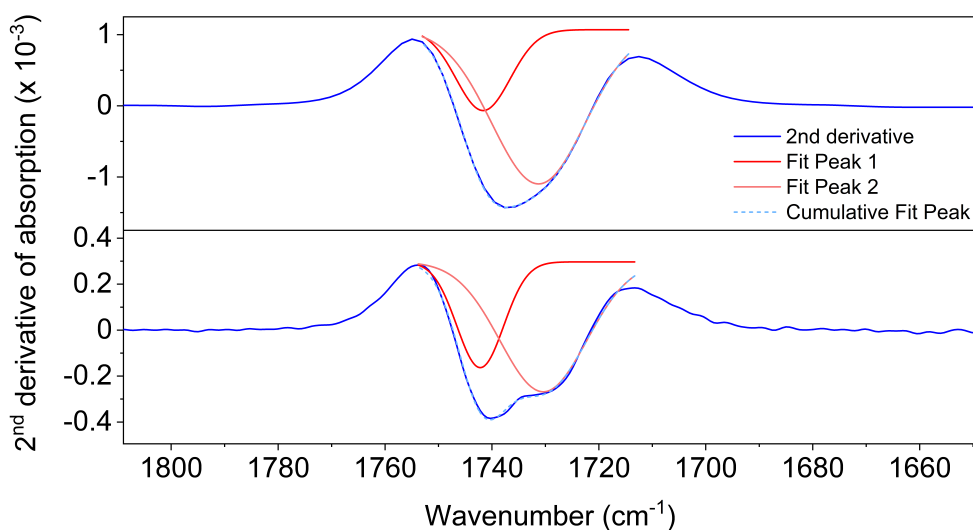
FIGURE B.5: **Second derivative of the carbonyl absorption band.** It is possible to separate the two components at 1742 and 1730 cm^{-1}, respectively from the anhydrous and hydrated esters. Different hydration conditions of the same sample change the contribution of the two components to the band.

This vibration is very sensitive to hydrogen bonding changes on the oxygen. Since these spectra were measured from AzoPC dried from chloroform on the ATR crystal in ambient conditions, with no control on hair humidity, changes in the hydration conditions of the dry film can lead to a more or less visible separation of peaks in the second derivative of the band.

B.4 DFT data treatment and additional spectra

The DFT simulation has been run from Rubén Cruz in Gaussian with the method BP66 and the basis set 6-311G with polarization and diffuse functions (bp66/6-311+g*). The output file returns a list of vibrational frequencies with the relative intensity value. A plot of these is shown in Figure B.6.
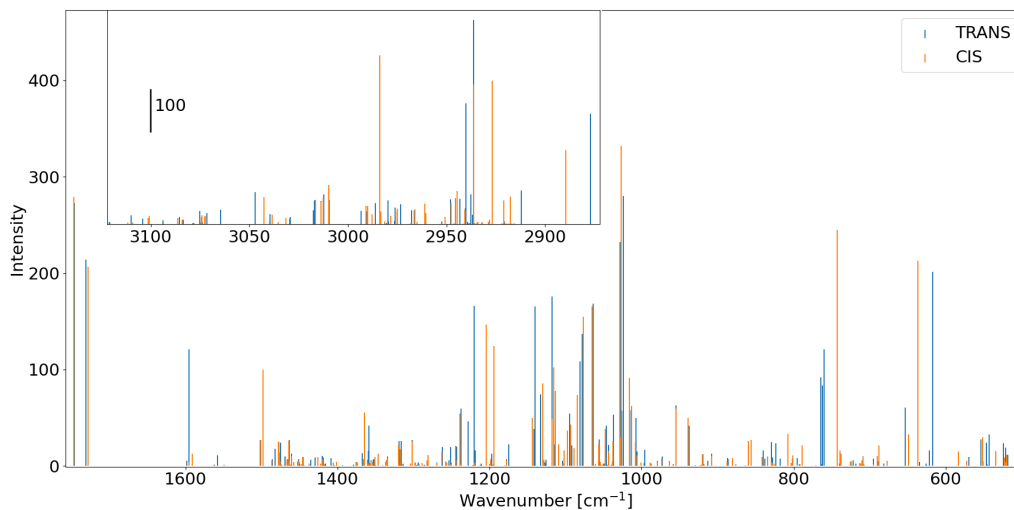
Figure B.6: DFT simulated vibrational spectrum of AzoPC. Frequencies and intensities calculated from the DFT simulation on the two isomers of an AzoPC molecule in vacuum.

The output frequencies and relative intensities have then been convoluted with a gaussian function to simulate a spectrum. The result is then a sum of gaussians, each defined as

$$G(x) = A\ e^{\frac{-(x-x_0)^2}{2\sigma^2}}$$

where x_0 is the peak frequency, A the corresponding intensity, and σ an arbitrary width for all gaussians. We have chosen $\sigma = 7$, as it reproduced best the width of the C=O band of the experimental spectrum at 1735 cm^{-1}.

No specific factor has been used to correct the frequencies, but a fitting algorithm has been applied instead. The assignment of some bands (listed in Table B.1) from a comparison with the literature on lipids and on azobenzenes is highly reliable and it could be easely matched with the assignment from the DFT. The frequencies relative to these bands from the ATR measurement and from the DFT calculation have been plotted against each other and the data have been fitted for a linear correlation (Figure B.7). Then, all other DFT-calculated frequencies have been shifted to the corresponding value on the fitted line, adapting linearly the correction factor based on how the known peaks were shifted.

Table B.1: *AzoPC marker bands assigned both in the ATR-measured and the DFT-calculated spectra, used in the linear fit to adjust the correction factor of all other DFT-calculated frequencies.*

ASSIGNMENT	ATR FREQUENCY	DFT FREQUENCY
$\nu_{as}(CH_3)$	2957 cm^{-1}	3010 cm^{-1}
$\nu_{as}(CH_2)$	2922 cm^{-1}	2984 cm^{-1}
$\nu_s(CH_3)$	2873 cm^{-1}	2945 cm^{-1}
$\nu_s(CH_2)$	2852 cm^{-1}	2936 cm^{-1}
$\nu(C=O$ hydrated$)$	1742 cm^{-1}	1746 cm^{-1}
$\nu(C=O$ anhydrous$)$	1730 cm^{-1}	1731 cm^{-1}
N=N + ring $\nu_s(CC)$	1603 cm^{-1}	1596 cm^{-1}
ring $\nu(CC)$	1580 cm^{-1}	1558 cm^{-1}
$\delta(CH_2)$	1468 cm^{-1}	1477 cm^{-1}
$\nu_{as}(PO_2^-)$	1237 cm^{-1}	1220 cm^{-1}
$\nu_s(PO_2^-)$	1090 cm^{-1}	1024 cm^{-1}
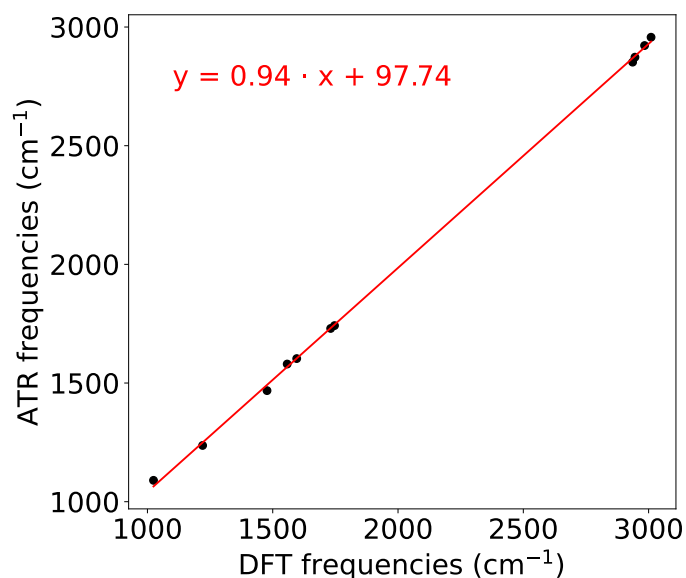
FIGURE B.7: LINEAR FIT OF THE CORRELATION BETWEEN DFT CALCULATED AND ATR MEASURED FREQUENCIES OF AZOPC The linear fit has been calculated on the correlation scatter plot of the frequencies with known assignment. All the other DFT-calculated frequencies (not shown in this plot) are then shifted to the corresponding value on the fitted line.
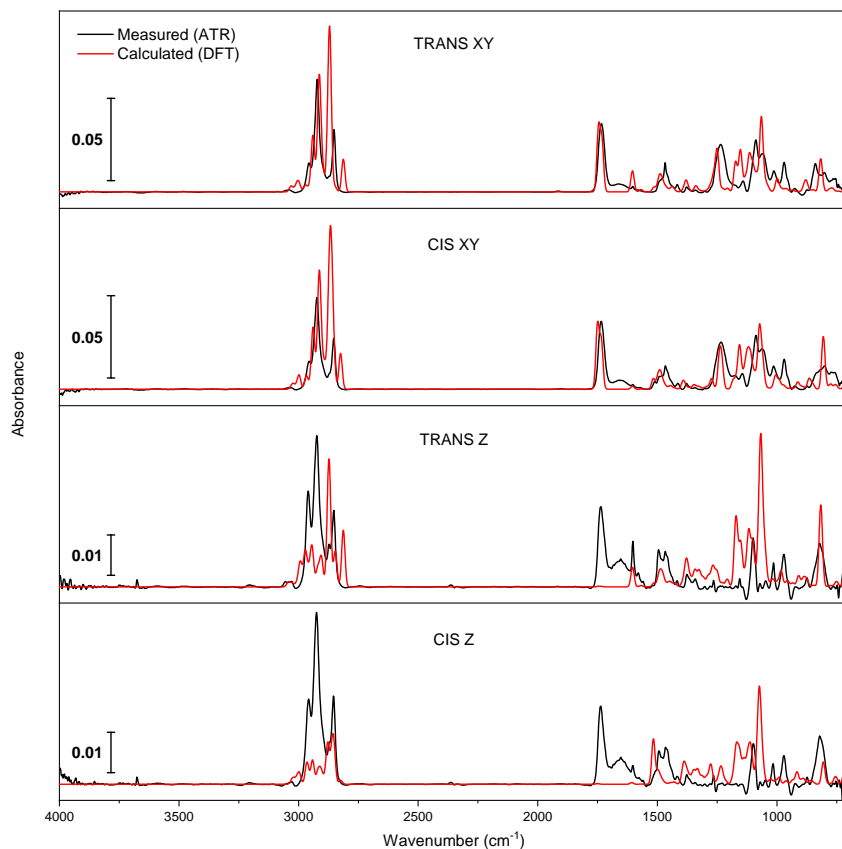
FIGURE B.8: COMPARISON BETWEEN EXPERIMENTAL AND DFT CALCULATED SPECTRA OF AZOPC.

B.5 Polarised spectra of liquid water and determination of the ATR angle

The spectra taken with linearly polarised light, either parallel or perpendicular to the plane of incidence, of an isotropic substance such as pure water, can be used to determine the ATR incident angle (using the formula presented in section 2.5.3). The ratio of band intensity $\frac{perpendicular}{parallel}$ for the absorption of water is 2.0 at 1600 cm^{-1} and 2.1 at 3340 cm^{-1}. A value of 2 is then used for the determination of the ATR angle, then resulting 45∘.
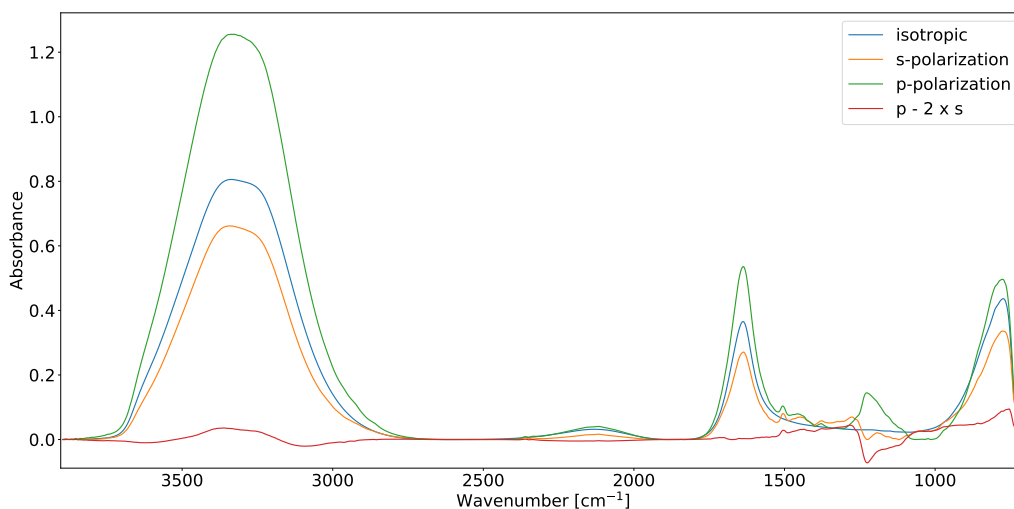
FIGURE B.9: POLARIZED ATR SPECTRA OF PURE WATER. The intensity of the band at 1637 cm^{-1}, the H-O-H bending mode of water, in the spectrum recorded with parallel polarized light with respect to the plane of incidence (p-polarized, green curve) is double the intensity of the one recorded with perpendicular polarization (s-polarized, orange curve), as suggested by the zero line obtained by their normalized subtraction (red curve). An isotropic spectrum of water (light blue curve), recorded with non-polarized light, is overlayed to show that the bands visible in the polarised spectra between 1550 and 1000 cm^{-1} are artifacts introduced by the polarizer.

B.6 Spectrum of the PBS buffer used for MscL

A spectrum of the PBS buffer used in all sample preparations of MscL is reported in Figure B.10. The profile of the spectrum of liquid water can be recognized: the broad OH stretching band around 3200 cm^{-1}, the broad and shallow libration band around 2100 cm^{-1}, and the sharper O-H-O bending at 1640 cm^{-1}. This water was naturally retained by the sample in the open lab environment. It is important to notice the three intense bands at 1067, 977 and 856 cm^{-1} because they are often visible in absolute spectra of MscL, possibly osbcuring the fingerprint region of the protein.
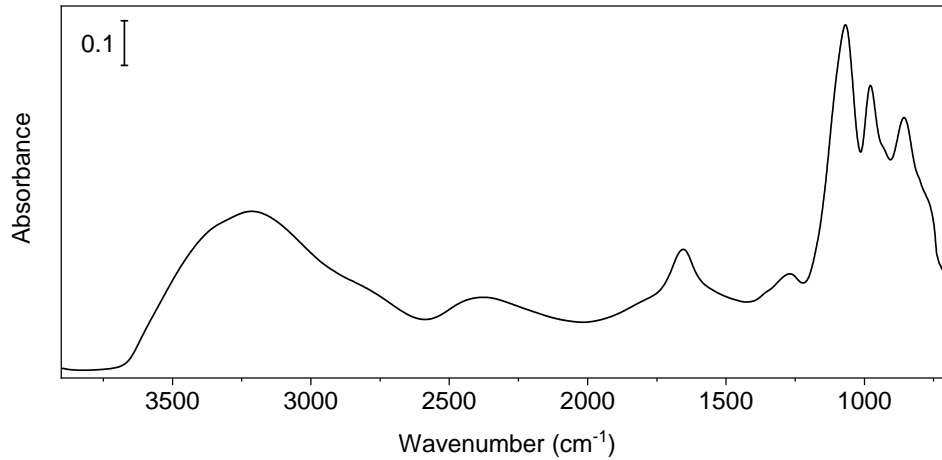
Figure B.10: ATR spectrum of the PBS buffer used for all MscL samples. PBS buffer was dried on the Si ATR crystal with a dry air flux.

B.7 Varying the lipid composition in the MscL lipid reconstitutions: absolute spectra

The lipid composition in the micelles (MscL:lipids molar ratio is 1:200) and liposomes (1:500) MscL reconstitutions was varied. The ion channel was reconstituted in 100% AzoPC, 100% POPC, as well as the 50:50 AzoPC:POPC molar ratio presented in the main body of this work. This variation was done, in the case of 100% AzoPC, to investigate if a higher change in lateral pressure would bring different results from the protein reaction and, in the case of 100% POPC, as a control. The absolute spectra do not show any particular difference across lipid compositions.

In Figure B.11 the absolute transmission spectra of MscL reconstituted in lipidic micelles of the three lipid compositions are compared. When drying the solution, not much water is retained by the sample, as it is the case for liposomes or nanodiscs, therefore the dry micelles were rehydrated with D_2O. In case of the POPC-reconstituted sample, the D_2O droplet used for rehydration touched the sample. These data are not fully reliable, since the hydration conditions of the sample were not controlled anymore.

FIGURE B.11: ABSOLUTE SPECTRA OF MSCL RECONSTITUTED IN MICELLES FOR DIFFERENT LIPID COMPOSITIONS. All spectra were taken in transmission, they are baseline corrected and normalized to the amide I band of the 50:50 sample. The AzoPC normalization factor is 1.435 and the POPC one is 1.26.

The spectra for the same variation in lipid composition in the liposome sample can be seen in Figure B.12. The only noticeable difference is the hydration level. Since the drying procedure was the same for all samples, we can hypothesize that AzoPC retains more water than POPC.
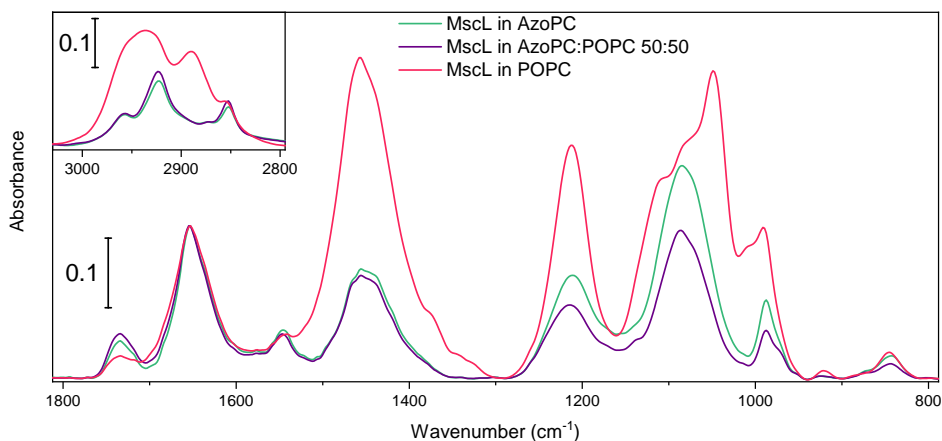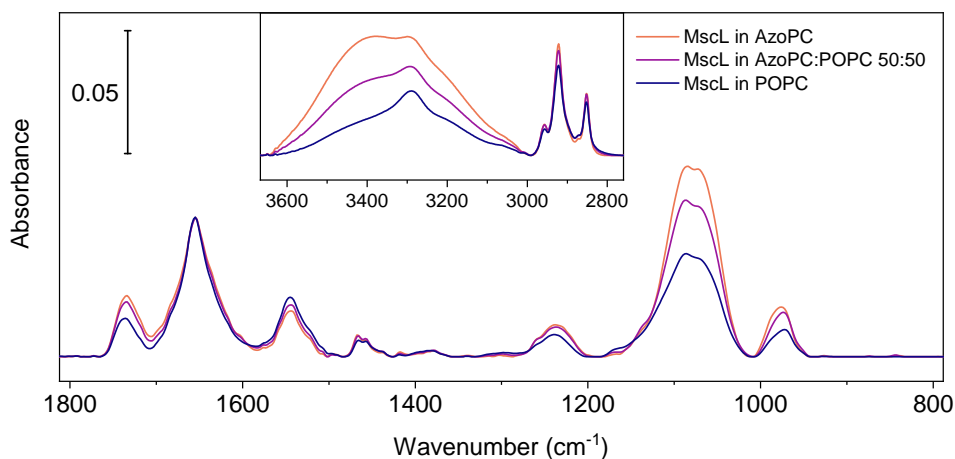

FIGURE B.12: ABSOLUTE SPECTRA OF MSCL RECONSTITUTED IN LIPOSOMES FOR DIFFERENT LIPID COMPOSITIONS. All spectra were taken in transmission, they are baseline corrected and normalized to the amide I band of the 50:50 sample. The AzoPC normalization factor is 1.54 and the POPC one is 1.

B.8 Absolute spectra of nanodisc samples

The nanodiscs are lipid bilayers surrounded by scaffold proteins. These proteins are also α-helical and appear in a FTIR spectrum at the same absorption frequency of the helices of MscL. To distinguish, upon light-triggering, the changes happening to the ion channel from the changes occurring in the scaffold protein, a comparison was carried out between the difference spectra of MscL reconstituted in nanodiscs with the difference spectra of control nanodiscs (see figure 3.33 in the Results). In Figure B.13 are reported the absolute spectra of the two nanodisc samples, with and without MscL.
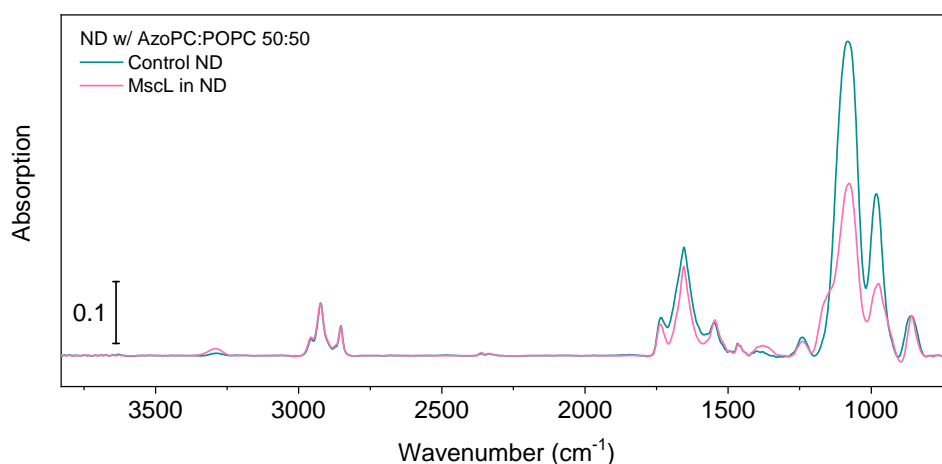
FIGURE B.13: ABSOLUTE SPECTRA OF MSCL IN NANODISCS COMPARED TO NANODISCS WITHOUT ION CHANNEL. Absolute transmission spectra of nanodiscs (ND) with and without MscL. The spectra are baseline corrected and normalized at the lipid band at 2924 cm^{-1} of the empty nanodiscs (normalization factor for the MscL in ND spectrum: 1.075).

It is evident from the amide I and II bands that both samples contain some α-helical protein. It might seem that the control sample contains more protein, but, as it is clear from the higher intensity of the buffer bands below 1300 cm^{-1} (see section B.10), the control sample contained more buffer solution. The higher intensity in the amide I region is therefore to be attributed to a hidden water band which was not eliminated by the baseline correction. The two frequencies where it is possible to appreciate the presence of something in the MscL sample absent from the empty nanodiscs are 1380 and 1160 cm^{-1}. No specific assignment is being proposed, but these two bands could be investigated in the future, as they allow for a distinction from the scaffold protein signal.

B.9 Decaying signal from MscL light switching in nanodiscs

The data presented in section 3.2.4 of the Results chapter are an average of seven light-switching cycles. The difference signal relative to the amide I is decreasing exponentially with the switching cycles. In Figure B.14 we can see how both the broad amide I band and the smaller shift-like feature decrease rapidly. The intensity difference between the peak and the trough is plotted in the inset and fitted with a decaying exponential. As discussed in more detail in the Discussion chapter, the nanodisc might rearrange its structure upon repeated switching, depleting its potential constraint ability. The other MscL preparations, micelles and proteoliposomes, were not tested for more than 7 cycles.
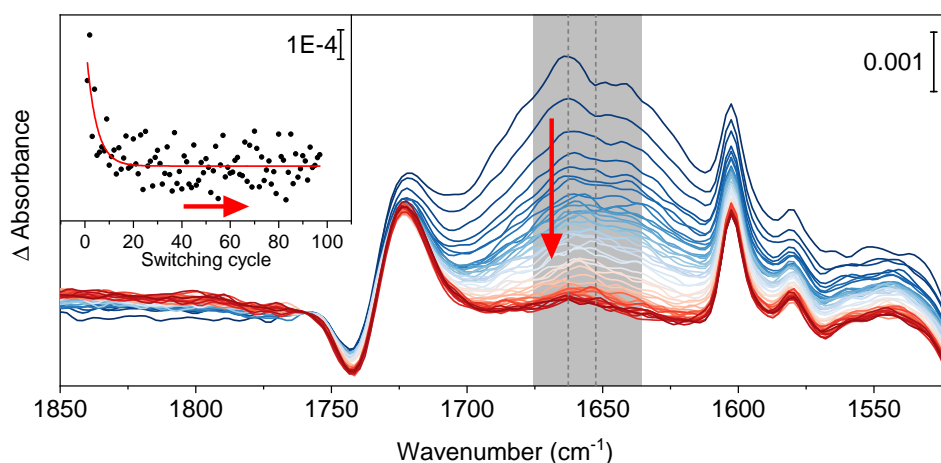
FIGURE B.14: EXPONENTIAL DECREASE OF AMIDE I SIGNAL IN THE DIFFERENCE SPECTRUM OF MSCL IN NANODISCS. The intensity of the signal in the amide I region of the difference spectrum of MscL in nanodiscs decreases drastically with the number of cycles. Both the broad band and the finer feature tend to flatten out by repetitively light-switching the sample. In the inset, the intensity difference between the maximum and the minimum of the small differential band, indicated in the main figure with the two dashed vertical lines, is fitted with a decaying exponential function.

B.10 Emission spectra of the lights used to switch the photolipids

Given the absorption spectrum of AzoPC (Figure 3.1 in the chapter Results and Discussion), to induce the isomerization of the azobenzene moiety, it is reasonable to choose one UV light of about 365 nm wavelegth to switch from

the *trans* to the *cis* state, and one blue light of about 450 nm wavelegth to switch back from *cis* to *trans.* Although the maximum absorption of the *trans* state is at lower wavelegths (337 nm in chloroform, 319 nm as liposomes in water), it is convenient to use a light peaked at 365 nm, in order to minimize the excitement of the second *cis* absorption band in the UV (310 nm in chloroform, 295 nm as liposomes in water).

The lights used to illuminate the sample for the IR spectroscopy, for both the transmission and the ATR configuration, are high power LEDs. The LED, blue or UV, is placed at less then 1 cm of distance from the sample and the measured power density of the light at the sample is 30 mW/cm^2 for the blue LED and 3 mW/cm^2 for the UV LED.
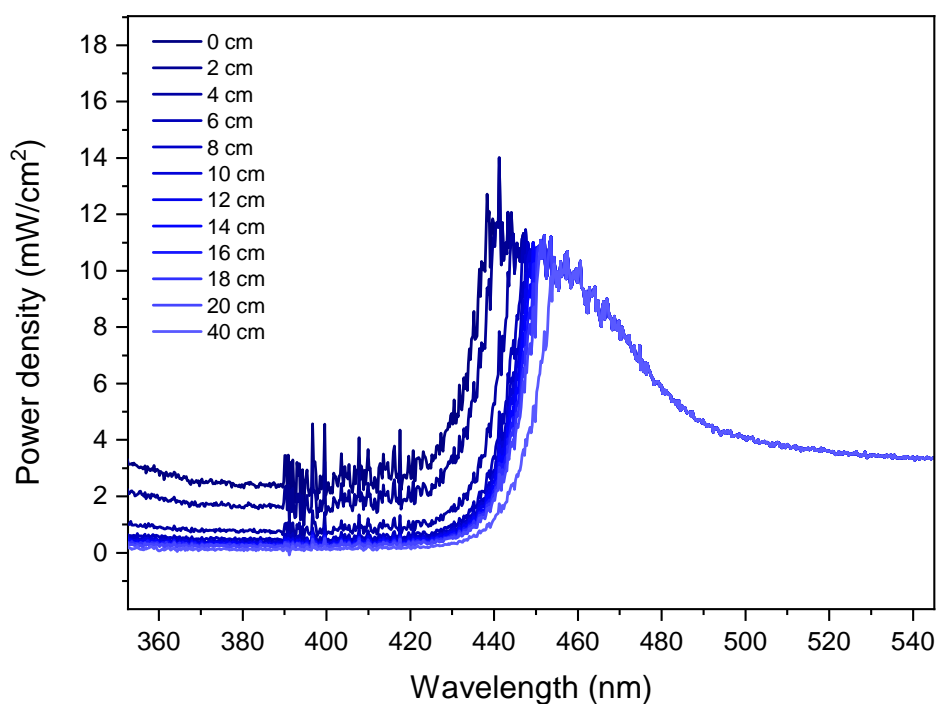
FIGURE B.15: EMISSION SPECTRUM OF THE BLUE LED ARRAY USED TO ILLUMI-NATE THE LB TROUGH. The distance from the surface of the photolipid monolayer has been varied to measure its effect on the power density. A distance of 14 cm ha been set for the expperiments at the LB trough as well as at the IRRAS setup.

In the case of the rheology measurements and of IRRAS, an extended light source was required to illuminate fully and evenly the surface of the LB trough, therefore the same LEDs employed for IR spectroscopy were unsuitable. A UV tube light (originally from a thin layer chromatography light box) has been used instead, and an array of blue LEDs, the same kind of the single one used in the spectroscopy, has been arranged on the same lamp, next to the UV tube,

to be able to alternate illumination on the lipidic monolayer without moving the light sources.
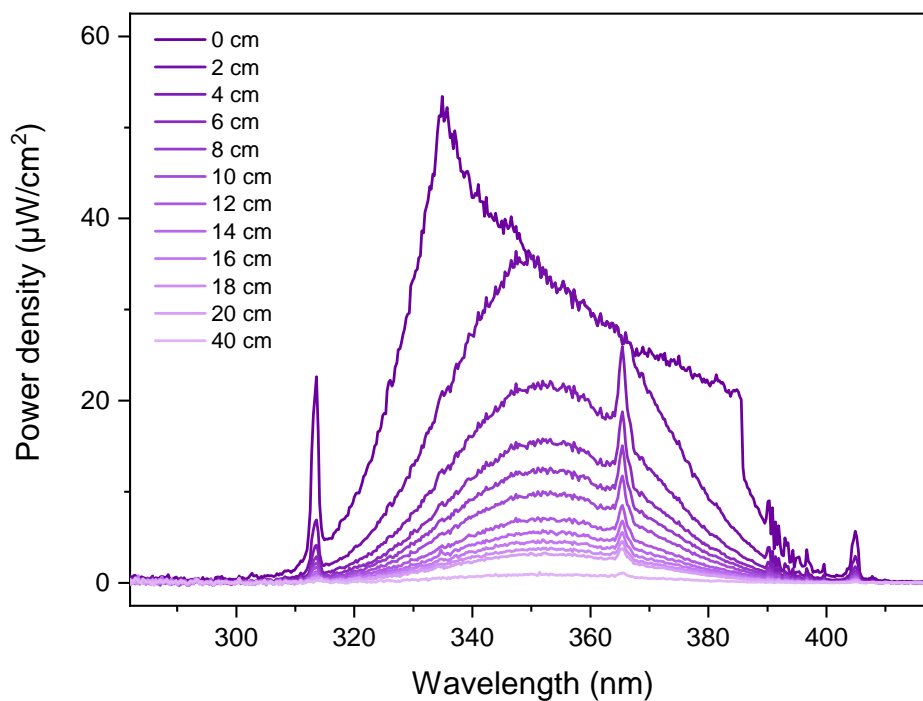
FIGURE B.16: EMISSION SPECTRUM OF THE UV TUBE LIGHT USED TO ILLUMINATE THE LB TROUGH.

Additional Supporting Information C

C.1 Determination of the starting density of lipids to build a monolayer in the Langmuir-Blodgett trough

In order to test if the initial density at which the lipids were deposited on the water surface in the so called "gas phase" had any influence on the monolayer that is created by compression on the LB trough, three different starting conditions were tested: 100, 130 and 200 Å^2/lipid. The isotherms recorded from these three different experiments do not deviate from one another (Figure C.1), and, for the scope of this thesis, the starting lipid density was excluded as a relevant parameter.

C.2 Calcein efflux

Calcein excitation-emission spectra and self-quenching

The calcein excitation-emission spectra of calcein are shown in Figure C.2. The spectra were measured with the Cary Eclipse fluorescence spectrometer. To measure the excitation spectrum, the detection scanned frequencies between 300 and 700 nm wavelegth, when the sample was illuminated at its excitation frequency, 495 nm wavelegth. To measure the excitation spectrum, the detection was fixed at 520 nm while the excitation frquencies were scanned.

The strong self-quenching property of calcein was exploited in the calcein efflux functional test. A calibration curve for concentrations between 0.3 μ M
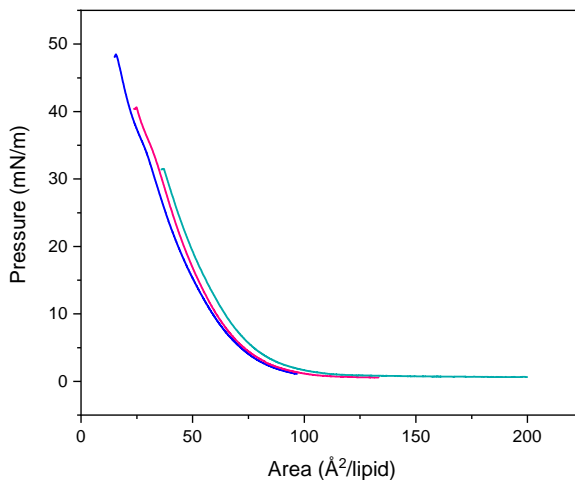
Figure C.1: *Trans azo*-PC compression isotherms. Three compression isotherms of AzoPC from different starting lipid densities.

and 50 mM was measured and it is shown in Figure C.3

Estimation of the efflux-induced dilution of calcein

The proteoliposomes for the calcein efflux assay were loaded with 50 mM calcein and their outer buffer was exchanged as not to contain free calcein. The following back-of-the-envelope calculation was used to determine the optimal concentration of proteoliposomes in solution to allow for fluorescence when the calcein is released upon light triggering.

The final calcein concentration c_f is the mass of encapsulated calcein m_e over the final total volume V_f

$$c_f = \frac{m_e}{V_f}$$

where the encapsulated calcein can be estimated from the initial calcein concentration internal to the proteoliposomes c_i, which is 50 mM, and the total enclosed volume of proteoliposomes V_e

$$m_e = c_i \cdot V_e$$

The volume V_e is the volume of a single liposome V multiplied by the number of liposomes n

$$V_e = V \cdot n$$
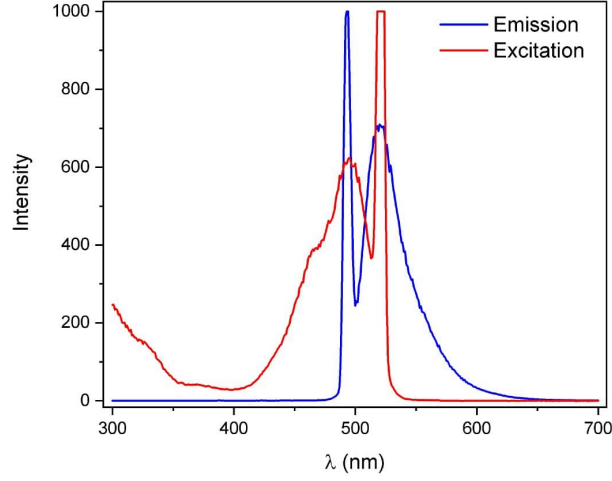
FIGURE C.2: EXCITATION-EMISSION SPECTRA OF CALCEIN. Calcein excitation wavelength is 495 nm and it emits through fluorescence at 520 nm. The large spikes correspond to the excitation light used during the recording of the emission spectrum and to the

Given the mesh used for the extrusion, we can use a liposome radius r of about 50 nm, and therefore a spherical liposome would have a volume of

$$V = \frac{4}{3}\pi r^3 = \frac{4}{3}\pi (5 \times 10^{-8} \text{ m})^3 = 5.23 \times 10^{-22} \text{ m}^3 = 5.23 \times 10^{-19} \text{ L}$$

The number of vescicles can be calculated from the total amount of lipids N divided by the number of lipids per vescicle l

$$n = \frac{N}{l}$$

where l can be estimated to be about 80000, from an average area occupancy of a phospholipid of $a = 0.71 \text{ nm}^2$, and considering two leaflets for the bilayer, one at a radius of $r_1 = 50$ nm and the inner one of $r_2 = 45$ nm

$$l = \frac{4\pi r_1^2 + 4\pi r_2^2}{a} = \frac{3.14 \times 10^{-14} \text{ m}^2 + 2.54 \times 10^{-14} \text{ m}^2}{0.71 \times 10^{-18} \text{ m}^2} \simeq 8 \times 10^4$$

The total amount of lipids N can be calculated from the moles of lipids in solution $N_{mol} = \frac{\text{grams of lipids}}{\text{molecular weight}}$ and Avogadro's number $N_A = 6 \times 10^{23} \text{ mol}^{-1}$

$$N = N_{mol} \cdot N_A = \frac{10^{-3} \text{ g}}{800 \text{ g/mol}} \cdot 6 \times 10^{23} \text{ mol}^{-1} \simeq 7 \times 10^{17}$$

where we used 1 mg of lipids and we approximated to 800 g/mol the molecular weight of PC lipids (DOPC: 786 g/mol, AzoPC = 830 g/mol). If we account
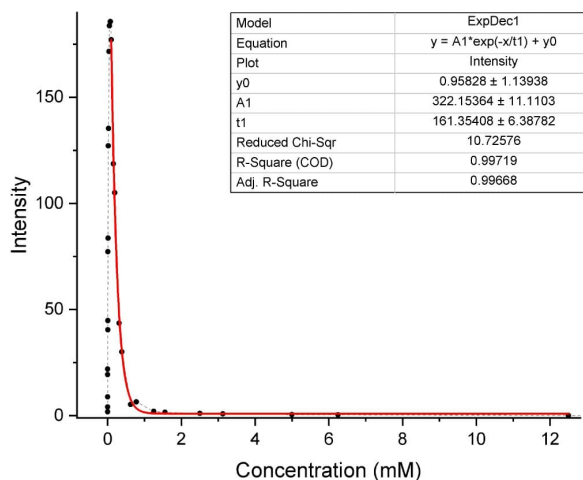
Figure C.3: Calcein self-qunches at high concentrations. Fluorescence intensity *vs.* concentration of free calcein in 10 mM PBS buffer solution, pH 7.2. The increase at lower concentrations is due to the increase of calcein in solution, the fitted exponential decrease at higher concentrations is due to self-quenching. The concentration used inside of the proteoliposomes is 50 mM.

for a $10 - 20\%$ lipid loss during the extrusion, the order of magnitude of N doesn't change and we can consider an effective number of lipids building the liposomes of $N \simeq 6 \times 10^{17}$.

Using the values obtained,

$$n = \frac{N}{l} = \frac{6 \times 10^{17}}{8 \times 10^4} = 7.5 \times 10^{12}$$

$$V_e = n \cdot V = 7.5 \times 10^{12} \cdot 5.23 \times 10^{-19} \text{ L} = 3.9 \times 10^{-6} \text{ L}$$

$$m_e = c_i \cdot V_e = 5 \times 10^{-2} \text{ mol/L} \cdot 3.9 \times 10^{-6} \text{ L} = 1.95 \times 10^{-7} \text{ mol}$$

$$c_f = \frac{m_e}{V_f} = \frac{1.95 \times 10^{-7} \text{ mol}}{3 \text{ mL}} = 6.5 \times 10^{-5} \text{ mol/L} = 65 \ \mu M$$

This concentration corresponds to the emission peak of calcein. Therefore, 0.5 mL of the proteoliposome solution (2 mg/mL), amounting to 1 mg of lipids, is to be diluted with the sucrose buffer as to reach the final desired volume $V_f = 3$ mL.

Reproducibility of the calcein efflux assay

The calcein fluorescence assay presents several difficulties. First of all, in order to keep the azo-lipids of the proteoliposomes as *cis* isomers, the state of lower

membrane tension, the whole sample preparation has to be done in darkness and intermittent UV-light illumination. The blue light is then used to trigger the isomerisation to the *trans* state of the lipid molecules, which cooperatively increase the tension, gating MscL.

A particularly critical step is the external buffer substitution (*cfr.* section 2.1.2 in the Materials and Methods chapter), where the osmotic pressure of the new external buffer without calcein has to equilibrate the one of the internal buffer by the presence of sucrose. A difference in osmotic pressure might otherwise activate the MscL channels while still in the PD-10 column, jeopardizing the whole sample preparation.

Another critical point is the actual measurement: since the fluorimeter does not offer the option to follow the kinetics of one emitted frequency after a triggered illumination, an external blue LED is used instead. The LED is placed on top of the cuvette, in the same position for each sample, but since it gets moved between each measurement, it is impossible to guarantee the exact same position.

Due to these technical issues, it has been very hard to reproduce the calcein efflux assay. On a couple of attempts no change in fluorescence could be observed upon blue light illumination. We suspect a mistake during the sample preparation. In the occasion the experiment did show the exponential increase in fluorescence, three batches of MscL proteoliposomes from the same sample preparation were tested. The traces of the two samples, in addition to the one presented in the Results chapter, are reported in Figure C.4.
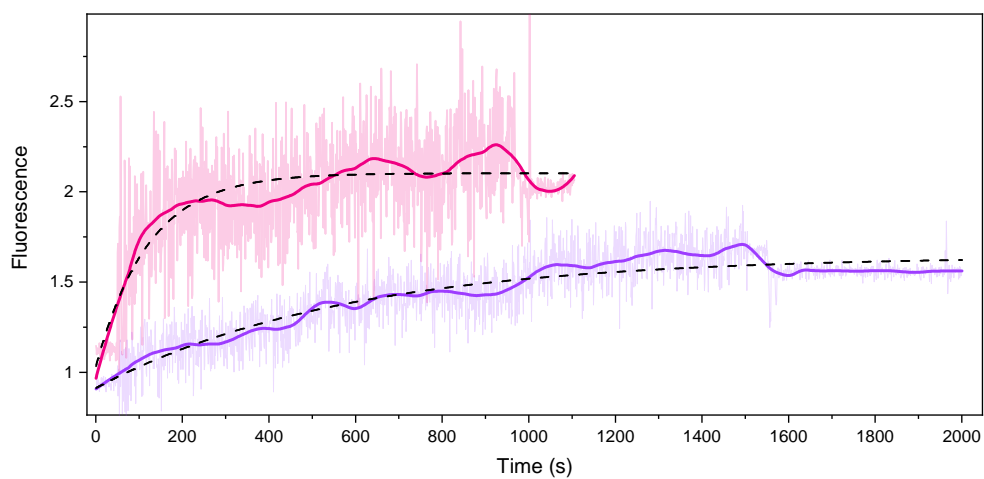
Figure C.4: Additional traces of the calcein efflux experiment. The same calcein efflux experiment on different batches of the same sample show different kinetics and a decrease in fluorescence when the LUVs get dissolved with detergent (1000 s for the pink trace, 1500 s for the lilac trace).

Bibliography

[1] Caroline Uhler and G. V. Shivashankar. Regulation of genome organization and gene expression by nuclear mechanotransduction. *Nature Reviews Molecular Cell Biology*, 18(12):717–727, December 2017. ISSN 1471-0080. doi: 10.1038/nrm.2017.101. URL `https://www.nature.com/articles/nrm.2017.101`. Number: 12 Publisher: Nature Publishing Group.

[2] Benoit Ladoux and René-Marc Mège. Mechanobiology of collective cell behaviours. *Nature Reviews Molecular Cell Biology*, 18(12):743–757, December 2017. ISSN 1471-0080. doi: 10.1038/nrm.2017.98. URL `https://www.nature.com/articles/nrm.2017.98`. Number: 12 Publisher: Nature Publishing Group.

[3] Michele A. Wozniak and Christopher S. Chen. Mechanotransduction in development: a growing role for contractility. *Nature Reviews Molecular Cell Biology*, 10(1):34–43, January 2009. ISSN 1471-0080. doi: 10.1038/nrm2592. URL `https://www.nature.com/articles/nrm2592`. Number: 1 Publisher: Nature Publishing Group.

[4] Carl-Philipp Heisenberg and Yohanns Bellaïche. Forces in Tissue Morphogenesis and Patterning. *Cell*, 153(5):948–962, May 2013. ISSN 0092-8674. doi: 10.1016/j.cell.2013.05.008. URL `http://www.sciencedirect.com/science/article/pii/S0092867413005734`.

[5] Nicoletta I. Petridou, Zoltán Spiró, and Carl-Philipp Heisenberg. Multiscale force sensing in development. *Nature Cell Biology*, 19(6):581–588, June 2017. ISSN 1476-4679. doi: 10.1038/ncb3524. URL `https://www.nature.com/articles/ncb3524`. Number: 6 Publisher: Nature Publishing Group.

[6] Gary R. Lewin and Rabih Moshourab. Mechanosensation and pain. *Journal of Neurobiology*, 61(1):30–44, 2004. ISSN 1097-4695. doi: 10.1002/neu.20078. URL `https://onlinelibrary.wiley.com/doi/abs/10.1002/neu.20078`. _eprint: https://onlinelibrary.wiley.com/doi/pdf/10.1002/neu.20078.

[7] Jeroen Eyckmans, Thomas Boudou, Xiang Yu, and Christopher S. Chen. A Hitchhiker's Guide to Mechanobiology. *Developmental Cell*, 21(1): 35–47, July 2011. ISSN 1534-5807. doi: 10.1016/j.devcel.2011.06. 015. URL `http://www.sciencedirect.com/science/article/pii/ S1534580711002498`.

[8] Thomas Iskratsch, Haguy Wolfenson, and Michael P. Sheetz. Appreciating force and shape — the rise of mechanotransduction in cell biology. *Nature Reviews Molecular Cell Biology*, 15(12):825–833, December 2014. ISSN 1471-0080. doi: 10.1038/nrm3903. URL `https: //www.nature.com/articles/nrm3903`. Number: 12 Publisher: Nature Publishing Group.

[9] Ching Kung. A possible unifying principle for mechanosensation. *Nature*, 436(7051):647–654, 2005. ISSN 0028-0836. doi: 10.1038/nature03896. URL `https://dx.doi.org/10.1038/nature03896`.

[10] Glen G. Ernstrom and Martin Chalfie. Genetics of Sensory Mechanotransduction. *Annual Review of Genetics*, 36(1):411–453, December 2002. ISSN 0066-4197. doi: 10.1146/annurev.genet.36. 061802.101708. URL `https://www.annualreviews.org/doi/10.1146/ annurev.genet.36.061802.101708`. Publisher: Annual Reviews.

[11] Jóhanna Árnadóttir and Martin Chalfie. Eukaryotic Mechanosensitive Channels. *Annual Review of Biophysics*, 39(1):111–137, 2010. doi: 10.1146/annurev.biophys.37.032807.125836. URL `https://doi.org/ 10.1146/annurev.biophys.37.032807.125836`. _eprint: https://-doi.org/10.1146/annurev.biophys.37.032807.125836.

[12] Peng Jin, Lily Yeh Jan, and Yuh-Nung Jan. Mechanosensitive Ion Channels: Structural Features Relevant to Mechanotransduction Mechanisms. *Annual Review of Neuroscience*, 43(1):207–229, 2020. doi: 10.1146/annurev-neuro-070918-050509. URL `https:// doi.org/10.1146/annurev-neuro-070918-050509`. _eprint: https://-doi.org/10.1146/annurev-neuro-070918-050509.

[13] J. M. Kefauver, A. B. Ward, and A. Patapoutian. Discoveries in structure and physiology of mechanically activated ion channels. *Nature*, 587(7835):567–576, November 2020. ISSN 0028-0836, 1476-4687. doi: 10.1038/s41586-020-2933-1. URL `http://www.nature.com/articles/ s41586-020-2933-1`.

[14] Charles D. Cox, Navid Bavi, and Boris Martinac. Bacterial Mechanosensors. *Annual Review of Physiology*, 80(1):71–93, 2018. doi: 10.1146/annurev-physiol-021317-121351. URL `https://doi. org/10.1146/annurev-physiol-021317-121351`. _eprint: https://-doi.org/10.1146/annurev-physiol-021317-121351.

[15] Jinfeng Teng, Stephen Loukin, Andriy Anishkin, and Ching Kung. The Force-From-Lipid (FFL) principle of mechanosensitivity, at large and in elements. *Pflugers Archiv : European journal of physiology*, 467(1): 27–37, January 2015. ISSN 0031-6768. doi: 10.1007/s00424-014-1530-2. URL https://www.ncbi.nlm.nih.gov/pmc/articles/PMC4254906/.

[16] B. Martinac, M. Buechner, A. H. Delcour, J. Adler, and C. Kung. Pressure-sensitive ion channel in Escherichia coli. *Proceedings of the National Academy of Sciences*, 84(8):2297–2301, April 1987. ISSN 0027-8424, 1091-6490. doi: 10.1073/pnas.84.8.2297. URL https://www.pnas.org/content/84/8/2297. Publisher: National Academy of Sciences Section: Research Article.

[17] Paul C. Moe, Paul Blount, and Ching Kung. Functional and structural conservation in the mechanosensitive channel MscL implicates elements crucial for mechanosensation. *Molecular Microbiology*, 28(3):583–592, 1998. ISSN 1365-2958. doi: 10.1046/j.1365-2958.1998.00821.x. URL https://onlinelibrary.wiley.com/doi/abs/10.1046/j.1365-2958.1998.00821.x. _eprint: https://onlinelibrary.wiley.com/doi/pdf/10.1046/j.1365-2958.1998.00821.x.

[18] Geoffrey Chang, Robert H. Spencer, Allen T. Lee, Margaret T. Barclay, and Douglas C. Rees. Structure of the MscL Homolog from Mycobacterium tuberculosis: A Gated Mechanosensitive Ion Channel. *Science*, 282(5397):2220–2226, December 1998. ISSN 0036-8075, 1095-9203. doi: 10.1126/science.282.5397.2220. URL https://science.sciencemag.org/content/282/5397/2220. Publisher: American Association for the Advancement of Science Section: Research Article.

[19] Paul Blount and Irene Iscla. Life with Bacterial Mechanosensitive Channels, from Discovery to Physiology to Pharmacological Target. *Microbiology and Molecular Biology Reviews*, 84(1), February 2020. ISSN 1092-2172, 1098-5557. doi: 10.1128/MMBR.00055-19. URL https://mmbr.asm.org/content/84/1/e00055-19. Publisher: American Society for Microbiology Section: Review.

[20] Sergei I. Sukharev, Paul Blount, Boris Martinac, Frederick R. Blattner, and Ching Kung. A large-conductance mechanosensitive channel in E. coli encoded by mscL alone. *Nature*, 368(6468):265–268, March 1994. ISSN 1476-4687. doi: 10.1038/368265a0. URL https://www.nature.com/articles/368265a0. Number: 6468 Publisher: Nature Publishing Group.

[21] Paul Moe and Paul Blount. Assessment of Potential Stimuli for Mechano-Dependent Gating of MscL: Effects of Pressure, Tension, and Lipid Headgroups. *Biochemistry*, 44(36):12239–12244, September 2005. ISSN

0006-2960. doi: 10.1021/bi0509649. URL https://doi.org/10.1021/bi0509649. Publisher: American Chemical Society.

[22] Boris Martinac, Julius Adler, and Ching Kung. Mechanosensitive ion channels of E. coli activated by amphipaths. *Nature*, 348(6298): 261–263, November 1990. ISSN 1476-4687. doi: 10.1038/348261a0. URL https://www.nature.com/articles/348261a0. Number: 6298 Publisher: Nature Publishing Group.

[23] S. I. Sukharev, B. Martinac, V. Y. Arshavsky, and C. Kung. Two types of mechanosensitive channels in the Escherichia coli cell envelope: solubilization and functional reconstitution. *Biophysical Journal*, 65(1): 177–183, July 1993. ISSN 0006-3495. doi: 10.1016/S0006-3495(93) 81044-0. URL http://www.sciencedirect.com/science/article/pii/S0006349593810440.

[24] Andrew R. Battle, Evgeny Petrov, Prithwish Pal, and Boris Martinac. Rapid and improved reconstitution of bacterial mechanosensitive ion channel proteins MscS and MscL into liposomes using a modified sucrose method. *FEBS Letters*, 583(2):407–412, January 2009. ISSN 0014-5793. doi: 10.1016/j.febslet.2008.12.033. URL http://www.sciencedirect.com/science/article/pii/S0014579308010247.

[25] Boris Martinac, Paul R. Rohde, Andrew R. Battle, Evgeny Petrov, Prithwish Pal, Alexander Fook Weng Foo, Valeria Vásquez, Thuan Huynh, and Anna Kloda. Studying Mechanosensitive Ion Channels Using Liposomes. In Volkmar Weissig, editor, *Liposomes: Methods and Protocols, Volume 2: Biological Membrane Models*, Methods in Molecular Biology™, pages 31–53. Humana Press, Totowa, NJ, 2010. ISBN 978-1-60761-447-0. doi: 10.1007/978-1-60761-447-0_4. URL https://doi.org/10.1007/978-1-60761-447-0_4.

[26] Maria Barthmes, Mac Donald F. Jose, Jan Peter Birkner, Andrea Brüggemann, Christian Wahl-Schott, and Armağan Koçer. Studying mechanosensitive ion channels with an automated patch clamp. *European Biophysics Journal*, 43(2):97–104, March 2014. ISSN 1432-1017. doi: 10.1007/s00249-014-0944-2. URL https://doi.org/10.1007/s00249-014-0944-2.

[27] Hanna M. G. Barriga, Paula Booth, Stuart Haylock, Richard Bazin, Richard H. Templer, and Oscar Ces. Droplet interface bilayer reconstitution and activity measurement of the mechanosensitive channel of large conductance from Escherichia coli. *Journal of The Royal Society Interface*, 11(98):20140404, September 2014. doi: 10.1098/rsif.2014.0404. URL https://royalsocietypublishing.org/doi/10.1098/rsif.2014.0404. Publisher: Royal Society.

[28] Joseph S. Najem, Myles D. Dunlap, Ian D. Rowe, Eric C. Freeman, John W. Grant, Sergei Sukharev, and Donald J. Leo. Activation of bacterial channel MscL in mechanically stimulated droplet interface bilayers. *Scientific Reports*, 5(1):13726, September 2015. ISSN 2045-2322. doi: 10.1038/srep13726. URL `https://www.nature.com/articles/srep13726`. Number: 1 Publisher: Nature Publishing Group.

[29] Kadla R. Rosholm, Matthew A. B. Baker, Pietro Ridone, Yoshitaka Nakayama, Paul R. Rohde, Luis G. Cuello, Lawrence K. Lee, and Boris Martinac. Activation of the mechanosensitive ion channel MscL by mechanical stimulation of supported Droplet-Hydrogel bilayers. *Scientific Reports*, 7(1):45180, March 2017. ISSN 2045-2322. doi: 10. 1038/srep45180. URL `https://www.nature.com/articles/srep45180`. Number: 1 Publisher: Nature Publishing Group.

[30] Navid Bavi, D. Marien Cortes, Charles D. Cox, Paul R. Rohde, Weihong Liu, Joachim W. Deitmer, Omid Bavi, Pavel Strop, Adam P. Hill, Douglas Rees, Ben Corry, Eduardo Perozo, and Boris Martinac. The role of MscL amphipathic N terminus indicates a blueprint for bilayer-mediated gating of mechanosensitive channels. *Nature Communications*, 7(1):11984, June 2016. ISSN 2041-1723. doi: 10.1038/ncomms11984. URL `https://www.nature.com/articles/ncomms11984`. Number: 1 Publisher: Nature Publishing Group.

[31] C. D. Cox, N. Bavi, and B. Martinac. Origin of the Force: The Force-From-Lipids Principle Applied to Piezo Channels. *Current Topics in Membranes*, 79:59–96, 2017. ISSN 1063-5823. doi: 10.1016/bs.ctm.2016. 09.001.

[32] Juan M. Vanegas and Marino Arroyo. Force Transduction and Lipid Binding in MscL: A Continuum-Molecular Approach. *PLoS ONE*, 9 (12):e113947, December 2014. ISSN 1932-6203. doi: 10.1371/journal. pone.0113947. URL `https://dx.plos.org/10.1371/journal.pone.0113947`.

[33] Bharat Reddy, Navid Bavi, Allen Lu, Yeonwoo Park, and Eduardo Perozo. Molecular basis of force-from-lipids gating in the mechanosensitive channel MscS. *eLife*, 8:e50486, December 2019. ISSN 2050-084X. doi: 10.7554/eLife.50486. URL `https://doi.org/10.7554/eLife.50486`. Publisher: eLife Sciences Publications, Ltd.

[34] Eduardo Perozo, D. Marien Cortes, Pornthep Sompornpisut, Anna Kloda, and Boris Martinac. Open channel structure of MscL and the gating mechanism of mechanosensitive channels. *Nature*, 418(6901):942–948, August 2002. ISSN 1476-4687. doi: 10.1038/nature00992. URL `https:`

//www.nature.com/articles/nature00992. Number: 6901 Publisher: Nature Publishing Group.

[35] Eduardo Perozo, Anna Kloda, D. Marien Cortes, and Boris Martinac. Physical principles underlying the transduction of bilayer deformation forces during mechanosensitive channel gating. *Nature Structural Biology*, 9(9):696–703, September 2002. ISSN 1545-9985. doi: 10.1038/nsb827. URL https://www.nature.com/articles/nsb827. Number: 9 Publisher: Nature Publishing Group.

[36] Stefan Steinbacher, Randal Bass, Pavel Strop, and Douglas C. Rees. Structures of the Prokaryotic Mechanosensitive Channels MscL and MscS. In *Current Topics in Membranes*, volume 58 of *Mechanosensitive Ion Channels, Part A*, pages 1–24. Academic Press, January 2007. doi: 10.1016/S1063-5823(06)58001-9. URL https://www.sciencedirect.com/science/article/pii/S1063582306580019.

[37] Zhenfeng Liu, Chris S. Gandhi, and Douglas C. Rees. Structure of a tetrameric MscL in an expanded intermediate state. *Nature*, 461 (7260):120–124, September 2009. ISSN 1476-4687. doi: 10.1038/nature08277. URL https://www.nature.com/articles/nature08277. Bandiera_abtest: a Cg_type: Nature Research Journals Number: 7260 Primary_atype: Research Publisher: Nature Publishing Group.

[38] Eamonn Reading, Troy A. Walton, Idlir Liko, Michael T. Marty, Arthur Laganowsky, Douglas C. Rees, and Carol V. Robinson. The Effect of Detergent, Temperature, and Lipid on the Oligomeric State of MscL Constructs: Insights from Mass Spectrometry. *Chemistry & Biology*, 22 (5):593–603, May 2015. ISSN 1074-5521. doi: 10.1016/j.chembiol.2015.04.016. URL https://www.sciencedirect.com/science/article/pii/S107455211500160X.

[39] Daniel Balleza and Froylan Gómez-Lagunas. Conserved motifs in mechanosensitive channels MscL and MscS. *European biophysics journal: EBJ*, 38(7):1013–1027, September 2009. ISSN 1432-1017. doi: 10.1007/s00249-009-0460-y.

[40] Isaiah T. Arkin, Sergei I. Sukharev, Paul Blount, Ching Kung, and Axel T. Brünger. Helicity, membrane incorporation, orientation and thermal stability of the large conductance mechanosensitive ion channel from E. coli. *Biochimica et Biophysica Acta (BBA) - Biomembranes*, 1369(1): 131–140, February 1998. ISSN 0005-2736. doi: 10.1016/S0005-2736(97)00219-8. URL https://www.sciencedirect.com/science/article/pii/S0005273697002198.

[41] Paul Blount, Sergei I Sukharev, Moe, Matthew J. Schroeder, H. Robert Guy, and Ching Kung. Membrane topology and multimeric structure of a

mechanosensitive channel protein of Escherichia coli. *The EMBO Journal*, 15(18):4798–4805, September 1996. ISSN 0261-4189. doi: 10.1002/ j.1460-2075.1996.tb00860.x. URL `https://www.embopress.org/doi/ abs/10.1002/j.1460-2075.1996.tb00860.x`. Publisher: John Wiley & Sons, Ltd.

[42] Paul Blount, Sergei I Sukharev, Paul C Moe, Scott K Nagle, and Ching Kung. Towards an understanding of the structural and functional properties of MscL, a mechanosensitive channel in bacteria. *Biology of the Cell*, 87(1):1–8, January 1996. ISSN 0248-4900. doi: 10.1016/S0248-4900(97)89832-2. URL `https://www.sciencedirect. com/science/article/pii/S0248490097898322`.

[43] P. Blount, S. I. Sukharev, M. J. Schroeder, S. K. Nagle, and C. Kung. Single residue substitutions that change the gating properties of a mechanosensitive channel in Escherichia coli. *Proceedings of the National Academy of Sciences*, 93(21):11652–11657, October 1996. ISSN 0027-8424, 1091-6490. doi: 10.1073/pnas.93.21.11652. URL `https: //www.pnas.org/content/93/21/11652`. Publisher: National Academy of Sciences Section: Research Article.

[44] C. C. Häse, A. C. Le Dain, and B. Martinac. Molecular dissection of the large mechanosensitive ion channel (MscL) of E. coli: Mutants with altered channel gating and pressure sensitivity. *The Journal of Membrane Biology*, 157(1):17–25, May 1997. ISSN 1432-1424. doi: 10.1007/ s002329900212. URL `https://doi.org/10.1007/s002329900212`.

[45] Sergei Sukharev, Monica Betanzos, Chien-Sung Chiang, and H. Robert Guy. The gating mechanism of the large mechanosensitive channel MscL. *Nature*, 409(6821):720–724, February 2001. ISSN 1476-4687. doi: 10. 1038/35055559. URL `https://www.nature.com/articles/35055559`. Bandiera_abtest: a Cg_type: Nature Research Journals Number: 6821 Primary_atype: Research Publisher: Nature Publishing Group.

[46] S. Sukharev, S. R. Durell, and H. R. Guy. Structural models of the MscL gating mechanism. *Biophysical Journal*, 81(2):917–936, August 2001. ISSN 0006-3495. doi: 10.1016/S0006-3495(01)75751-7.

[47] H. Valadié, J.J. Lacapčre, Y.-H. Sanejouand, and C. Etchebest. Dynamical Properties of the MscL of Escherichia coli: A Normal Mode Analysis. *Journal of Molecular Biology*, 332(3):657–674, September 2003. ISSN 00222836. doi: 10.1016/S0022-2836(03)00851-9. URL `https: //linkinghub.elsevier.com/retrieve/pii/S0022283603008519`.

[48] Irene Iscla, Robin Wray, and Paul Blount. On the Structure of the N-Terminal Domain of the MscL Channel: Helical Bundle or Membrane Interface. *Biophysical Journal*, 95(5):2283–2291, September 2008.

ISSN 0006-3495. doi: 10.1529/biophysj.107.127423. URL `https://www.sciencedirect.com/science/article/pii/S0006349508783760`.

[49] Ben Corry, Annette C. Hurst, Prithwish Pal, Takeshi Nomura, Paul Rigby, and Boris Martinac. An improved open-channel structure of MscL determined from FRET confocal microscopy and simulation. *Journal of General Physiology*, 136(4):483–494, September 2010. ISSN 0022-1295. doi: 10.1085/jgp.200910376. URL `https://doi.org/10.1085/jgp.200910376`.

[50] Adam D. Martinac, Navid Bavi, Omid Bavi, and Boris Martinac. Pulling MscL open via N-terminal and TM1 helices: A computational study towards engineering an MscL nanovalve. *PLOS ONE*, 12(8): e0183822, August 2017. ISSN 1932-6203. doi: 10.1371/journal.pone.0183822. URL `https://journals.plos.org/plosone/article?id=10.1371/journal.pone.0183822`. Publisher: Public Library of Science.

[51] Andriy Anishkin, Vyacheslav Gendel, Neda A. Sharifi, Chien-Sung Chiang, Lena Shirinian, H. Robert Guy, and Sergei Sukharev. On the Conformation of the COOH-terminal Domain of the Large Mechanosensitive Channel MscL. *Journal of General Physiology*, 121(3):227–244, February 2003. ISSN 0022-1295. doi: 10.1085/jgp.20028768. URL `https://doi.org/10.1085/jgp.20028768`.

[52] Navid Bavi, Adam D. Martinac, D. Marien Cortes, Omid Bavi, Pietro Ridone, Takeshi Nomura, Adam P. Hill, Boris Martinac, and Eduardo Perozo. Structural Dynamics of the MscL C-terminal Domain. *Scientific Reports*, 7(1):17229, December 2017. ISSN 2045-2322. doi: 10.1038/s41598-017-17396-w. URL `https://www.nature.com/articles/s41598-017-17396-w`. Bandiera_abtest: a Cc_license_type: cc_by Cg_type: Nature Research Journals Number: 1 Primary_atype: Research Publisher: Nature Publishing Group Subject_term: Ion transport;Molecular conformation Subject_term_id: ion-transport;molecular-conformation.

[53] Anna Kloda, Alexandre Ghazi, and Boris Martinac. C-Terminal Charged Cluster of MscL, RKKEE, Functions as a pH Sensor. *Biophysical Journal*, 90(6):1992–1998, March 2006. ISSN 0006-3495. doi: 10.1529/biophysj.105.075481. URL `https://www.sciencedirect.com/science/article/pii/S0006349506723840`.

[54] Nadia Herrera, Grigory Maksaev, Elizabeth S. Haswell, and Douglas C. Rees. Elucidating a role for the cytoplasmic domain in the Mycobacterium tuberculosis mechanosensitive channel of large conductance. *Scientific Reports*, 8(1):14566, October 2018. ISSN 2045-2322. doi: 10.1038/s41598-018-32536-6. URL `https://www.nature.com/`

articles/s41598-018-32536-6. Bandiera_abtest: a Cc_license_type: cc_by Cg_type: Nature Research Journals Number: 1 Primary_atype: Research Publisher: Nature Publishing Group Subject_term: Permeation and transport;X-ray crystallography Subject_term_id: permeation-and-transport;x-ray-crystallography.

[55] Chie Ando, Naili Liu, and Kenjiro Yoshimura. A cytoplasmic helix is required for pentamer formation of the Escherichia coli MscL mechanosensitive channel. *The Journal of Biochemistry*, 158(2):109–114, August 2015. ISSN 0021-924X. doi: 10.1093/jb/mvv019. URL `https://doi.org/10.1093/jb/mvv019`.

[56] Li-Min Yang, Robin Wray, Juandell Parker, Danyell Wilson, Randolph S. Duran, and Paul Blount. Three Routes To Modulate the Pore Size of the MscL Channel/Nanovalve. *ACS Nano*, 6(2):1134–1141, February 2012. ISSN 1936-0851. doi: 10.1021/nn203703j. URL `https://doi.org/10.1021/nn203703j`. Publisher: American Chemical Society.

[57] Bassam Ajouz, Catherine Berrier, Madeleine Besnard, Boris Martinac, and Alexandre Ghazi. Contributions of the Different Extramembranous Domains of the Mechanosensitive Ion Channel MscL to Its Response to Membrane Tension *. *Journal of Biological Chemistry*, 275(2):1015–1022, January 2000. ISSN 0021-9258, 1083-351X. doi: 10.1074/jbc.275.2.1015. URL `https://www.jbc.org/article/S0021-9258(18)31212-2/abstract`. Publisher: Elsevier.

[58] Kenjiro Yoshimura, Takeshi Nomura, and Masahiro Sokabe. Loss-of-Function Mutations at the Rim of the Funnel of Mechanosensitive Channel MscL. *Biophysical Journal*, 86(4):2113–2120, April 2004. ISSN 0006-3495. doi: 10.1016/S0006-3495(04)74270-8. URL `https://www.sciencedirect.com/science/article/pii/S0006349504742708`.

[59] Kyu-Ho Park, Catherine Berrier, Boris Martinac, and Alexandre Ghazi. Purification and Functional Reconstitution of N- and C-Halves of the MscL Channel. *Biophysical Journal*, 86(4):2129–2136, April 2004. ISSN 0006-3495. doi: 10.1016/S0006-3495(04)74272-1. URL `https://www.cell.com/biophysj/abstract/S0006-3495(04)74272-1`. Publisher: Elsevier.

[60] Li-Min Yang, Dalian Zhong, and Paul Blount. Chimeras Reveal a Single Lipid-Interface Residue that Controls MscL Channel Kinetics as well as Mechanosensitivity. *Cell Reports*, 3(2):520–527, February 2013. ISSN 2211-1247. doi: 10.1016/j.celrep.2013.01.018. URL `https://www.sciencedirect.com/science/article/pii/S2211124713000259`.

[61] C. C. Cruickshank, R. F. Minchin, A. C. Le Dain, and B. Martinac. Estimation of the pore size of the large-conductance mechanosensitive ion channel of Escherichia coli. *Biophysical Journal*, 73(4): 1925–1931, October 1997. ISSN 0006-3495. doi: 10.1016/S0006-3495(97) 78223-7. URL `https://www.sciencedirect.com/science/article/pii/S0006349597782237`.

[62] Yong Wang, Yanxin Liu, Hannah A DeBerg, Takeshi Nomura, Melinda Tonks Hoffman, Paul R Rohde, Klaus Schulten, Boris Martinac, and Paul R Selvin. Single molecule FRET reveals pore size and opening mechanism of a mechano-sensitive ion channel. *eLife*, 3: e01834, February 2014. ISSN 2050-084X. doi: 10.7554/eLife.01834. URL `https://doi.org/10.7554/eLife.01834`. Publisher: eLife Sciences Publications, Ltd.

[63] Geert van den Bogaart, Victor Krasnikov, and Bert Poolman. Dual-Color Fluorescence-Burst Analysis to Probe Protein Efflux through the Mechanosensitive Channel MscL. *Biophysical Journal*, 92(4): 1233–1240, February 2007. ISSN 0006-3495. doi: 10.1529/biophysj.106. 088708. URL `https://www.sciencedirect.com/science/article/pii/S0006349507709347`.

[64] Xiaorong Ou, Paul Blount, Robert J. Hoffman, and Ching Kung. One face of a transmembrane helix is crucial in mechanosensitive channel gating. *Proceedings of the National Academy of Sciences of the United States of America*, 95(19):11471–11475, September 1998. ISSN 0027-8424. URL `https://www.ncbi.nlm.nih.gov/pmc/articles/PMC21667/`.

[65] Jan Peter Birkner, Bert Poolman, and Armağan Koçer. Hydrophobic gating of mechanosensitive channel of large conductance evidenced by single-subunit resolution. *Proceedings of the National Academy of Sciences of the United States of America*, 109(32):12944–12949, August 2012. ISSN 1091-6490. doi: 10.1073/pnas.1205270109.

[66] Kenjiro Yoshimura, Ann Batiza, Matt Schroeder, Paul Blount, and Ching Kung. Hydrophilicity of a Single Residue within MscL Correlates with Increased Channel Mechanosensitivity. *Biophysical Journal*, 77(4): 1960–1972, October 1999. ISSN 0006-3495. doi: 10.1016/S0006-3495(99) 77037-2. URL `https://www.sciencedirect.com/science/article/pii/S0006349599770372`.

[67] Kenjiro Yoshimura, Ann Batiza, and Ching Kung. Chemically Charging the Pore Constriction Opens the Mechanosensitive Channel MscL. *Biophysical Journal*, 80(5):2198–2206, May 2001. ISSN 0006-3495. doi: 10.1016/S0006-3495(01)76192-9. URL `https://www.sciencedirect.com/science/article/pii/S0006349501761929`.

[68] Irene Iscla, Christina Eaton, Juandell Parker, Robin Wray, Zoltán Kovács, and Paul Blount. Improving the Design of a MscL-Based Triggered Nanovalve. *Biosensors*, 3(1):171–184, 2013. ISSN 2079-6374. doi: 10. 3390/bios3010171.

[69] Joshua A. Maurer and Dennis A. Dougherty. Generation and Evaluation of a Large Mutational Library from the Escherichia coli Mechanosensitive Channel of Large Conductance, MscL: IMPLICATIONS FOR CHANNEL GATING AND EVOLUTIONARY DESIGN *. *Journal of Biological Chemistry*, 278(23):21076–21082, June 2003. ISSN 0021-9258, 1083-351X. doi: 10.1074/jbc.M302892200. URL `https://www.jbc.org/article/ S0021-9258(20)73415-0/abstract`. Publisher: Elsevier.

[70] Irene Iscla, Gal Levin, Robin Wray, Robert Reynolds, and Paul Blount. Defining the Physical Gate of a Mechanosensitive Channel, MscL, by Engineering Metal-Binding Sites. *Biophysical Journal*, 87(5):3172–3180, November 2004. ISSN 0006-3495. doi: 10. 1529/biophysj.104.049833. URL `https://www.cell.com/biophysj/ abstract/S0006-3495(04)73786-8`. Publisher: Elsevier.

[71] Yuezhou Li, Robin Wray, Christina Eaton, and Paul Blount. An open-pore structure of the mechanosensitive channel MscL derived by determining transmembrane domain interactions upon gating. *The FASEB Journal*, 23(7):2197–2204, 2009. ISSN 1530-6860. doi: 10.1096/fj.09-129296. URL `https://onlinelibrary.wiley.com/doi/ abs/10.1096/fj.09-129296`. _eprint: https://onlinelibrary.wiley.com/- doi/pdf/10.1096/fj.09-129296.

[72] Michael R. Dorwart, Robin Wray, Chad A. Brautigam, Youxing Jiang, and Paul Blount. S. aureus MscL Is a Pentamer In Vivo but of Variable Stoichiometries In Vitro: Implications for Detergent-Solubilized Membrane Proteins. *PLOS Biology*, 8(12): e1000555, December 2010. ISSN 1545-7885. doi: 10.1371/journal.pbio. 1000555. URL `https://journals.plos.org/plosbiology/article? id=10.1371/journal.pbio.1000555`. Publisher: Public Library of Science.

[73] Chris S Gandhi, Troy A Walton, and Douglas C Rees. OCAM: A new tool for studying the oligomeric diversity of MscL channels. *Protein Science : A Publication of the Protein Society*, 20(2):313–326, February 2011. ISSN 0961-8368. doi: 10.1002/pro.562. URL `https://www.ncbi. nlm.nih.gov/pmc/articles/PMC3048416/`.

[74] Andrew A. Beharry and G. Andrew Woolley. Azobenzene photoswitches for biomolecules. *Chemical Society Reviews*, 40(8):4422–4437, 2011. doi: 10.1039/C1CS15023E. URL `https://pubs.rsc.org/en/content/`

articlelanding/2011/cs/c1cs15023e. Publisher: Royal Society of Chemistry.

[75] Philipp Weis and Si Wu. Light-Switchable Azobenzene-Containing Macro-molecules: From UV to Near Infrared. *Macromolecular Rapid Communications*, 39(1):1700220, 2018. ISSN 1521-3927. doi: https://doi.org/ 10.1002/marc.201700220. URL `https://onlinelibrary.wiley.com/ doi/abs/10.1002/marc.201700220`. _eprint: https://onlinelibrary.wiley.com/doi/pdf/10.1002/marc.201700220.

[76] Katharina Hüll, Johannes Morstein, and Dirk Trauner. In Vivo Pho-topharmacology. *Chemical Reviews*, 118(21):10710–10747, November 2018. ISSN 0009-2665. doi: 10.1021/acs.chemrev.8b00037. URL `https://doi.org/10.1021/acs.chemrev.8b00037`. Publisher: American Chemical Society.

[77] Olga Bozovic, Brankica Jankovic, and Peter Hamm. Using azoben-zene photocontrol to set proteins in motion. *Nature Reviews Chemistry*, pages 1–13, December 2021. ISSN 2397-3358. doi: 10. 1038/s41570-021-00338-6. URL `https://www.nature.com/articles/ s41570-021-00338-6`. Bandiera_abtest: a Cg_type: Nature Research Journals Primary_atype: Reviews Publisher: Nature Publishing Group Subject_term: Biophysical chemistry;Physical chemistry Subject_term_id: biophysical-chemistry;physical-chemistry.

[78] Johannes Morstein, Anna C. Impastato, and Dirk Trauner. Photoswitch-able Lipids. *ChemBioChem*, 22(1):73–83, 2021. ISSN 1439-7633. doi: 10.1002/cbic.202000449. URL `https://onlinelibrary.wiley.com/ doi/abs/10.1002/cbic.202000449`. _eprint: https://onlinelibrary.wiley.com/doi/pdf/10.1002/cbic.202000449.

[79] Carla Pernpeintner, James A. Frank, Patrick Urban, Christian R. Roeske, Stefanie D. Pritzl, Dirk Trauner, and Theobald Lohmüller. Light-Controlled Membrane Mechanics and Shape Transitions of Pho-toswitchable Lipid Vesicles. *Langmuir*, 33(16):4083–4089, April 2017. ISSN 0743-7463. doi: 10.1021/acs.langmuir.7b01020. URL `https: //doi.org/10.1021/acs.langmuir.7b01020`. Publisher: American Chemical Society.

[80] Claudia C. Häse, Alexander C. Le Dain, and Boris Martinac. Pu-rification and Functional Reconstitution of the Recombinant Large Mechanosensitive Ion Channel (MscL) of Escherichia coli. *Journal of Biological Chemistry*, 270(31):18329–18334, August 1995. ISSN 0021-9258, 1083-351X. doi: 10.1074/jbc.270.31.18329. URL `http: //www.jbc.org/content/270/31/18329`. Publisher: American Society for Biochemistry and Molecular Biology.

[81] Patrick Urban, Stefanie D. Pritzl, David B. Konrad, James A. Frank, Carla Pernpeintner, Christian R. Roeske, Dirk Trauner, and Theobald Lohmüller. Light-Controlled Lipid Interaction and Membrane Organization in Photolipid Bilayer Vesicles. *Langmuir*, 34(44):13368–13374, November 2018. ISSN 0743-7463. doi: 10.1021/acs.langmuir.8b03241. URL https://doi.org/10.1021/acs.langmuir.8b03241. Publisher: American Chemical Society.

[82] Patrick Urban, Stefanie D. Pritzl, Martina F. Ober, Christina F. Dirscherl, Carla Pernpeintner, David B. Konrad, James A. Frank, Dirk Trauner, Bert Nickel, and Theobald Lohmueller. A Lipid Photoswitch Controls Fluidity in Supported Bilayer Membranes. *Langmuir*, 36(10):2629–2634, March 2020. ISSN 0743-7463. doi: 10.1021/acs.langmuir.9b02942. URL https://doi.org/10.1021/acs.langmuir.9b02942. Publisher: American Chemical Society.

[83] Mahmoudreza Doroudgar, Johannes Morstein, Johanna Becker-Baldus, Dirk Trauner, and Clemens Glaubitz. How Photoswitchable Lipids Affect the Order and Dynamics of Lipid Bilayers and Embedded Proteins. *Journal of the American Chemical Society*, 143(25):9515–9528, June 2021. ISSN 0002-7863. doi: 10.1021/jacs.1c03524. URL https://doi.org/10.1021/jacs.1c03524. Publisher: American Chemical Society.

[84] Ilia G. Denisov and Stephen G. Sligar. Nanodiscs in Membrane Biochemistry and Biophysics. *Chemical Reviews*, 117(6):4669–4713, March 2017. ISSN 0009-2665. doi: 10.1021/acs.chemrev.6b00690. URL https://doi.org/10.1021/acs.chemrev.6b00690. Publisher: American Chemical Society.

[85] Stephen G. Sligar and Ilia G. Denisov. Nanodiscs: A toolkit for membrane protein science. *Protein Science*, 30(2):297–315, 2021. ISSN 1469-896X. doi: 10.1002/pro.3994. URL https://onlinelibrary.wiley.com/doi/abs/10.1002/pro.3994. _eprint: https://onlinelibrary.wiley.com/doi/pdf/10.1002/pro.3994.

[86] Kenichi Ataka, Sven Timo Stripp, and Joachim Heberle. Surface-enhanced infrared absorption spectroscopy (SEIRAS) to probe monolayers of membrane proteins. *Biochimica et Biophysica Acta (BBA) - Biomembranes*, 1828(10):2283–2293, October 2013. ISSN 0005-2736. doi: 10.1016/j.bbamem.2013.04.026. URL https://www.sciencedirect.com/science/article/pii/S0005273613001442.

[87] Axel Baumann, Silke Kerruth, Jörg Fitter, Georg Büldt, Joachim Heberle, Ramona Schlesinger, and Kenichi Ataka. In-Situ Observation of Membrane Protein Folding during Cell-Free Expression. *PLOS ONE*, 11(3): e0151051, March 2016. ISSN 1932-6203. doi: 10.1371/journal.pone.

0151051. URL `https://journals.plos.org/plosone/article?id=10.1371/journal.pone.0151051`. Publisher: Public Library of Science.

[88] J. J. Domínguez Pardo, C. A. van Walree, M. R. Egmond, M. C. Koorengevel, and J. A. Killian. Nanodiscs bounded by styrene-maleic acid allow trans-cis isomerization of enclosed photoswitches of azobenzene labeled lipids. *Chemistry and Physics of Lipids*, 220:1–5, May 2019. ISSN 0009-3084. doi: 10.1016/j.chemphyslip.2019.02.002. URL `https://www.sciencedirect.com/science/article/pii/S0009308418302457`.

[89] Meghedi Babakhanian, Limin Yang, Bryan Nowroozi, George Saddik, Lilian Boodaghians, Paul Blount, and Warren Grundfest. Effects of Low Intensity Focused Ultrasound on Liposomes Containing Channel proteins. *Scientific Reports*, 8(1):17250, November 2018. ISSN 2045-2322. doi: 10.1038/s41598-018-35486-1. URL `https://www.nature.com/articles/s41598-018-35486-1`. Bandiera_abtest: a Cc_license_type: cc_by Cg_type: Nature Research Journals Number: 1 Primary_atype: Research Publisher: Nature Publishing Group Subject_term: Epilepsy;Ion transport;Permeation and transport Subject_term_id: epilepsy;ion-transport;permeation-and-transport.

[90] Jia Ye, Siyang Tang, Long Meng, Xia Li, Xiaoxu Wen, Sihan Chen, Lili Niu, Xiangyao Li, Weibao Qiu, Hailan Hu, Mizu Jiang, Shiqiang Shang, Qiang shu, Hairong Zheng, Shumin Duan, and Yuezhou Li. Ultrasonic Control of Neural Activity through Activation of the Mechanosensitive Channel MscL. *Nano Letters*, 18(7):4148–4155, July 2018. ISSN 1530-6984. doi: 10.1021/acs.nanolett.8b00935. URL `https://doi.org/10.1021/acs.nanolett.8b00935`. Publisher: American Chemical Society.

[91] Zhihai Qiu, Shashwati Kala, Jinghui Guo, Quanxiang Xian, Jiejun Zhu, Ting Zhu, Xuandi Hou, Kin Fung Wong, Minyi Yang, Haoru Wang, and Lei Sun. Targeted Neurostimulation in Mouse Brains with Non-invasive Ultrasound. *Cell Reports*, 32(7):108033, August 2020. ISSN 2211-1247. doi: 10.1016/j.celrep.2020.108033. URL `https://www.sciencedirect.com/science/article/pii/S2211124720310184`.

[92] Armağan Koçer, Martin Walko, Wim Meijberg, and Ben L. Feringa. A Light-Actuated Nanovalve Derived from a Channel Protein. *Science*, July 2005. doi: 10.1126/science.1114760. URL `https://www.science.org/doi/abs/10.1126/science.1114760`. Publisher: American Association for the Advancement of Science.

[93] Armağan Koçer, Martin Walko, and Ben L. Feringa. Synthesis and utilization of reversible and irreversible light-activated nanovalves derived from the channel protein MscL. *Nature Protocols*, 2(6):1426–1437, June 2007. ISSN 1750-2799. doi: 10.1038/nprot.2007.196. URL `https:`

//www.nature.com/articles/nprot.2007.196. Bandiera_abtest: a Cg_type: Nature Research Journals Number: 6 Primary_atype: Protocols Publisher: Nature Publishing Group.

[94] Duygu Yilmaz, Anna I. Dimitrova, Martin Walko, and Armagan Kocer. Study of light-induced MscL gating by EPR spectroscopy. *European Biophysics Journal*, 44(7):557–565, October 2015. ISSN 1432-1017. doi: 10.1007/s00249-015-1063-4. URL `https://doi.org/10.1007/s00249-015-1063-4`.

[95] Joost H. A. Folgering, Johanna M. Kuiper, Alex H. de Vries, Jan B. F. N. Engberts, and Bert Poolman. Lipid-Mediated Light Activation of a Mechanosensitive Channel of Large Conductance. *Langmuir*, 20(17): 6985–6987, August 2004. ISSN 0743-7463. doi: 10.1021/la048942v. URL `https://doi.org/10.1021/la048942v`. Publisher: American Chemical Society.

[96] ThermoFisher Scientific. Protein assay technical handook. `https://assets.thermofisher.com/TFS-Assets/LSG/brochures/protein-assay-technical-handook.pdf`. Accessed: 8/2/2021.

[97] Marion M. Bradford. A rapid and sensitive method for the quantitation of microgram quantities of protein utilizing the principle of protein-dye binding. *Analytical Biochemistry*, 72(1):248–254, May 1976. ISSN 0003-2697. doi: 10.1016/0003-2697(76)90527-3. URL `https://www.sciencedirect.com/science/article/pii/0003269776905273`.

[98] Annela M. Seddon, Paul Curnow, and Paula J. Booth. Membrane proteins, lipids and detergents: not just a soap opera. *Biochimica et Biophysica Acta (BBA) - Biomembranes*, 1666(1):105–117, November 2004. ISSN 0005-2736. doi: 10.1016/j.bbamem.2004.04.011. URL `http://www.sciencedirect.com/science/article/pii/S0005273604001610`.

[99] Jean-Louis Rigaud, Bruno Pitard, and Daniel Levy. Reconstitution of membrane proteins into liposomes: application to energy-transducing membrane proteins. *Biochimica et Biophysica Acta (BBA) - Bioenergetics*, 1231(3):223–246, October 1995. ISSN 0005-2728. doi: 10.1016/0005-2728(95)00091-V. URL `http://www.sciencedirect.com/science/article/pii/000527289500091V`.

[100] Christian J. Braun, Tom Baer, Anna Moroni, and Gerhard Thiel. Pseudo painting/air bubble technique for planar lipid bilayers. *Journal of Neuroscience Methods*, 233:13–17, August 2014. ISSN 0165-0270. doi: 10.1016/j.jneumeth.2014.05.031. URL `http://www.sciencedirect.com/science/article/pii/S016502701400199X`.

[101] Ekaterina Zaitseva, Alison Obergrussberger, Conrad Weichbrodt, Mord-jane Boukhet, Frank Bernhard, Christopher Hein, Gerhard Baaken, Niels Fertig, and Jan C. Behrends. Electrophysiology on Channel-Forming Proteins in Artificial Lipid Bilayers: Next-Generation Instrumentation for Multiple Recordings in Parallel. In Mark Dallas and Damian Bell, editors, *Patch Clamp Electrophysiology: Methods and Protocols*, Methods in Molecular Biology, pages 67–92. Springer US, New York, NY, 2021. ISBN 978-1-07-160818-0. doi: 10.1007/978-1-0716-0818-0_4. URL `https://doi.org/10.1007/978-1-0716-0818-0_4`.

[102] Laura-Marie Winterstein, Kerri Kukovetz, Oliver Rauh, Daniel L. Tur-man, Christian Braun, Anna Moroni, Indra Schroeder, and Gerhard Thiel. Reconstitution and functional characterization of ion channels from nanodiscs in lipid bilayers. *Journal of General Physiology*, 150(4): 637–646, February 2018. ISSN 0022-1295. doi: 10.1085/jgp.201711904. URL `https://doi.org/10.1085/jgp.201711904`.

[103] Steffen Hamann, Jens Folke Kiilgaard, Thomas Litman, Francisco J. Alvarez-Leefmans, Benny R. Winther, and Thomas Zeuthen. Measure-ment of Cell Volume Changes by Fluorescence Self-Quenching. *Journal of Fluorescence*, 12(2):139–145, June 2002. ISSN 1573-4994. doi: 10.1023/A: 1016832027325. URL `https://doi.org/10.1023/A:1016832027325`.

[104] Andrew M. Powl, J. Malcolm East, and Anthony G. Lee. Anionic Phospholipids Affect the Rate and Extent of Flux through the Mechano-sensitive Channel of Large Conductance MscL. *Biochemistry*, 47(14): 4317–4328, April 2008. ISSN 0006-2960. doi: 10.1021/bi702409t. URL `https://doi.org/10.1021/bi702409t`. Publisher: American Chemical Society.

[105] Ching Kung, Boris Martinac, and Sergei Sukharev. Mechanosensi-tive Channels in Microbes. *Annual Review of Microbiology*, 64(1): 313–329, 2010. doi: 10.1146/annurev.micro.112408.134106. URL `https://doi.org/10.1146/annurev.micro.112408.134106`. _eprint: https://doi.org/10.1146/annurev.micro.112408.134106.

[106] Takeshi Nomura, Charles G. Cranfield, Evelyne Deplazes, Dylan M. Owen, Alex Macmillan, Andrew R. Battle, Maryrose Constantine, Masahiro Sokabe, and Boris Martinac. Differential effects of lipids and lyso-lipids on the mechanosensitivity of the mechanosensitive chan-nels MscL and MscS. *Proceedings of the National Academy of Sciences*, 109(22):8770–8775, May 2012. ISSN 0027-8424, 1091-6490. doi: 10.1073/ pnas.1200051109. URL `https://www.pnas.org/content/109/22/8770`. Publisher: National Academy of Sciences Section: Biological Sciences.

[107] Sergei I. Sukharev, Wade J. Sigurdson, Ching Kung, and Frederick Sachs. Energetic and Spatial Parameters for Gating of the Bacterial Large Conductance Mechanosensitive Channel, MscL. *Journal of General Physiology*, 113(4):525–540, April 1999. ISSN 0022-1295. doi: 10.1085/jgp.113.4.525. URL https://doi.org/10.1085/jgp.113.4.525.

[108] Agnès P Girard-Egrot and Loïc J Blum. Langmuir-blodgett technique for synthesis of biomimetic lipid membranes. In *Nanobiotechnology of biomimetic membranes*, pages 23–74. Springer, 2007.

[109] José Luis R. Arrondo and Félix M. Goñi. Structure and dynamics of membrane proteins as studied by infrared spectroscopy. *Progress in Biophysics and Molecular Biology*, 72(4):367–405, November 1999. ISSN 0079-6107. doi: 10.1016/S0079-6107(99)00007-3. URL http://www.sciencedirect.com/science/article/pii/S0079610799000073.

[110] Lie Wu and Xiue Jiang. Infrared Spectroscopy for Studying Plasma Membranes. In Hongda Wang and Guohui Li, editors, *Membrane Biophysics*, pages 319–354. Springer Singapore, Singapore, 2018. ISBN 978-981-10-6822-5 978-981-10-6823-2. doi: 10.1007/978-981-10-6823-2_11. URL http://link.springer.com/10.1007/978-981-10-6823-2_11.

[111] Suren A. Tatulian. Structural Characterization of Membrane Proteins and Peptides by FTIR and ATR-FTIR Spectroscopy. In Jörg H. Kleinschmidt, editor, *Lipid-Protein Interactions*, volume 974, pages 177–218. Humana Press, Totowa, NJ, 2013. ISBN 978-1-62703-274-2 978-1-62703-275-9. doi: 10.1007/978-1-62703-275-9_9. URL http://link.springer.com/10.1007/978-1-62703-275-9_9. Series Title: Methods in Molecular Biology.

[112] Andreas Barth and Christian Zscherp. What vibrations tell about proteins. *Quarterly Reviews of Biophysics*, 35(4):369–430, November 2002. ISSN 1469-8994, 0033-5835. doi: 10.1017/S0033583502003815. URL https://www.cambridge.org/core/journals/quarterly-reviews-of-biophysics/article/what-vibrations-tell-about-proteins/F16333B39A8E96B4941966314BD890CC. Publisher: Cambridge University Press.

[113] Andreas Barth. Infrared spectroscopy of proteins. *Biochimica et Biophysica Acta (BBA) - Bioenergetics*, 1767(9):1073–1101, September 2007. ISSN 0005-2728. doi: 10.1016/j.bbabio.2007.06.004. URL http://www.sciencedirect.com/science/article/pii/S0005272807001375.

[114] Heinz Fabian and Werner Mäntele. Infrared Spectroscopy of Proteins. In John M. Chalmers and Peter R. Griffiths, editors, *Handbook of Vibrational*

Spectroscopy, page s8201. John Wiley & Sons, Ltd, Chichester, UK, August 2006. ISBN 978-0-471-98847-2 978-0-470-02732-5. doi: 10.1002/ 0470027320.s8201. URL http://doi.wiley.com/10.1002/0470027320. s8201.

[115] Lukas K. Tamm and Suren A. Tatulian. Infrared spectroscopy of proteins and peptides in lipid bilayers. *Quarterly Reviews of Biophysics*, 30(4):365–429, November 1997. ISSN 1469-8994, 0033-5835. doi: 10.1017/S0033583597003375. URL https://www.cambridge. org/core/journals/quarterly-reviews-of-biophysics/article/ infrared-spectroscopy-of-proteins-and-peptides-in-lipid-bilayers/ F0904FF869B5CF57FE17D770533EE229. Publisher: Cambridge University Press.

[116] A. Blume, W. Huebner, and G. Messner. Fourier transform infrared spectroscopy of 13C:O labeled phospholipids hydrogen bonding to carbonyl groups. *Biochemistry*, 27(21):8239–8249, October 1988. ISSN 0006-2960, 1520-4995. doi: 10.1021/bi00421a038. URL https://pubs.acs.org/doi/abs/10.1021/bi00421a038.

[117] R.N. Lewis, R.N. McElhaney, W. Pohle, and H.H. Mantsch. Components of the carbonyl stretching band in the infrared spectra of hydrated 1,2-diacylglycerolipid bilayers: a reevaluation. *Biophysical Journal*, 67(6):2367–2375, December 1994. ISSN 00063495. doi: 10.1016/S0006-3495(94)80723-4. URL https://linkinghub.elsevier. com/retrieve/pii/S0006349594807234.

[118] Kenichi Ataka, Janina Drauschke, Valentina Stulberg, Beate Koksch, and Joachim Heberle. pH-induced insertion of pHLIP into a lipid bilayer: In-situ SEIRAS characterization of a folding intermediate at neutral pH. *Biochimica et Biophysica Acta (BBA) - Biomembranes*, 1864(6): 183873, June 2022. ISSN 0005-2736. doi: 10.1016/j.bbamem.2022. 183873. URL https://www.sciencedirect.com/science/article/ pii/S0005273622000153.

[119] Jean-Joseph Max and Camille Chapados. Isotope effects in liquid water by infrared spectroscopy. iii. h 2 o and d 2 o spectra from 6000 to 0 cm-1. *The Journal of chemical physics*, 131(18):184505, 2009.

[120] Mike Reppert and Andrei Tokmakoff. Computational amide i 2d ir spectroscopy as a probe of protein structure and dynamics. *Annual Review of Physical Chemistry*, 67:359–386, 2016.

[121] Catherine Berthomieu and Rainer Hienerwadel. Fourier transform infrared (FTIR) spectroscopy. *Photosynthesis Research*, 101(2):157–170, September 2009. ISSN 1573-5079. doi: 10.1007/s11120-009-9439-x. URL https://doi.org/10.1007/s11120-009-9439-x.

[122] Victor A. Lorenz-Fonfria. Infrared Difference Spectroscopy of Proteins: From Bands to Bonds. *Chemical Reviews*, 120(7):3466–3576, April 2020. ISSN 0009-2665. doi: 10.1021/acs.chemrev.9b00449. URL `https://doi.org/10.1021/acs.chemrev.9b00449`. Publisher: American Chemical Society.

[123] Erik Goormaghtigh, Vincent Raussens, and Jean-Marie Ruysschaert. Attenuated total re£ection infrared spectroscopy of proteins and lipids in biological membranes. *Biochimica et Biophysica Acta*, page 81.

[124] HR Phillip and EA Taft. Kramers-kronig analysis of reflectance data for diamond. *Physical Review*, 136(5A):A1445, 1964.

[125] Tatiana Amotchkina, Michael Trubetskov, Daniel Hahner, and Vladimir Pervak. Characterization of e-beam evaporated ge, ybf 3, zns, and laf 3 thin films for laser-oriented coatings. *Applied Optics*, 59(5):A40–A47, 2020.

[126] Deane Chandler-Horowitz and Paul M Amirtharaj. High-accuracy, mid-infrared (450 cm- 1 ω 4000 cm- 1) refractive index values of silicon. *Journal of Applied physics*, 97(12):123526, 2005.

[127] Marvin R Querry. *Optical constants of minerals and other materials from the millimeter to the ultraviolet.* Chemical Research, Development & Engineering Center, US Army Armament …, 1987.

[128] Stephanie A. Tristram-Nagle. Preparation of Oriented, Fully Hydrated Lipid Samples for Structure Determination Using X-Ray Scattering. *Methods in molecular biology (Clifton, N.J.)*, 400:63–75, 2007. ISSN 1064-3745. URL `https://www.ncbi.nlm.nih.gov/pmc/articles/PMC2697614/`.

[129] Derek Marsh. Quantitation of Secondary Structure in ATR Infrared Spectroscopy. *Biophysical Journal*, 77(5):2630–2637, November 1999. ISSN 0006-3495. doi: 10.1016/S0006-3495(99)77096-7. URL `http://www.sciencedirect.com/science/article/pii/S0006349599770967`.

[130] Víctor A. Lórenz-Fonfría, Meritxell Granell, Xavier León, Gérard Leblanc, and Esteve Padrós. In-Plane and Out-of-Plane Infrared Difference Spectroscopy Unravels Tilting of Helices and Structural Changes in a Membrane Protein upon Substrate Binding. *Journal of the American Chemical Society*, 131(42):15094–15095, October 2009. ISSN 0002-7863. doi: 10.1021/ja906324z. URL `https://doi.org/10.1021/ja906324z`. Publisher: American Chemical Society.

[131] Richard Mendelsohn, Joseph W. Brauner, and Arne Gericke. External Infrared Reflection Absorption Spectrometry of Monolayer Films at the Air-Water Interface. *Annual Review of Physical Chemistry*, 46

(1):305–334, 1995. doi: 10.1146/annurev.pc.46.100195.001513. URL `https://doi.org/10.1146/annurev.pc.46.100195.001513`. _eprint: https://doi.org/10.1146/annurev.pc.46.100195.001513.

[132] M. Handke, M. Milosevic, and N. J. Harrick. External reflection Fourier transform infrared spectroscopy: Theory and experimental problems. *Vibrational Spectroscopy*, 1(3):251–262, April 1991. ISSN 0924-2031. doi: 10.1016/0924-2031(91)85002-5. URL `https://www.sciencedirect.com/science/article/pii/0924203191850025`.

[133] R. A. Dluhy. Infrared Spectroscopy of Biophysical Monomolecular Films at Interfaces: Theory and Applications. *Applied Spectroscopy Reviews*, 35(4):315–351, November 2000. ISSN 0570-4928. doi: 10.1081/ASR-100101228. URL `https://doi.org/10.1081/ASR-100101228`. Publisher: Taylor & Francis _eprint: https://doi.org/10.1081/ASR-100101228.

[134] Richard Mendelsohn, Guangru Mao, and Carol R. Flach. Infrared reflection–absorption spectroscopy: Principles and applications to lipid–protein interaction in Langmuir films. *Biochimica et Biophysica Acta (BBA) - Biomembranes*, 1798(4):788–800, April 2010. ISSN 0005-2736. doi: 10.1016/j.bbamem.2009.11.024. URL `https://www.sciencedirect.com/science/article/pii/S0005273609004209`.

[135] John R. Ferraro and Louis J. Basile. *Fourier Transform Infrared Spectra: Applications to Chemical Systems*. Academic Press, December 2012. ISBN 978-0-323-14018-8. Google-Books-ID: pWb4UlG4j8kC.

[136] Richard A Dluhy and Donald G Cornell. In situ measurement of the infrared spectra of insoluble monolayers at the air-water interface. *The Journal of Physical Chemistry*, 89(15):3195–3197, 1985.

[137] Richard A Dluhy. Quantitative external reflection infrared spectroscopic analysis of insoluble monolayers spread at the air-water interface. *The Journal of Physical Chemistry*, 90(7):1373–1379, 1986.

[138] Richard A Dluhy, Norman A Wright, and Peter R Griffiths. In situ measurement of the ft-ir spectra of phospholipid monolayers at the air/water interface. *Applied spectroscopy*, 42(1):138–141, 1988.

[139] Richard A Dluhy, Melody L Mitchell, Thomas Pettenski, and Jeffery Beers. Design and interfacing of an automated langmuir-type film balance to an ft-ir spectrometer. *Applied spectroscopy*, 42(7):1289–1293, 1988.

[140] VL Kuzmin and AV Mikhailov. Molecular theory of light reflection and applicability limits of the macroscopic approach. *Optics and Spectroscopy*, 51(4):383–385, 1981.

[141] VL Kuzmin, VP Romanov, and AV Mikhailov. Reflection of light at the boundary of liquid systems and structure of the surface layer: A review. *Optics and spectroscopy*, 73(1):1–26, 1992.

[142] Arne Gericke, Alexander V Michailov, and Heinrich Hühnerfuss. Polarized external infrared reflection-absorption spectrometry at the air/water interface: comparison of experimental and theoretical results for different angles of incidence. *Vibrational spectroscopy*, 4(3):335–348, 1993.

[143] Derek Marsh. Structural and thermodynamic determinants of chain-melting transition temperatures for phospholipid and glycolipids membranes. *Biochimica et Biophysica Acta (BBA) - Biomembranes*, 1798(1): 40–51, January 2010. ISSN 0005-2736. doi: 10.1016/j.bbamem.2009.10. 010. URL `https://www.sciencedirect.com/science/article/pii/S0005273609003630`.

[144] Johanna M. Kuiper and Jan B. F. N. Engberts. H-Aggregation of Azobenzene-Substituted Amphiphiles in Vesicular Membranes. *Langmuir*, 20(4):1152–1160, February 2004. ISSN 0743-7463. doi: 10.1021/la0358724. URL `https://doi.org/10.1021/la0358724`. Publisher: American Chemical Society.

[145] Oskar Klaja, James A. Frank, Dirk Trauner, and Ana-Nicoleta Bondar. Potential energy function for a photo-switchable lipid molecule. *Journal of Computational Chemistry*, 41(27):2336–2351, 2020. ISSN 1096-987X. doi: 10.1002/jcc.26387. URL `https://onlinelibrary.wiley.com/doi/abs/10.1002/jcc.26387`. _eprint: https://onlinelibrary.wiley.com/doi/pdf/10.1002/jcc.26387.

[146] Fucsia Crea, Antreas Vorkas, Aoife Redlich, Rubén Cruz, Chaowei Shi, Dirk Trauner, Adam Lange, Ramona Schlesinger, and Joachim Heberle. Photoactivation of a Mechanosensitive Channel. *Frontiers in Molecular Biosciences*, 9, 2022. ISSN 2296-889X. URL `https://www.frontiersin.org/articles/10.3389/fmolb.2022.905306`.

[147] Alfred Blume. Properties of lipid vesicles: FT-IR spectroscopy and fluorescence probe studies. *Current Opinion in Colloid & Interface Science*, 1 (1):64–77, February 1996. ISSN 1359-0294. doi: 10.1016/S1359-0294(96) 80046-X. URL `http://www.sciencedirect.com/science/article/pii/S135902949680046X`.

[148] DR Armstrong, J Clarkson, and WE Smith. Vibrational analysis of trans-azobenzene. *The Journal of Physical Chemistry*, 99(51):17825–17831, 1995.

[149] M. Preuss and F. Bechstedt. Vibrational spectra of ammonia, benzene, and benzene adsorbed on Si (001) by *first principles* calculations with

periodic boundary conditions. *Physical Review B*, 73(15):155413, April 2006. ISSN 1098-0121, 1550-235X. doi: 10.1103/PhysRevB.73.155413. URL https://link.aps.org/doi/10.1103/PhysRevB.73.155413.

[150] Xuedong Song, Jerry Perlstein, and David G. Whitten. Supramolecular Aggregates of Azobenzene Phospholipids and Related Compounds in Bilayer Assemblies and Other Microheterogeneous Media: Structure, Properties, and Photoreactivity1. *Journal of the American Chemical Society*, 119(39):9144–9159, October 1997. ISSN 0002-7863. doi: 10.1021/ja971291n. URL https://doi.org/10.1021/ja971291n. Publisher: American Chemical Society.

[151] Takeshi Kawai, Junzo Umemura, and Tohru Takenaka. UV absorption spectra of azobenzene-containing long-chain fatty acids and their barium salts in spread monolayers and Langmuir-Blodgett films. *Langmuir*, 5(6): 1378–1383, November 1989. ISSN 0743-7463. doi: 10.1021/la00090a020. URL https://doi.org/10.1021/la00090a020. Publisher: American Chemical Society.

[152] Sue-Hwa Lin and Guido Guidotti. Chapter 35 Purification of Membrane Proteins. In Richard R. Burgess and Murray P. Deutscher, editors, *Methods in Enzymology*, volume 463 of *Guide to Protein Purification, 2nd Edition*, pages 619–629. Academic Press, January 2009. doi: 10.1016/S0076-6879(09)63035-4. URL https://www.sciencedirect.com/science/article/pii/S0076687909630354.

[153] Dylan T. Murray, James Griffin, and Timothy A. Cross. Detergent Optimized Membrane Protein Reconstitution in Liposomes for Solid State NMR. *Biochemistry*, 53(15):2454–2463, April 2014. ISSN 0006-2960. doi: 10.1021/bi500144h. URL https://pubs.acs.org/doi/10.1021/bi500144h. Publisher: American Chemical Society.

[154] Mohammed Mouhib, Andrea Benediktsdottir, Caroline Svensson Nilsson, and Celestine N. Chi. Influence of Detergent and Lipid Composition on Reconstituted Membrane Proteins for Structural Studies. *ACS Omega*, 6 (38):24377–24381, September 2021. doi: 10.1021/acsomega.1c02542. URL https://doi.org/10.1021/acsomega.1c02542. Publisher: American Chemical Society.

[155] Samuel Krimm and Jagdeesh Bandekar. Vibrational Spectroscopy and Conformation of Peptides, Polypeptides, and Proteins. In C. B. Anfinsen, John T. Edsall, and Frederic M. Richards, editors, *Advances in Protein Chemistry*, volume 38, pages 181–364. Academic Press, January 1986. doi: 10.1016/S0065-3233(08)60528-8. URL https://www.sciencedirect.com/science/article/pii/S0065323308605288.

[156] Yongliang Liu, Rae-Kwang Cho, Kaori Sakurai, Tsuyoshi Miura, and Yukihiro Ozaki. Studies on Spectra/Structure Correlations in Near-Infrared Spectra of Proteins and Polypeptides. Part I: A Marker Band for Hydrogen Bonds. *Applied Spectroscopy*, 48(10):1249–1254, October 1994. ISSN 0003-7028. doi: 10.1366/0003702944027408. URL `https://doi.org/10.1366/0003702944027408`. Publisher: SAGE Publications Ltd STM.

[157] Chungwen Liang, Martti Louhivuori, Siewert J. Marrink, Thomas L. C. Jansen, and Jasper Knoester. Vibrational Spectra of a Mechanosensitive Channel. *The Journal of Physical Chemistry Letters*, 4(3):448–452, February 2013. ISSN 1948-7185. doi: 10.1021/jz3019258. URL `https://pubs.acs.org/doi/10.1021/jz3019258`.

[158] Burkhard Bechinger, Jean-Marie Ruysschaert, and Erik Goormaghtigh. Membrane Helix Orientation from Linear Dichroism of Infrared Attenuated Total Reflection Spectra. *Biophysical Journal*, 76(1):552–563, January 1999. ISSN 0006-3495. doi: 10.1016/S0006-3495(99) 77223-1. URL `https://www.sciencedirect.com/science/article/pii/S0006349599772231`.

[159] Derek Marsh, Martin Müller, and Franz-Josef Schmitt. Orientation of the Infrared Transition Moments for an -Helix. *Biophysical Journal*, 78 (5):2499–2510, May 2000. ISSN 0006-3495. doi: 10.1016/S0006-3495(00) 76795-6. URL `https://www.sciencedirect.com/science/article/pii/S0006349500767956`.

[160] Federico Baserga, Antreas Vorkas, Fucsia Crea, Luiz Schubert, Jheng-Liang Chen, Aoife Redlich, Mariafrancesca La Greca, Julian Storm, Sabine Oldemeyer, Kirsten Hoffmann, Ramona Schlesinger, and Joachim Heberle. Membrane Protein Activity Induces Specific Molecular Changes in Nanodiscs Monitored by FTIR Difference Spectroscopy. *Frontiers in Molecular Biosciences*, 9, 2022. ISSN 2296-889X. URL `https://www.frontiersin.org/articles/10.3389/fmolb.2022.915328`.

[161] Flavia Aleotti, Lorenzo Soprani, Artur Nenov, Roberto Berardi, Alberto Arcioni, Claudio Zannoni, and Marco Garavelli. Multidimensional Potential Energy Surfaces Resolved at the RASPT2 Level for Accurate Photoinduced Isomerization Dynamics of Azobenzene. *Journal of Chemical Theory and Computation*, 15(12):6813–6823, December 2019. ISSN 1549-9618. doi: 10.1021/acs.jctc.9b00561. URL `https://doi.org/10.1021/acs.jctc.9b00561`. Publisher: American Chemical Society.

[162] Marek Pederzoli, Jiří Pittner, Mario Barbatti, and Hans Lischka. Nonadiabatic Molecular Dynamics Study of the cis–trans Photoisomerization

of Azobenzene Excited to the S1 State. *The Journal of Physical Chemistry A*, 115(41):11136–11143, October 2011. ISSN 1089-5639. doi: 10.1021/jp2013094. URL https://doi.org/10.1021/jp2013094. Publisher: American Chemical Society.

[163] Anna Kristina Schnack-Petersen, Mátyás Pápai, and Klaus Braagaard Møller. Azobenzene photoisomerization dynamics: Revealing the key degrees of freedom and the long timescale of the trans-to-cis process. *Journal of Photochemistry and Photobiology A: Chemistry*, 428: 113869, June 2022. ISSN 1010-6030. doi: 10.1016/j.jphotochem.2022. 113869. URL https://www.sciencedirect.com/science/article/pii/S1010603022000995.

[164] Oliver Weingart, Zhenggang Lan, Axel Koslowski, and Walter Thiel. Chiral Pathways and Periodic Decay in cis-Azobenzene Photodynamics. *The Journal of Physical Chemistry Letters*, 2(13):1506–1509, July 2011. doi: 10.1021/jz200474g. URL https://doi.org/10.1021/jz200474g. Publisher: American Chemical Society.

[165] Mina Aleksanyan, Andrea Grafmüller, Fucsia Crea, Vasil N. Georgiev, Naresh Yandrapalli, Stephan Block, Joachim Heberle, and Rumiana Dimova. Photomanipulation of Minimal Synthetic Cells: Area Increase, Softening, and Interleaflet Coupling of Membrane Models Doped with Azobenzene-Lipid Photoswitches. *Advanced Science*, n/a(n/a):2304336. ISSN 2198-3844. doi: 10.1002/advs. 202304336. URL https://onlinelibrary.wiley.com/doi/abs/10. 1002/advs.202304336. _eprint: https://onlinelibrary.wiley.com/-doi/pdf/10.1002/advs.202304336.

[166] Alessandro Cembran, Fernando Bernardi, Marco Garavelli, Laura Gagliardi, and Giorgio Orlandi. On the Mechanism of the cis−trans Isomerization in the Lowest Electronic States of Azobenzene: S0, S1, and T1. *Journal of the American Chemical Society*, 126(10): 3234–3243, March 2004. ISSN 0002-7863. doi: 10.1021/ja038327y. URL https://doi.org/10.1021/ja038327y. Publisher: American Chemical Society.

[167] Evgenii Titov, Giovanni Granucci, Jan Philipp Götze, Maurizio Persico, and Peter Saalfrank. Dynamics of Azobenzene Dimer Photoisomerization: Electronic and Steric Effects. *The Journal of Physical Chemistry Letters*, 7(18):3591–3596, September 2016. doi: 10.1021/acs.jpclett.6b01401. URL https://doi.org/10.1021/acs.jpclett.6b01401. Publisher: American Chemical Society.

[168] Tripta Bhatia, Tom Robinson, and Rumiana Dimova. Membrane permeability to water measured by microfluidic trapping of giant vesicles. *Soft Matter*, 16(31):7359–7369, 2020.

[169] Ryan S. Ries, Hyeon Choi, Rikard Blunck, Francisco Bezanilla, and James R. Heath. Black Lipid Membranes: Visualizing the Structure, Dynamics, and Substrate Dependence of Membranes. *The Journal of Physical Chemistry B*, 108(41):16040–16049, October 2004. ISSN 1520-6106. doi: 10.1021/jp048098h. URL https://doi.org/10.1021/jp048098h. Publisher: American Chemical Society.

[170] Halil I. Okur, Orly B. Tarun, and Sylvie Roke. Chemistry of Lipid Membranes from Models to Living Systems: A Perspective of Hydration, Surface Potential, Curvature, Confinement and Heterogeneity. *Journal of the American Chemical Society*, 141(31):12168–12181, August 2019. ISSN 0002-7863. doi: 10.1021/jacs.9b02820. URL https://doi.org/10.1021/jacs.9b02820. Publisher: American Chemical Society.

[171] OliverH. Lowry, NiraJ. Rosebrough, A. Lewis Farr, and RoseJ. Randall. PROTEIN MEASUREMENT WITH THE FOLIN PHENOL REAGENT. *Journal of Biological Chemistry*, 193(1):265–275, November 1951. ISSN 0021-9258. doi: 10.1016/S0021-9258(19)52451-6. URL https://www.sciencedirect.com/science/article/pii/S0021925819524516.